



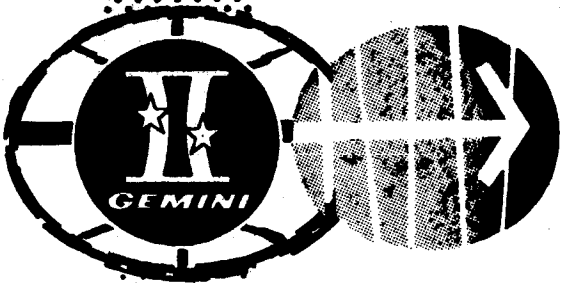
NATIONAL AERONAUTICS AND SPACE ADMINISTRATION

INTERIM REPORT
MANNED SPACEFLIGHT EXPERIMENTS

GEMINI X MISSION

JULY 18 - 21, 1966

FACILITY FORM 6	N 6 8 - 1 4 1 5 0 1	N 6 8 - 1 4 1 6 4
	(ACCESSION NUMBER)	(THRU)
	145	1
	(PAGES)	(CODE)
	TMX-60791	30
	(NASA CR OR TMX OR AD NUMBER)	(CATEGORY)



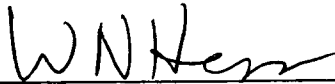
SCIENCE AND APPLICATIONS DIRECTORATE
MANNED SPACECRAFT CENTER
HOUSTON, TEXAS

807-49154

INTERIM REPORT
MANNED SPACEFLIGHT EXPERIMENTS
GEMINI X MISSION
July 18 - 21, 1966

Prepared by: Mission and Data Management Office
Science and Applications Directorate

Approved by:



Wilmot N. Hess
Director

Science and Applications Directorate

NATIONAL AERONAUTICS AND SPACE ADMINISTRATION
Manned Spacecraft Center
Houston, Texas
March 1967

CONTENTS

Section	Page
INTRODUCTION	1
1. EXPERIMENT M405 (MSC-3), TRIAXIS MAGNETOMETER	9 ✓
2. EXPERIMENT M408 (MSC-6), BETA SPECTROMETER	21 ✓
3. EXPERIMENT M409 (MSC-7), BREMSSTRAHLUNG SPECTROMETER	37 ✓
4. EXPERIMENT M410 (MSC-8), COLOR PATCH PHOTOGRAPHY	49 ✓
5. EXPERIMENT M412 (MSC-12), LANDMARK CONTRAST MEASUREMENTS	55 ✓
6. EXPERIMENT S001 (S-1), ZODIACAL LIGHT PHOTOGRAPHY	59 ✓
7. EXPERIMENT S005 (S-5), SYNOPTIC TERRAIN PHOTOGRAPHY	63 ✓
8. EXPERIMENT S006 (S-6), SYNOPTIC WEATHER PHOTOGRAPHY	73 ✓
9. EXPERIMENT S010 (S-10), AGENA MICROMETEORITE COLLECTION	81 ✓
10. EXPERIMENT S012 (S-12), MICROMETEORITE COLLECTION	89 ✓
11. EXPERIMENT S013 (S-13), ULTRAVIOLET ASTRONOMICAL CAMERA	97 ✓
12. EXPERIMENT S026 (S-26), ION-WAKE MEASUREMENT	105 ✓
13. EXPERIMENT D005 (D-5), STAR OCCULTATION NAVIGATION	115 ✓
14. EXPERIMENT D010 (D-10), ION-SENSING ATTITUDE CONTROL	125 ✓
DISTRIBUTION LIST	135

TABLES

Tables		Page
I	EXPERIMENTS ON GEMINI X	2
II	EXPERIMENT FLIGHT PLAN FOR GEMINI X	4
6-I	PHOTOGRAPHS TAKEN DURING EXPERIMENT S001 (S-1)	61
11-I	REVISED CENSUS OF STARS ON GEMINI X S013 (S-13) FILM	100

FIGURES

Figure		Page
1-1	Triaxis magnetometer	13
1-2	Electronics unit	14
1-3	Sensor unit	15
1-4	Boom on test fixture	16
1-5	Measurement of earth magnetic field in South Atlantic Anomaly	17
1-6	Measured field versus theoretical field	18
1-7	Field magnitude at varying altitudes	19
2-1	Beta Spectrometer	29
2-2	Electron detector cross section	30
2-3	Detector/analyzer block diagram	31
2-4	Pulse height analyzer	32
2-5	Program control circuitry	33
2-6	Spectrometer view angle with magnetic field lines versus relative counting rate	34
2-7	Measured average electron spectrum	35
2-8	Predicted decay of artificial electron belt based on Gemini X data	36
3-1	Bremsstrahlung Spectrometer	42
3-2	Bremsstrahlung Spectrometer block diagram	43
3-3	Data processor circuit	44
3-4	Relative count-time distributions for revolution 20	45

Figure		Page
3-5	Relative count-time distributions for revolution 32	46
3-6	Bremsstrahlung relative countrate-time spectra for revolution 6	47
3-7	Bremsstrahlung relative countrate-time spectra for revolution 34	48
4-1	Color patch photography experiment equipment	52
4-2	Method of photography by spacecraft pilot	53
7-1	View to the northeast over the Spanish Sahara and Morocco	66
7-2	A second view over the Sahara with Hamada du Dra to the left	67
7-3	View to the southeast over Niger	68
7-4	The Rio Grande Delta	69
7-5	The China coast	70
7-6	Southern Formosa	71
7-7	Atolls in the Maldine Islands	72
8-1	Convective cloud patterns of northern South America . . .	76
8-2	Open polygonal cells, 3 to 6 miles in diameter, formed over the oceans	77
8-3	Convective activity in a cloud mass over Indian Ocean	78
8-4	Equatorial cloud condition taken over Sumatra and Malaya	79
9-1	Agena micrometeorite collection unit before flight . . .	84
9-2	Collection unit after 4-months exposure	85
9-3	Macroscopic crater in stainless steel plate (light micrograph - 500X)	86

Figure	Page	
9-4	Second macroscopic crater in stainless steel plate (light micrograph - 500X)	87
9-5	The second macroscopic crater stainless steel plate (scanning electron micrograph - 500X)	88
10-1	Mounted micrometeorite collection hardware	92
10-2	Micrometeorite collection unit with one cover open	93
10-3	Sample slides in second compartment in micrometeorite collection unit	94
10-4	Sample locations and descriptions	95
11-1	Ultraviolet Astronomical Camera assembly mounted to spacecraft	102
11-2	Ultraviolet spectra of stars in the Carina-Vela region of the southern Milky Way	103
11-3	Key chart for figure 11-2	104
12-1	Placement of ion-wake measurement equipment on GATV	110
12-2	General ion-wake profile	111
12-3	An electron detector sensor	112
12-4	View of sensor circuitry.	113
12-5	Gemini undocking maneuvers for ion-wake measurements	114
13-1	Star occultation photometer	121
13-2	Telemetry intensity profile of star Vega	122
13-3	Telemetry intensity profile of star Arcturus	123
13-4	Telemetry intensity profile of star Denebola	124
14-1	Location of ion-sensing attitude control equipment	130

Figure		Page
14-2	Ion-sensing configuration	131
14-3	Ion-sensing attitude control electronics system	132
14-4	Comparison of ion attitude yaw angle measurements with inertial system	133
14-5	Comparison of ion attitude pitch angle measurements with inertial system	134

INTERIM REPORT
MANNED SPACEFLIGHT EXPERIMENTS
GEMINI X MISSION

INTRODUCTION

This compilation of papers constitutes an interim report on the results of experiments conducted during the Gemini X manned spaceflight. The results of experiments conducted on earlier flights have been published in similar interim reports which are available on request from the Mission and Data Management Office, Science and Applications Directorate, Code TF2, Houston, Texas.

The Gemini Agena Target Vehicle for this mission was launched at 3:39:46 p.m. eastern standard time (e.s.t.) and the Gemini XII spacecraft was launched at 5:20:26 p.m. e.s.t. on July 18. The touchdown of the spacecraft was after 70 hours 46 minutes 39 seconds ground elapsed time (g.e.t.) on July 21.

Fifteen scientific or technological experiments were planned for the Gemini X mission, of which one was cancelled at the time of launch. Table I is a list of the experiments in alphanumeric order showing the title, sponsoring agency, principal investigator, and qualitative success on this mission. The experiment inflight operations schedule was considerably changed from the preflight flight plan. The actual schedule of experiment activities shown in table II was reconstructed from the onboard voice tapes, mission notes, crew flight logs, and scientific debriefing. The Lunar Ultraviolet Spectral Reflectance (M407) experiment was scheduled contingent upon the phase of the moon at the time of launch, and would have been performed only if the launch had been postponed to a later time.

Preliminary analyses of data indicated that the basic objectives of 12 out of the 14 experiments were met. Each experiment scheduled for the Gemini X mission is described in the sections that follow. Success or failure of each experiment is so indicated. Detailed analyses and evaluation of the data, particularly the photographic information, requires more time to reach definitive conclusions. Additional scientific or technological reports will be published as appropriate.

TABLE I.- EXPERIMENTS ON GEMINI X

Experiment number	Experiment title	Principal investigator	Sponsor	Data obtained	Completion of planned objectives
D005 (D-5)	Star Occultation Navigation	Air Force Avionics Laboratory, Wright Patterson AFB, Ohio	Department of the Air Force, Detachment 2, Space Systems Division (AFSC)	Two periods of useful data	Partial
D010 (D-10)	Ion-Sensing Attitude Control	Air Force Cambridge Research Laboratory, Hanscom AFB, Massachusetts	Department of the Air Force, Detachment 2, Space Systems Division (AFSC)	Five periods of useful data	Substantial
M405 (MSC-3)	Triaxis Magnetometer	NASA Manned Spacecraft Center, Space Sciences Division	NASA/Manned Spacecraft Center	Data available during all revolutions	Completed
M408 (MSC-6)	Beta Spectrometer	NASA Manned Spacecraft Center, Space Sciences Division	NASA/MSC	One period of useful data	Partial
M409 (MSC-7)	Bremsstrahlung Spectrometer	NASA Manned Spacecraft Center, Space Sciences Division	NASA/MSC	Data available during all revolutions	Completed
M410 (MSC-8)	Color Patch Photography	NASA Manned Spacecraft Center, Photographic Technology Laboratory	NASA/MSC	All photo-graphic data available	Substantial

TABLE I.- EXPERIMENTS ON GEMINI X - Concluded

Experiment number	Experiment title	Principal investigator	Sponsor	Data obtained	Completion of planned activities
M412 (MSC-12)	Landmark Contrast Measurements	NASA Manned Spacecraft Center, Guidance and Control Division	NASA/MSC	No data obtained	Not attempted
S001 (S-1)	Zodiacal Light Photography	University of Minnesota, Institute of Technology, Minneapolis, Minnesota	NASA/Office of Space Science and Applications	15 frames of photographic data	Partial
S005 (S-5)	Synoptic Terrain Photography	NASA Goddard Spaceflight Center	NASA/OSSA	75 frames of photographic data	Partial
S006 (S-6)	Synoptic Weather Photography	U.S. Weather Bureau, National Weather Satellite Center	NASA/OSSA	260 frames of photographic data	Completed
S010 (S-10)	Agena Micrometeorite Collection	Dudley University, Albany, New York	NASA/OSSA	4 plates of data	Partial
S012 (S-12)	Micrometeorite Collection	Dudley University, Albany, New York	NASA/OSSA	Data package not recovered	Not completed
S013 (S-13)	Ultraviolet Astronomical Camera	Dearborn Observatory, Northwestern University	NASA/OSSA	Several frames of photo data	Substantial
S026 (S-26)	Ion-Wake Measurement	Electro-Optical Systems, Inc., Pasadena, California	NASA/OSSA	Several periods of useful data including one undocking maneuver	Partial

TABLE II.- EXPERIMENT FLIGHT PLAN FOR GEMINI X

Experiment title	Priority	Activation time, g.e.t., hr:min	Revolution	Condition	Remarks
D005 (D-5) Star Occulation Navigation	1	26:30 to 26:50	17	Mode-A from flight plan	1. Stars Alioth and Alkaid were acquired and tracked. 2. Spacecraft was docked with GATV. Attitude was maintained using GATV attitude control. 3. Fifty pounds of GATV propellant gas used.
			18	Mode-A	Cancelled by Flight Director at 27:40 g.e.t. due to excessive fuel requirements.
			40	Modified mode-D	The computer function was to be deleted from mode-D if time prevented its use.
D010 (D-10) Ion-Sensing Attitude Control	2	51:45	32	Mode-A	Mode-A is equipment extension and activation.
			34 to 39	Mode-G (Random Data Accumulation)	All four temperature parameters stabilized to approximately 35° F during the-mission.
			40	Mode-E (Yaw Attitude Study)	Sensors were used for platform alignment. Good results were obtained.
			40	Mode-E	
		65:25 to 65:55	41	Mode-C (Roll Attitude Study)	
		65:55 to 66:10			

TABLE II.- EXPERIMENT FLIGHT PLAN FOR GEMINI X - Continued

Experiment title	Priority	Activation time, G.e.t., hr:min	Revolution	Condition	Remarks
D010 (D-10) Ion-Sensing Attitude Control - continued	2	66:05 to 66:40	41	Mode-D (Pitch Attitude Study)	Mode-B (Ambient Data Accumulation) Mode-F (Photo Emission Effects) and Mode-H (Translation Thruster Effects) were not accomplished due to fuel constraints.
M405 (MSC-3) Triaxis Magnetometer	10	00:20 to 70:10	All	Boom extended	1. Experiment was on at all times. Orbits of particular interest were those passing through the South Atlantic Anomaly region. 2. Sensors performed satisfactorily throughout the mission.
M407 (MSC-5) Lunar Ultraviolet Spectral Reflectance	13	--	--	Deleted	Experiment cancelled at launch in accordance with contingency plan.
M408 (MSC-6) Beta Spectrometer	10	--	All	Free flight	1. Attitude control was desired but not provided due to a fuel constraint. Data for revolutions 32 and 33 showed good correlation with M405 data. Spacecraft was tumbling at this time. 2. Approximately 2 minutes of useful data were obtained.
M409 (MSC-7) Bremsstrahlung Spectrometer	11	--	All	Sensors on during entire orbital flight	1. Data from revolutions 4, 16, 17, 18, 19, 20, 32, and 33 showed sensors functioned normally. 2. Quick-look data showed useful results throughout mission.

TABLE II.- EXPERIMENT FLIGHT PLAN FOR GEMINI X - Continued

Experiment title	Priority	Activation time, g.e.t., hr:min	Revolution	Condition	Remarks
M410 (MSC-8) Color Patch Photography	14	23:42	15	Photos taken during standup EVA	Three sunlight and one shadow exposures were taken.
M412 (MSC-12) Landmark Contrast Measurements	12	--	--	--	Because of fuel limitation and time allocation, the experiment could not be accomplished.
S001 (S-1) Zodiacal Light Photography	7	66:30	41	Attitude Control	1. Several photos taken were underexposed. 2. Quality of picture sharpness showed excellent attitude control hold.
S005 (S-5) Synoptic Terrain Photography	8	Varied	28 29	Targets of opportunity	Approximately 10 straight-down 70-mm pictures taken. A total of 75 are useful.
S006 (S-6) Synoptic Weather	9	Varied	27 28 29	Targets of opportunity	1. The crew confirmed that weather photos were taken during state- side passes on revolutions 27, 28, and 29. An attempt was made to photograph Hurricane Celia located northeast of Bermuda. 2. Approximately 260 pictures were taken.
S010 (S-10) Agena Micro- meteorite Collection	6	Gemini VIII GATV launch to 49:06	30	Closed position only; 4-month operating period	1. The crew retrieved S010 from Gemini VIII GATV during umbil- ical EVA. 2. The EVA pilot did not place additional hardware on the GATV due to lack of handrails and possible umbilical entan- glement.

TABLE II.- EXPERIMENT FLIGHT PLAN FOR GEMINI X - Concluded

Experiment title	Priority	Activation time, g.e.t., hr:min	Revolution	Condition	Remarks
S012 (S-12) Micrometeorite Collection	5	9:00 to 17:00 Retrieved at 48:50	6 to 11 30	Opened during first crew sleep period Umbilical EVA	<ol style="list-style-type: none"> The crew reported locking of the S012 collector door at 29:06 g.e.t. The crew stated retrieval was accomplished just prior to umbilical EVA and prior to M410 operation. The crew indicated at 64:15 g.e.t. the S012 hardware could not be located in the spacecraft. They surmised the experiment hardware floated through the open hatch during umbilical EVA.
S013 (S-13) Ultraviolet Astronomical Camera	4	23:28 to 24:00	15	Standup EVA	<ol style="list-style-type: none"> 18 exposures were reported taken of the β Crucis star field. 24 stars have usable spectra. 22 additional stars show usable energy density.
S026 (S-26) Ion-Wake Measurement	3	44:40	29	Mode-A (Linear Mapping)	Undocking was accomplished over Cape Kennedy. S026 was performed over Canary Islands. Real-time data showed wake activity at approximately 100 feet.

1. EXPERIMENT M405 (MSC-3), TRIAXIS MAGNETOMETER

By William Dan Womack
NASA Manned Spacecraft Center

SUMMARY

N 6 8 - 1 4 1 5 1

Knowledge of the magnetic field magnitude and direction is most important for the evaluation of charged particle measurements, especially where directional instrumentation is employed. Due to the directionality of charged particles within magnetic fields, the measurement of those particles becomes impossible when employing a directional measuring instrument without determining the direction of the magnetic field lines.

This report provides a description of the triaxis magnetometric experimental equipment and operation, and the experimental results obtained from the Gemini Titan 10 (GT-10) spacecraft. The results discussed are based solely on data which were evaluated when this report was compiled.

OBJECTIVE

The object was to determine the direction and magnitude of the earth's geomagnetic field in the South Atlantic Anomaly regions with respect to experiment M408 (MSC-6). Experiment M408 (MSC-6), described in section 2 of this report, consisted of a beta spectrometer, with a half-angle of 15° , attached to the GT-10 spacecraft. The experiment M408 (MSC-6) was to determine the flux of charged particles external to spacecraft. The South Atlantic Anomaly region is between South America and Africa. This region, bounded approximately by 30° E and 60° W longitude and 15° S and 50° S latitude, is the only portion of the spacecraft trajectory that presents any significant electron intensities.

EQUIPMENT

The experimental equipment consisted of the triaxis magnetometer and an extendible boom.

The triaxis magnetometer was a flux-gate variety which included an electronic package, a sensor unit, and an interconnecting cable (fig. 1-1).

The electronic package contained a dc-to-dc converter and three electronic subassemblies which supplied the necessary sensor-drive voltages, detected and transformed the vector field ac second-harmonic signals, and converted these signals to a 0- to 5-volt analog dc signal.

The sensor unit contains three identical second-harmonic sensors which have a core material driven into saturation by a 15-kc signal through a primary winding. A secondary winding obtains the second-harmonic frequency when an external field is applied, and an auxiliary winding nulls the residual field. The three sensor probes are mounted orthogonally in one package.

The three sensor probes are mounted orthogonally to measure vector components H_x , H_y , and H_z of the magnetic field. By measuring the vector components, the direction and total field could be calculated from the following equations:

$$H_t = \sqrt{H_x^2 + H_y^2 + H_z^2}$$

$$\theta_x = \cos^{-1} \left(\frac{H_x}{H_t} \right)$$

$$\theta_y = \cos^{-1} \left(\frac{H_y}{H_t} \right)$$

$$\theta_z = \cos^{-1} \left(\frac{H_z}{H_t} \right)$$

where

H_t is total field; H_x , H_y , and H_z are vector components of the field; and θ_x , θ_y , and θ_z are the component angles measured from their respective axes.

If the location of the sensor unit with respect to the spacecraft is known, the direction of the field with respect to the spacecraft can be calculated.

The interconnection is a 110-inch cable that supplies the electrical continuity between the electronics and sensor units.

The electronics unit and the sensor unit are located in the retro-adapter section (figs. 1-2 and 1-3). Figure 1-2 shows the interior of the retroadapter section with the electronics unit mounted to the retro-beam. Figure 1-3 shows the skin of the adapter section with the magnetometer boom door open and the boom extended. This photograph was taken during experiment hardware checkout at McDonnell Aircraft Corporation (MAC) in St. Louis.

The boom, spring-loaded and telescopic, extends the sensor unit approximately 42 inches from the spacecraft for attenuating any residual magnetic field produced by the electrical cables, instrumentation, or material within the area of the sensor assembly. The boom was fabricated from titanium tubes, loaded with a beryllium-copper spring, and actuated with pyrotechnics during sustainer engine cutoff (SECO). A view of the boom on a test fixture at MAC is shown in figure 1-4.

PROCEDURE

Since experiment M405 (MSC-3) was flown in direct support of the experiment M408 (MSC-6), the experimental operation was determined by the requirements established by the latter. All requirements imposed upon the spacecraft or crew are described in experiment M408 (MSC-6) report.

The triaxis magnetometer was turned on during the preinsertion checklist and remained on until the crew performed the preretro checklist. These were the only operational requirements necessary for the experiment.

The magnetometer and beta spectrometer were scheduled to operate for at least ten revolutions while spacecraft passed over the South Atlantic Anomaly region. In addition, the equipment was to be operated for a period of at least 15 minutes while the spacecraft was not within this region.

RESULTS

The data shown in this portion of the report are not conclusive and are given only as an example of the data that may be of interest to the scientific community. All computations made on the data to obtain direction of the magnetic field are referenced to the beta spectrometer only.

Other computations and analyses would have to be made before the direction of the magnetic field could be determined with respect to any other portion of the spacecraft or the earth.

An example of data obtained through an anomaly pass is presented in figure 1-5. For a typical pass, these data illustrate values of the total magnetic field vector and the angle made with respect to the center line of the spectrometer detector. The figure shows the total field vector, expressed in thousands of gammas, and the angle alpha, in degrees, for a ground elapsed time from 51 hours 20 minutes to 51 hours 30 minutes. The total field vector between 20 100 gammas and 23 800 gammas for this pass agrees with the theoretical calculated total field. The wide variation in angle can be explained by a tumbling motion of the spacecraft or its random attitude during this time period. The data shown in the figure were measured during a sleep period of the Gemini X flight crew. Additional analysis is continuing as computer-determined computations become available.

Figure 1-6 gives the magnitude of the geomagnetic field measured during revolution 20 of the GT-10 spacecraft through the South Atlantic Anomaly. This magnitude is compared to the calculated theoretical magnetic field magnitude by Dr. C. E. McIlwain's computer codes (ref. 1). The pattern formed by the data points of the measured field can best be explained by the random-sample rate of the telemetry system and the accuracy of the flight hardware itself. If the measured field was interpolated to acquire a smooth curve, the measured field and the theoretical field would agree favorably. The trend in this figure seems to hold throughout all data which have been analyzed.

Figure 1-7 shows the comparison of the geomagnetic field magnitude measured at altitudes approximately 350 km apart. These measurements were taken in the South Atlantic Anomaly region between 10° S and 28° S latitude and 60° W and 30° E longitude, with altitudes as noted. The data from 383 to 400 km were taken during revolution 36, and the data from 700 to 762 km were taken during revolutions 6 and 7. The effect seen here is the attenuation of the field strength with increasing altitudes as is common with magnetic field sources.

REFERENCE

1. McIlwain, Carl E.: Coordinates for Mapping the Distribution of Magnetically Trapped Particles. *J. Geophys. Res.*, vol. 66, no. 11, Nov. 1961, pp. 3681-3691.

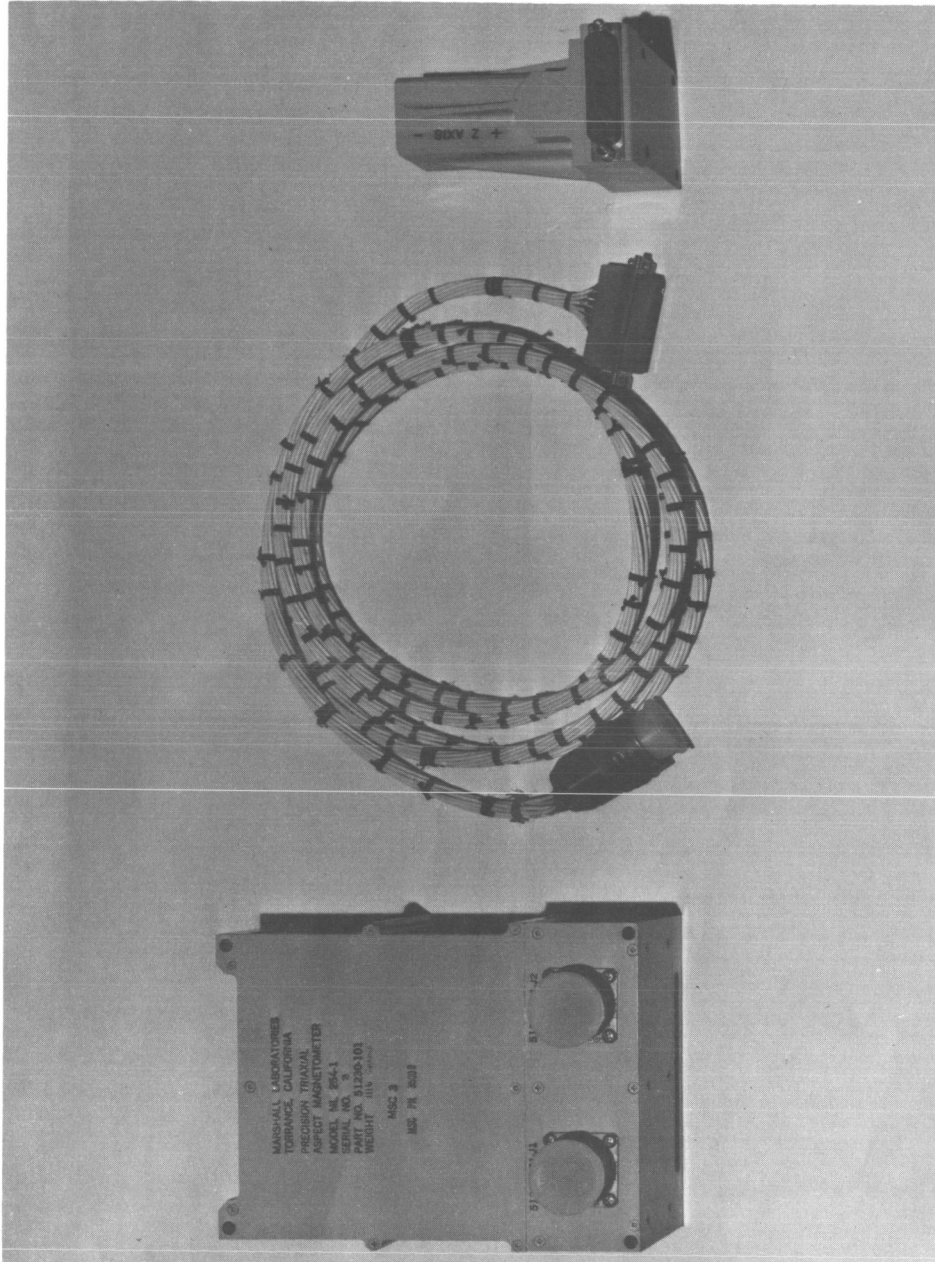


Figure 1-1-1. - Triaxis magnetometer.

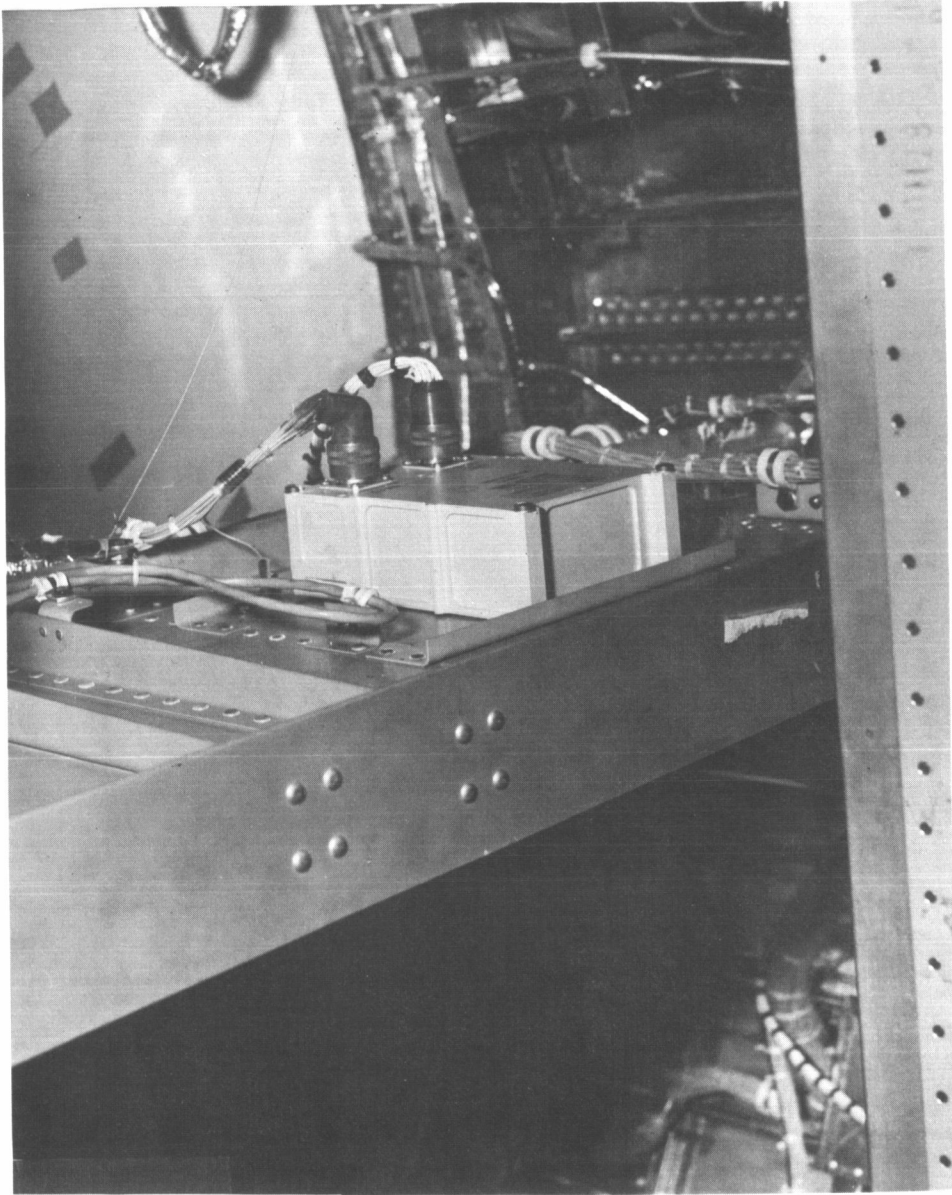


Figure 1-2. - Electronics unit attached to Gemini adapter section.



Figure 1-3. - Sensor unit.

MAGNETOMETER BOOM EXTENDED VERTICALLY DOWNWARD

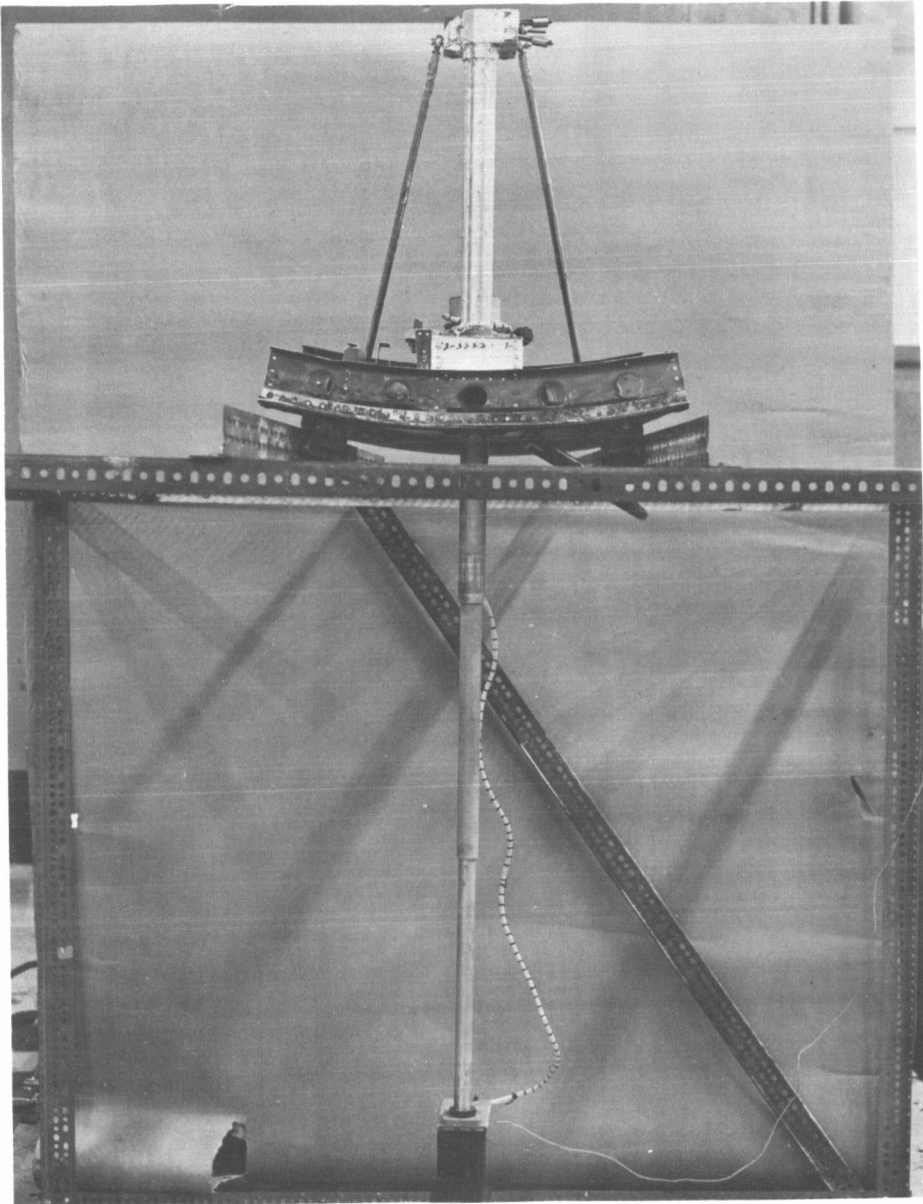


Figure 1-4. - Boom on test fixture.

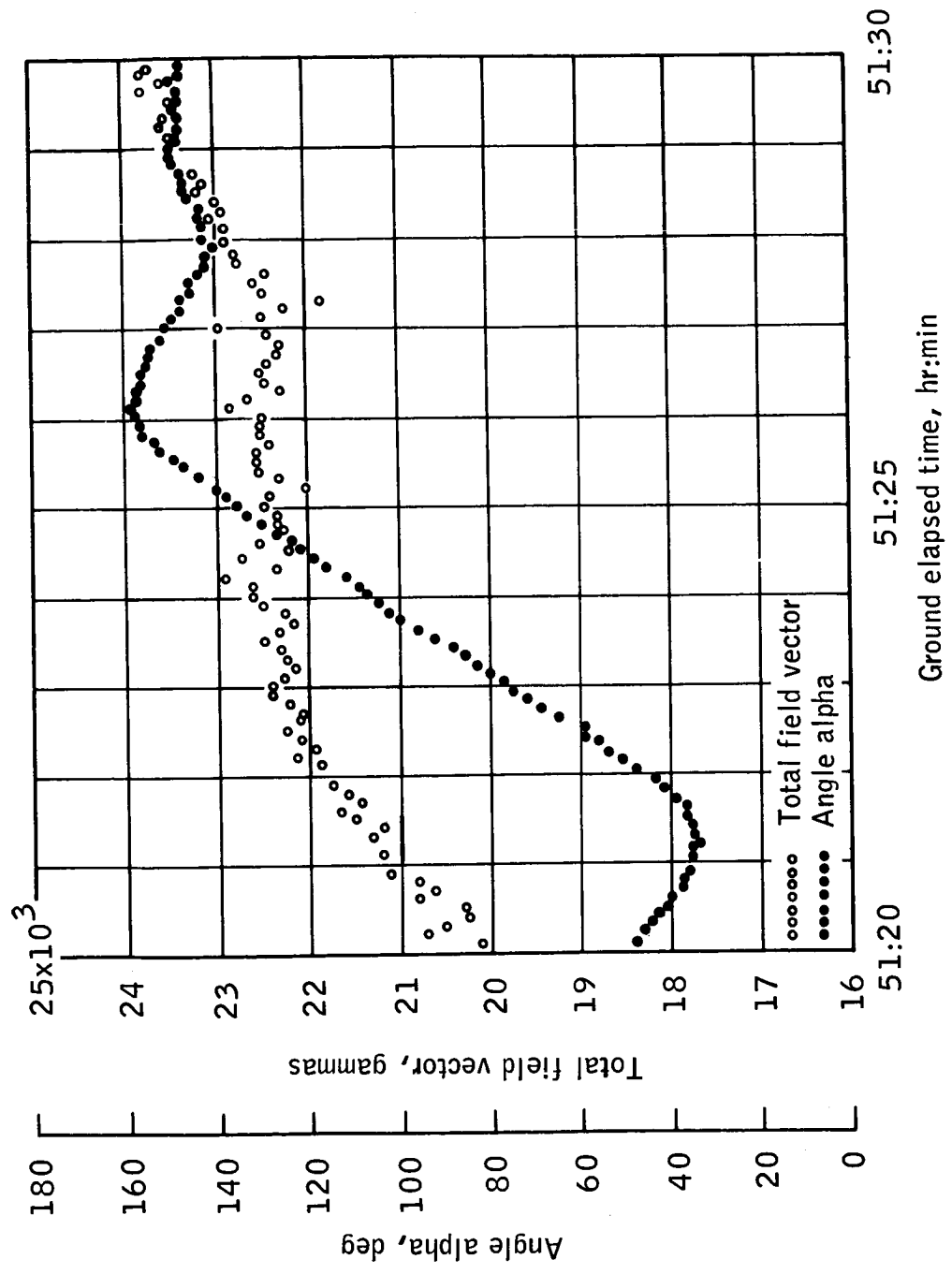


Figure 1-5. - Measurement of earth magnetic field in South Atlantic Anomaly.

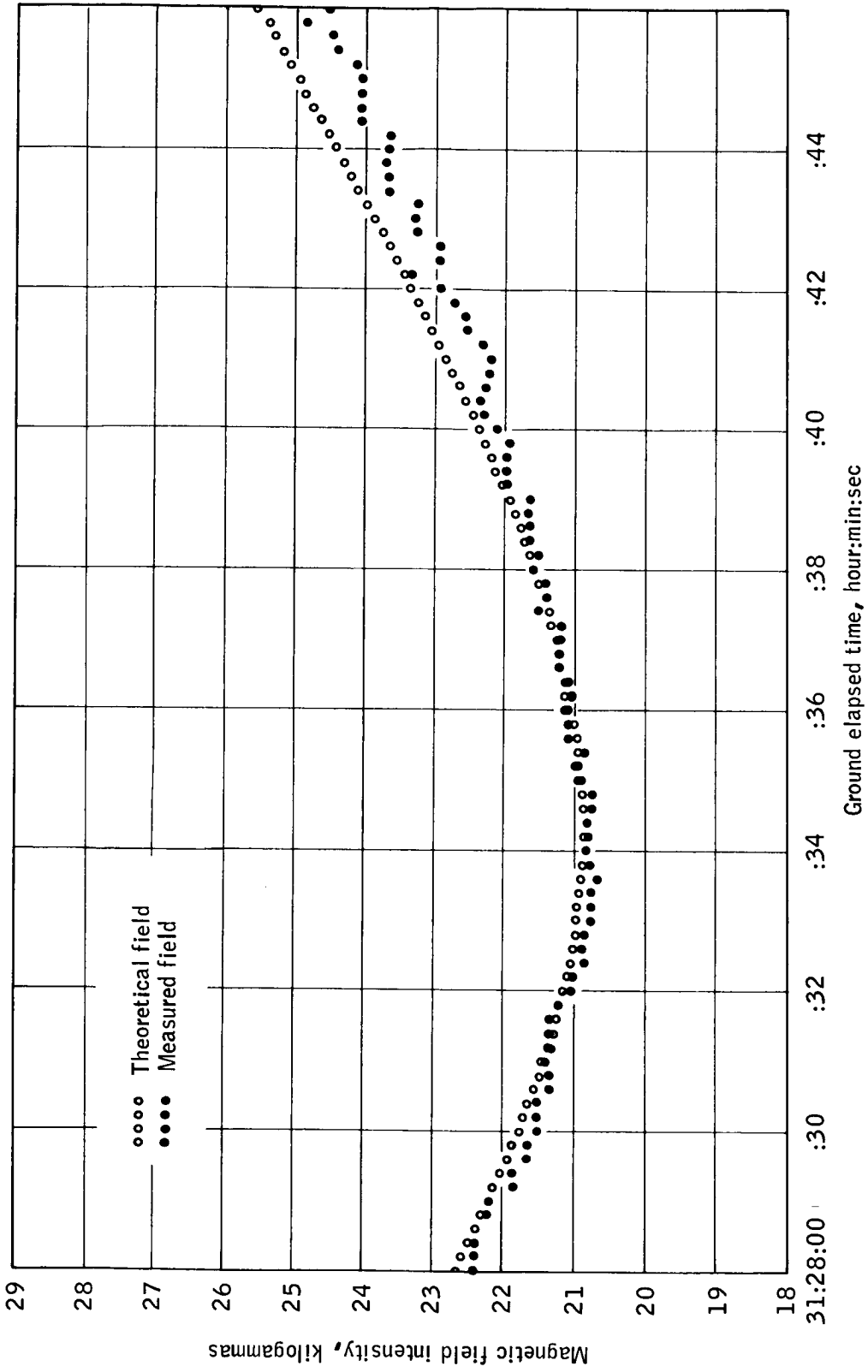


Figure 1-6. - Measured field versus theoretical field.

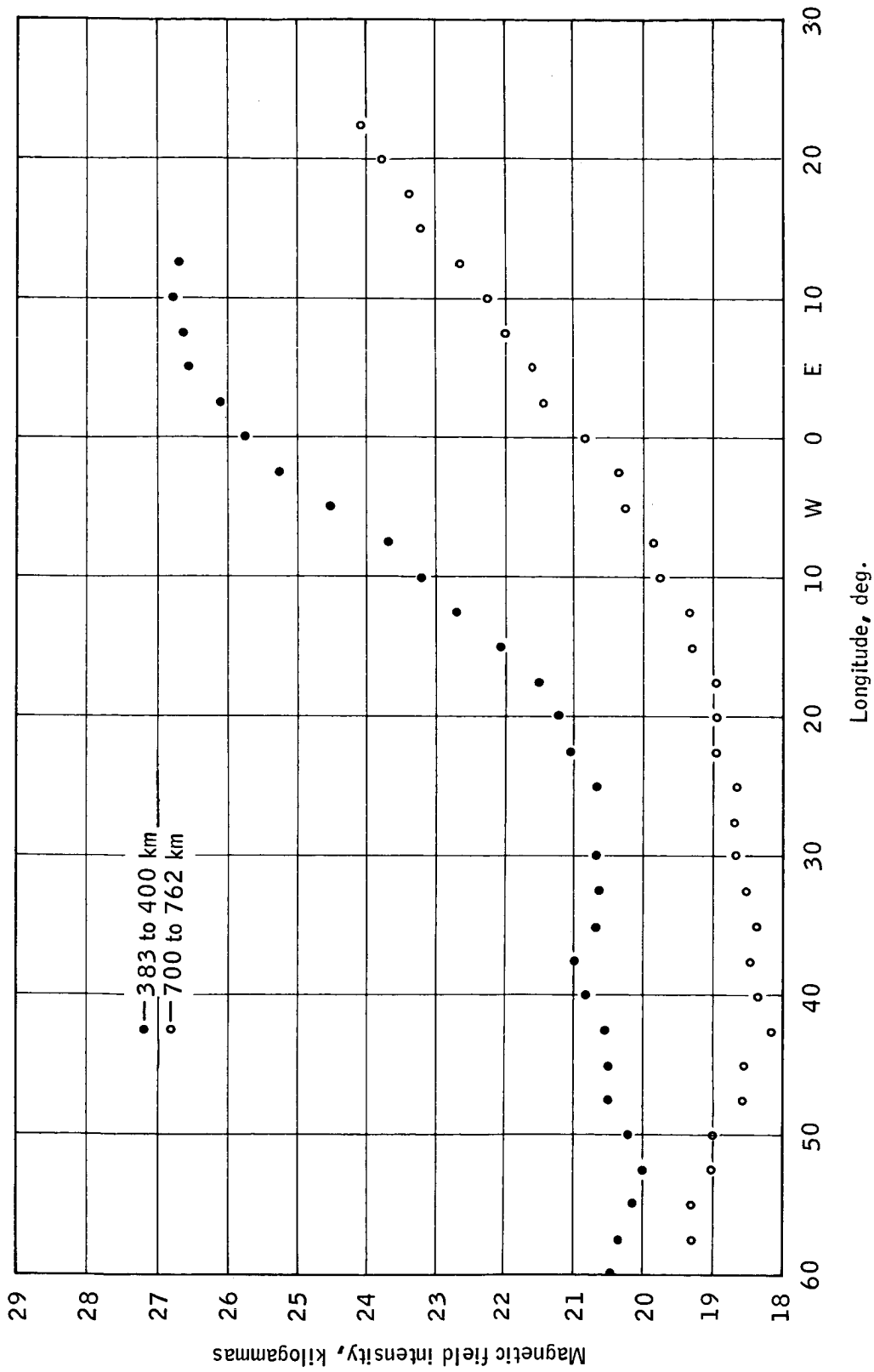


Figure 1-7. - Field magnitude at varying altitudes.

2. EXPERIMENT M408 (MSC-6), BETA SPECTROMETER

By James Marbach
NASA Manned Spacecraft Center

SUMMARY

N 6 8 - 1 4 1 5 2

The beta spectrometer experiment was flown on the Gemini X mission to determine, together with experiments M405 (MSC-3) and M409 (MSC-7), the radiation environment both inside and outside the spacecraft throughout the mission. Its specific purpose was to measure the flux, energy, and spatial distribution of electrons encountered in the South Atlantic Anomaly region of the inner Van Allen radiation belt. The equipment utilized semiconductor detectors in a straightforward pulse-height-analyzer (PHA) design to provide seven channels of flux information over the energy range $0.41 \leq E \leq 4.61$ MeV. A 15° half-angle collimator allowed a determination of the directional distribution of the incident radiation.

The data revealed a spectrum similar to those measured on the Gemini IV and the Gemini VII missions. There is evidence that the electron directions are almost entirely confined within a plane normal to the earth's magnetic field direction as has been suggested by previous scientific measurements.

OBJECTIVE

The beta spectrometer experiment flown on the Gemini X mission was the third in a series of such measurements on Project Gemini. It was designed to determine the radiation environment external to the spacecraft encountered throughout typical manned earth-orbital missions. The data from these experiments are necessary to assemble a concise and up-to-date picture of the environment in order to estimate the radiation hazard to be encountered on any specific mission. By comparing dose estimates using this environment with actual measured doses made on each flight, a knowledge of the reliability and accuracy of the mathematical technique of hazard prediction is realized.

EQUIPMENT

The beta spectrometer is similar in function to the proton-electron spectrometer for experiment M404, flown on previous Gemini missions; however, it is quite different in design.

The beta spectrometer consists of two containers, one housing the detector and analyzer system, and the other the data processing system. The total weight is approximately 16 pounds. Power consumption is about 5.5 watts at 28 volts dc. All data are processed in digital form and are relayed via Gemini pulse code modulation (PCM) telemetry system. Figure 2-1 is a photograph of the completed assembly.

Particles are detected by solid-state detectors in a dE/dx , total E arrangement providing seven channels of flux information over the energy bands of 0.41 to 0.67, 0.67 to 1.0, 1.0 to 1.22, 1.22 to 2.00, 2.00 to 2.88, 2.88 to 3.63, and 3.63 to 4.61 MeV.

Figure 2-2 is a cross section of the detector/analyzer system. The total E detector is a stack of four lithium-drifted silicon detectors providing a total active region approximately 1 cm in depth. The outputs of all four detectors are connected in parallel to a common amplifier and pulse shaper. The dE/dx detector is a 60-micron surface barrier and functions solely as an anticoincidence device in conjunction with the total E detector to discriminate against protons. To minimize the probability of electrons being scattered out of the dE/dx detector and completely (or partially) missing the total E detector, the two are physically mounted as close to each other as practical. This requires that mass shielding be used for collimation. As indicated in figure 2-2, lead spacers are arranged to provide a solid angle aperture of approximately 0.25 steradian (half-angle approximately 15°). To eliminate analysis of particles entering the total E detector from a direction other than through the collimator, the rear and sides of the detector assembly are surrounded with plastic scintillator (NE102). This third detector is viewed by an RCA 4460 photomultiplier (pm) tube, the output of which feeds an anticoincidence circuit similar to that of the dE/dx detector. Additional aluminum acts as both support and a shield to minimize anticoincidence rate (and subsequent dead-time) around the plastic and pm tube assembly. The aluminized Mylar and aluminum housing surrounds the silicon detectors and serves as an electromagnetic shield to minimize noise in the detector outputs.

The effect of the combination of shielding and coincidence circuitry can be summarized as follows:

- (1) All particles entering the instrument through any other portion other than the entrance aperture are either stopped in shielding or rejected by anticoincidence as they enter the plastic scintillator.

- (2) Protons of $E < 2$ MeV entering the aperture are completely stopped in the front detector.

(3) Protons of $0.2 < E < 20$ MeV will deposit greater than 200 keV in the front detector. The threshold for coincidence rejection is adjusted to 200 keV and these particles are not analyzed.

(4) Protons with $E > 5.5$ MeV will deposit more than 4.6 MeV in the total E detector and will be out of the range of the PHA and rejected on that basis.

(5) Protons with $E > 70$ MeV will penetrate both silicon detectors and enter the plastic coincidence scintillator for rejection.

(6) Electrons of $E < 410$ keV and of $4.6 < E < 10$ MeV will deposit energies in the total E detector that are outside the range of the PHA.

(7) Electrons of $E > 10$ MeV will penetrate to the scintillator for rejection.

(8) Electrons of $0.41 \geq E \geq 4.6$ MeV will be analyzed.

A block diagram of the detector/analyzer system is shown in figure 2-3.

Pulses from either the dE/dx , total E, or scintillator detector are routed into essentially identical charge-sensitive amplifiers. The amplified and shaped pulses from the dE/dx and scintillator detectors are fed into level discriminators which are adjusted to equivalent energy deposited of 200 keV and 100 keV, respectively. When an incoming pulse exceeds the threshold level, the discriminator triggers and remains latched on for approximately 0.7 microsecond. The two discriminator outputs are then routed through a complementary AND gate to a strobe control circuit.

The strobe pulse feeds an AND gate together with the inhibit/enable logic discriminator outputs. Its function is to hold the analyzer storage input closed to an analyzed pulse from the total E detector until the inhibit circuits have enough time to present an output should they have one.

Firing time of the strobe is adjusted to occur sufficiently down on the decay slope of the pulse to allow the latest and shortest, as well as the earliest and shortest, inhibit pulses to be recognized.

Figure 2-4 is a simplified block diagram of the pulse height analyzer. The amplified and shaped signals from the total E detector are applied to eight voltage-to-current converters, each of which feeds a tunnel diode discriminator. Each discriminator is adjustable, to allow flexibility of the selected energy thresholds of about 50 percent of its nominal levels. The first and eighth discriminators serve to define the

energy window of the analyzer. The discriminators are similar in operation to the inhibit logic discriminators, that is, they detect a level and then latch on for approximately 0.7 microsecond. The ninth circuit in the diagram is a dE/dt -to-I converter which operates the previously mentioned strobe.

To obtain differential rather than integral spectra, interconnecting logic circuitry is provided between each discriminator output after strobe interrogation. As each discriminator fires, it inhibits the output of its next lower neighbor, leaving a pulse present on the highest energy line actuated.

A pulse that has been interrogated and accepted by the strobe circuit then feeds a one-shot multivibrator which is connected to the data processing package.

Data pulses from the one shot multivibrators at the output of each of the seven energy channels are routed directly to the digital data processing system. Each channel is routed through a gate which is controlled by the time-base generator to control sampling time. When the gate is opened, pulses are fed into seven parallel, 14-bit scaler accumulators. After the preset sampling has occurred, the gate is closed and the information in the accumulators is shifted in parallel into seven 14-bit shift registers. The registers are connected to seven parallel-sampled, bilevel PCM telemetry channels. Each time the telemetry (TM) channels are sampled the next register bit is shifted for readout. Sampling rate is 10 per second so that 1.4 seconds are required to read out each seven channel spectrum. Immediately after the accumulated data are transferred, the input gates are opened to begin another sample. In this way data are accumulated and read out at the same time.

Figure 2-5 is a block diagram of the program control circuitry. All sequences are slaved to a 10-per-second gate pulse that is obtained from the PCM telemetry system. If it is assumed initially that the index pulse is set and the counters in the control circuitry are at zero, the sequencing can be traced as follows: A sync pulse enters the N/14 counter. The falling edge of this pulse triggers the N/14 counter one step and flips the index signal off. The index signal is routed to an eighth bilevel TM channel that is sampled in parallel with the seven energy channels. Its function is to define the first register bit being sampled. Simultaneously, this first sync pulse sends a shift command to all registers. The 2nd to 13th sync pulses advance the N/14 counter and shift the register leaving them cleared. The N/14 counter, now filled, sends a pulse to a three-position sequencer. This sequencer consists of six cascaded one-shot multivibrators. After a 75-microsecond delay, a pulse appears at terminal 1 of the sequencer, resets the N/14 counter and the index flip-flop, and transfers data from the accumulators into the now depleted registers. After another 75-microsecond delay, a pulse appears

at terminal 2 of the sequencer which resets all accumulators. After a third 75-microsecond delay, a pulse appears at terminal 3 of the sequencer initiating the time-base for controlling the input gates to the accumulators. This completes the cycle and the next sequence can begin.

The time-base generator works as follows. The pulse from terminal 3 of the sequencer opens the input gates to the accumulator and simultaneously gates a 100-kc crystal-controlled square wave oscillator into a 17-bit scaler. After 2^{17} pulses, the time-base flip-flop is toggled, closing the input gates to the accumulators and the oscillator gate to the scaler. The circuit will now wait until a pulse from the sequencer reinitiates the cycle. The accumulator gates are open for $131\,075 \pm 15$ counts in the scaler which corresponds to 1.31057 ± 0.00015 seconds. Stability is better than 3 parts per 13 000 over the temperature range of -65° to $+170^{\circ}$ F or ± 0.102 percent.

It should be noted that although the output registers require 1.4 seconds to be sampled, the accumulators are filled for only 1.31 seconds. The difference is to allow for time required to transfer the accumulator information into the output registers.

To assure that the silicon semiconductor detectors are maintained at room temperature or below (the noise figure improves with decreasing temperature), an evaporative cooling device is incorporated into the detector/analyzer. Water, stored in the cylindrical reservoir on the top of the assembly in the left of figure 2-1, is fed to two identical evaporators mounted to the side of the detector subassembly. The evaporators consist of ceramic disks which allow the water to evaporate through to the vacuum maintained inside the instrument during orbit. The water is sealed inside the reservoir in a polyethylene bag which leaves approximately half of the tank for air which is sealed at atmospheric pressure. During orbit, the 1-atmosphere pressure differential between the inside of the tank and the vacuum outside forces the water to the ceramic evaporators where it slowly bleeds out and evaporates, absorbing the heat of vaporization. The bleed rate is adjusted to approximately 5 grams per hour total, which will maintain the detectors at room temperature or lower for 4 hours with the equipment mounting structure temperature at 120° F.

PROCEDURE

The experimental equipment on GT-10 was located in the retrograde section of the spacecraft adapter. The detector/analyzer was mounted on the adapter ring structure and had an unobstructed view of the exterior environment through a hole in the spacecraft skin. The hole was

covered with a half-hinged door to protect the instrument during the launch phase of the mission. It was automatically jettisoned during spacecraft separation from the booster.

Operation of the equipment during the flight was accomplished by means of a toggle switch on the control console of the pilot, who turned on the instrument after orbit insertion and left it on throughout the mission until just prior to retrofire.

To obtain information on the directionality of the electron radiation encountered, it was necessary that the instrument see as many different directions in space as possible. Since the radiation is concentrated in the relatively small South Atlantic Anomaly region at Gemini altitudes and is known to be trapped in the geomagnetic field, it was important that the instrument be made to look at several angles with respect to the magnetic field while in this area. To accomplish this the crew was requested to execute a slow roll maneuver while in the South Atlantic Anomaly which would rotate the instrument about the magnetic field lines. This maneuver sweeps the experiment sensors through the normal to the field twice for every 360-degree roll of the spacecraft. In addition to providing directionality information, this would also assure several data points taken while the instrument is normal to the magnetic field direction where the electron intensity is known to be greatest.

The principal investigator was stationed at the Kokee tracking site in Hawaii, where the dumped telemetry data were evaluated following each of the anomaly passes. The requirements for controlled spacecraft attitude could then be augmented or reduced during the mission, depending on quick-look data obtained during other mission operations. The Triaxis Magnetometer experiment (M405) provided instantaneous "magnetic attitude" of the beta spectrometer so that the data received could be continuously related to spacecraft attitude.

RESULTS

The unexpected high fuel usage during the first and second days of the mission eliminated the possibility of controlled altitude passes for the beta spectrometer experiment. Evaluation of data from the first 2 days indicates that very little, if any, usable data were obtained. On the third day, the spacecraft was flown in a random or tumbling mode through the anomaly and one good traversal of the magnetic field resulted. All results and conclusions are necessarily based on this one set of data points. The location within the anomaly of these few data points was fortuitously good, however, in that much data from previous scientific measurements are available for comparison.

Figure 2-6 is a plot of relative counting rate as measured by the spectrometer versus the angle the spectrometer viewed with respect to the magnetic field direction. The indicated angle is derived directly from magnetometer data. Although the ordinate has not been amply corrected for X-ray contributions or geometric factor, the data indicate a strongly peaked intensity distribution about the normal to the magnetic field. The full-width-half-maximum points of $\pm 10^\circ$ about the normal are in general agreement with measurements made previously on scientific satellites.

Figure 2-7 is a plot of the average electron spectrum as measured. As mentioned previously the available data occurred at a convenient location ($B = 0.22$, $L = 1.250$ in B, L space) so as to be comparable with other measurements. The solid curve is the theoretical spectrum predicted by Walt (ref. 1) which for convenience of comparison was normalized to the measured differential flux at approximately 2.45 MeV. The Gemini X data points were obtained by averaging five spectra that were measured within $\pm 3.5^\circ$ of the normal to the magnetic field. This average spectrum was then corrected for X-rays using count rates observed when the instrument was well away from the normal to the field immediately prior to this time. The resulting spectrum was then corrected for backscatter effects using calibration data and assuming an incident spec-

trum of the form $\phi(E) = \phi_0(10) \frac{E_0 - E}{1.34}$. The error bars indicated are due to statistics only. Actually, a somewhat harder spectrum in the energy band between 0.5 MeV and 1.5 MeV would be more realistic, but calculations indicate the overall effect of such an assumed spectrum would be to raise the data point at 1.1 MeV more in line with that suggested by the other data points. The overall measured spectrum is in good agreement with that measured on the Gemini IV and Gemini VII missions, and is in excellent agreement with the theoretical spectrum of Walt except at low energies. The divergence at low energies has been suggested to be due to the presence of natural Van Allen belt electrons which are now becoming a significant fraction of the fission electrons still present from the high-altitude nuclear tests of 1962.

Figure 2-8 is a plot of omnidirectional electron flux for energies above about 1.2 MeV versus time after the Starfish high-altitude nuclear tests. The data points are from measurements as indicated on the graph. No explanation is offered for the high flux measured on the Gemini X mission compared to the measured values on the Gemini IV and Gemini VII missions except that in both cases the data are still preliminary and require more detailed evaluation. Particularly, the Gemini X mission data have no corrections for geometric factor applied, and the error bar, which allows for statistics only, needs adjustment. It is anticipated that data from the Gemini XII mission (the beta spectrometer experiment will be repeated) will be extremely helpful in explaining the difference

in decay constants as measured on the Gemini X, Gemini IV, and Gemini VII missions.

Summaries of the real-time data obtained during the mission indicate that the equipment functioned exactly as planned. The detector was provided with a specially designed cooler, and the detector temperature followed a satisfactory profile. Shortly after being turned on, the detector temperature sensor indicated temperatures of less than 10° C and cooled to about 3° C on the second revolution. Throughout the rest of the mission, temperatures remained between 2° and 3.5° C.

CONCLUSIONS

The beta spectrometer functioned as planned throughout the Gemini X mission. The cool temperatures recorded from the instrument during the mission indicate that the evaporative cooler, coupled with apparently lower-than-expected spacecraft adapter temperatures, provided ideal operating conditions. The data provide a good picture of the electron directional distribution. The omnidirectional flux calculated appears to be in good agreement with previous measurements. Detailed reports will be published when additional data are received and evaluated.

REFERENCE

1. Walt, Martin: The Effects of Atmospheric Collisions on Geomagnetically Trapped Electrons. J. Geophysical Res., vol. 69, 1964, pp. 3947-3958.

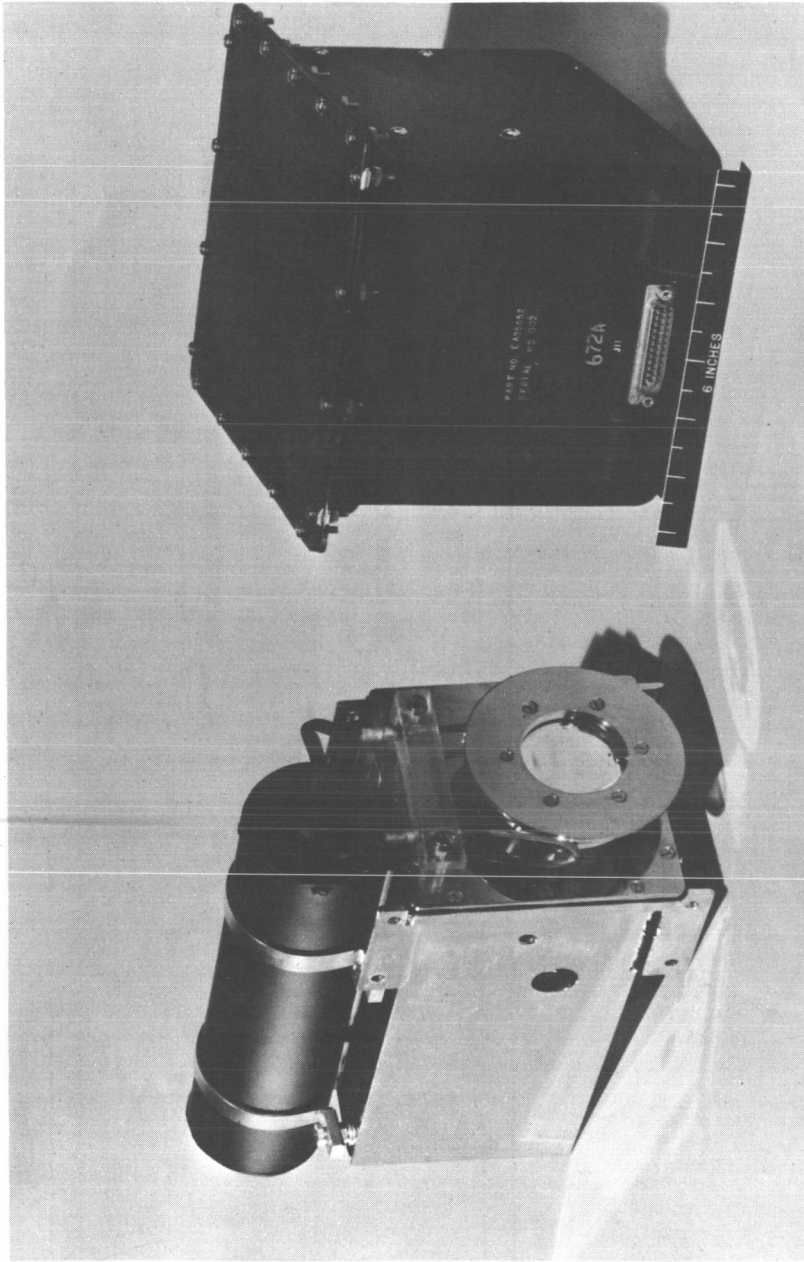


Figure 2-1-1. - Beta spectrometer.

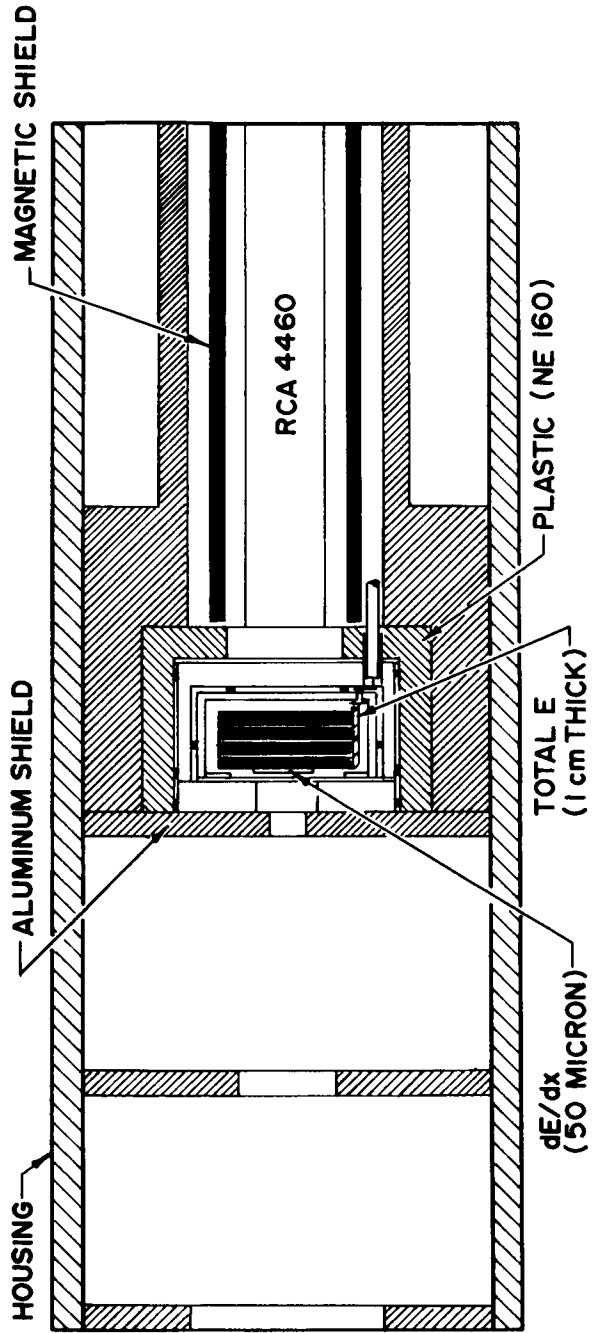


Figure 2-2. - Electron detector cross section.

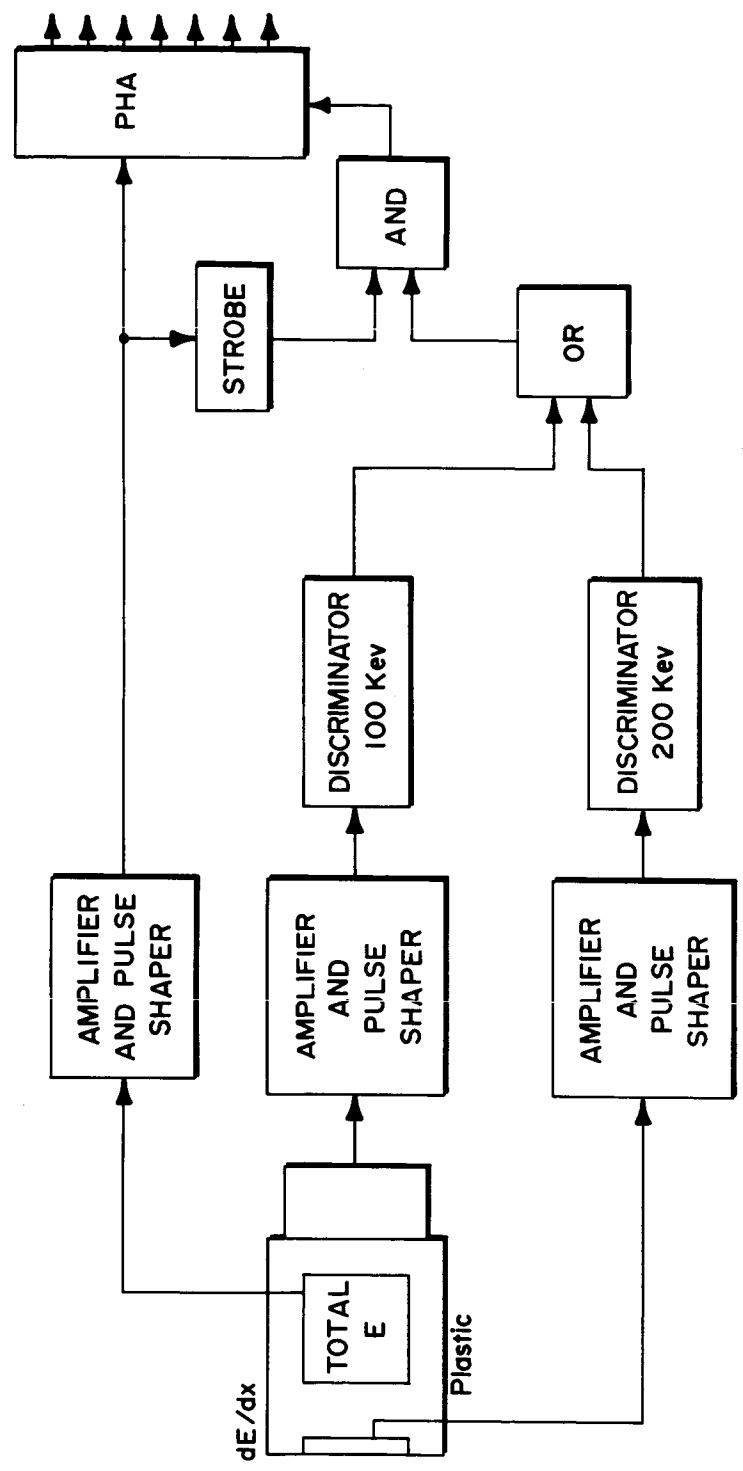


Figure 2-3. - Detector/analyzer block diagram.

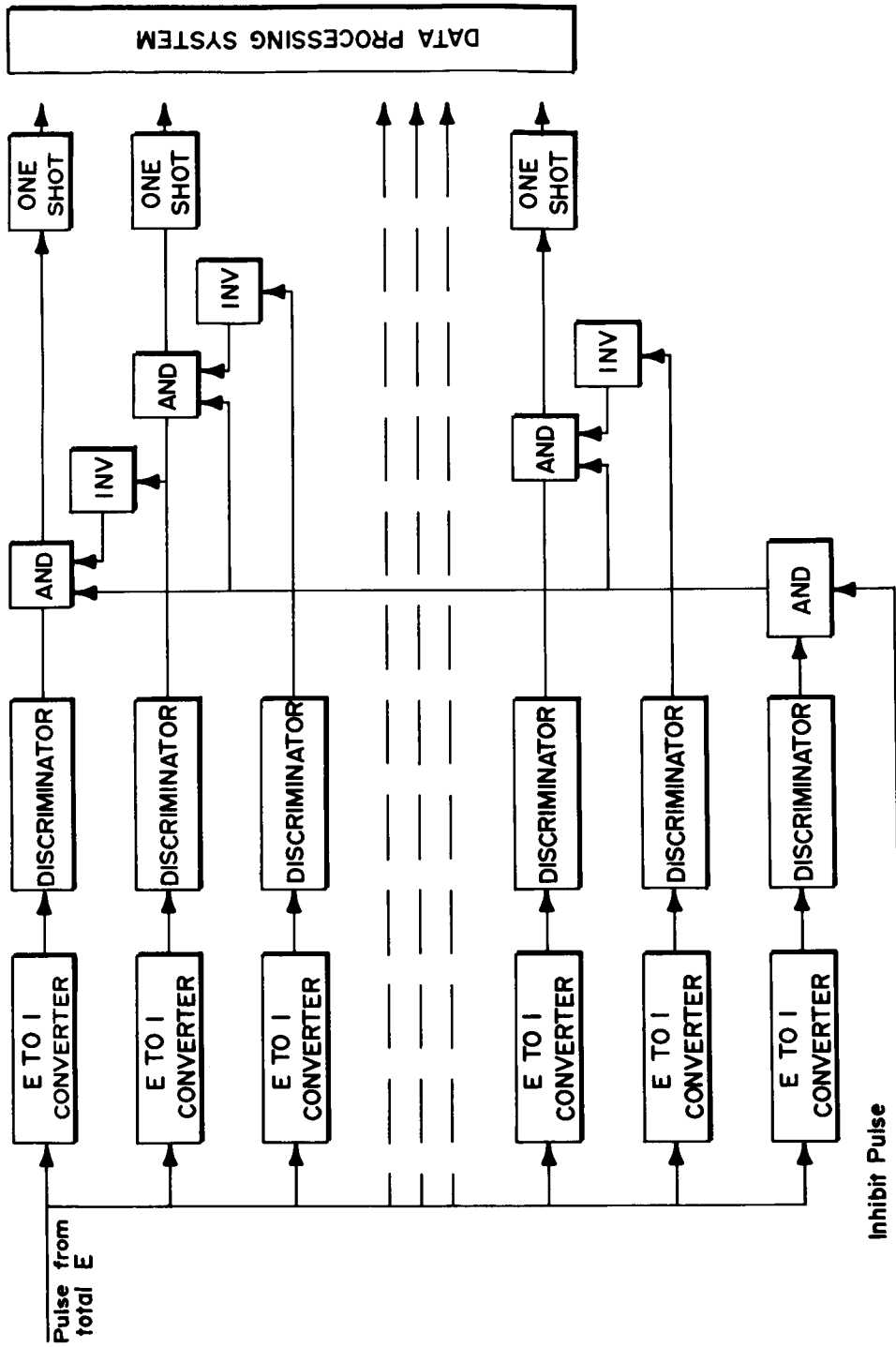


Figure 2-4. - Pulse height analyzer.

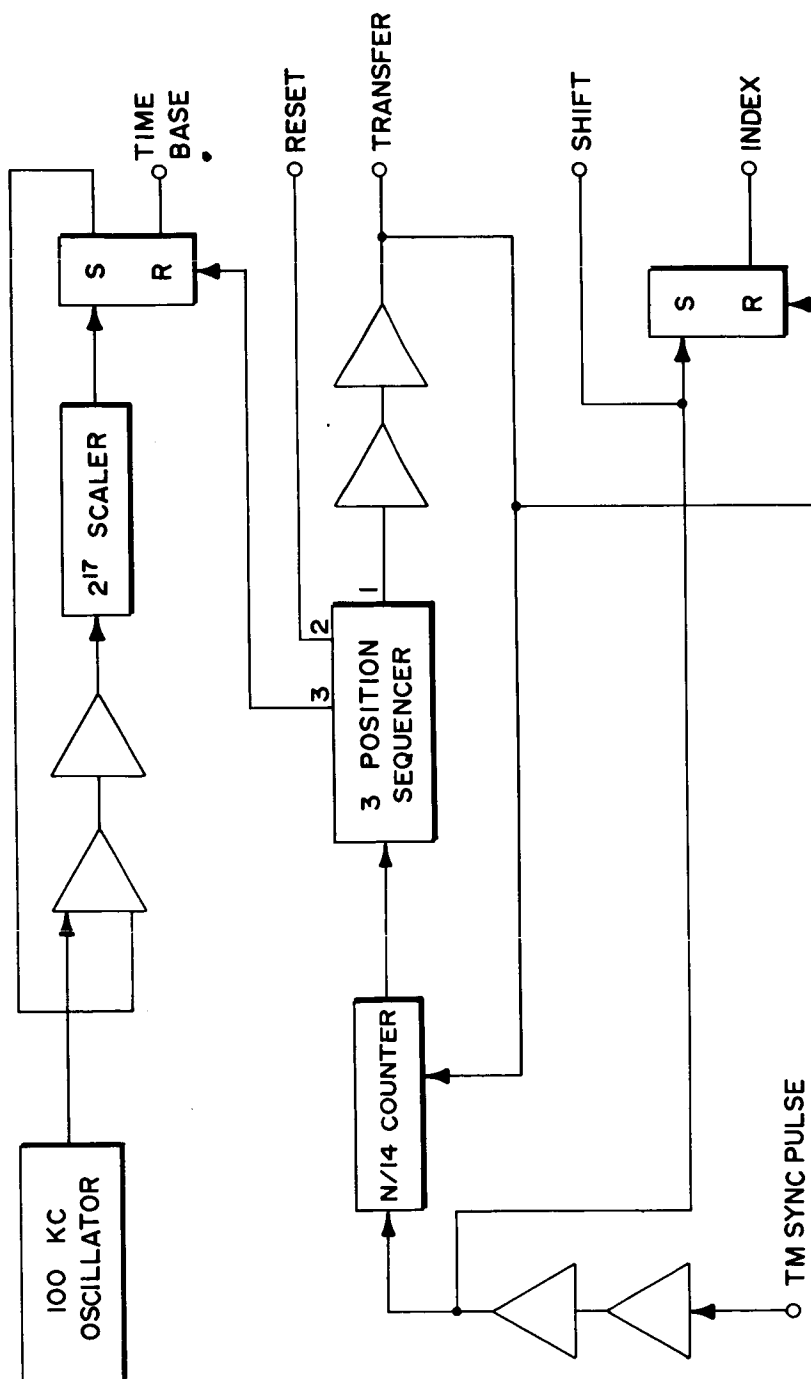


Figure 2-5.- Program control circuitry.

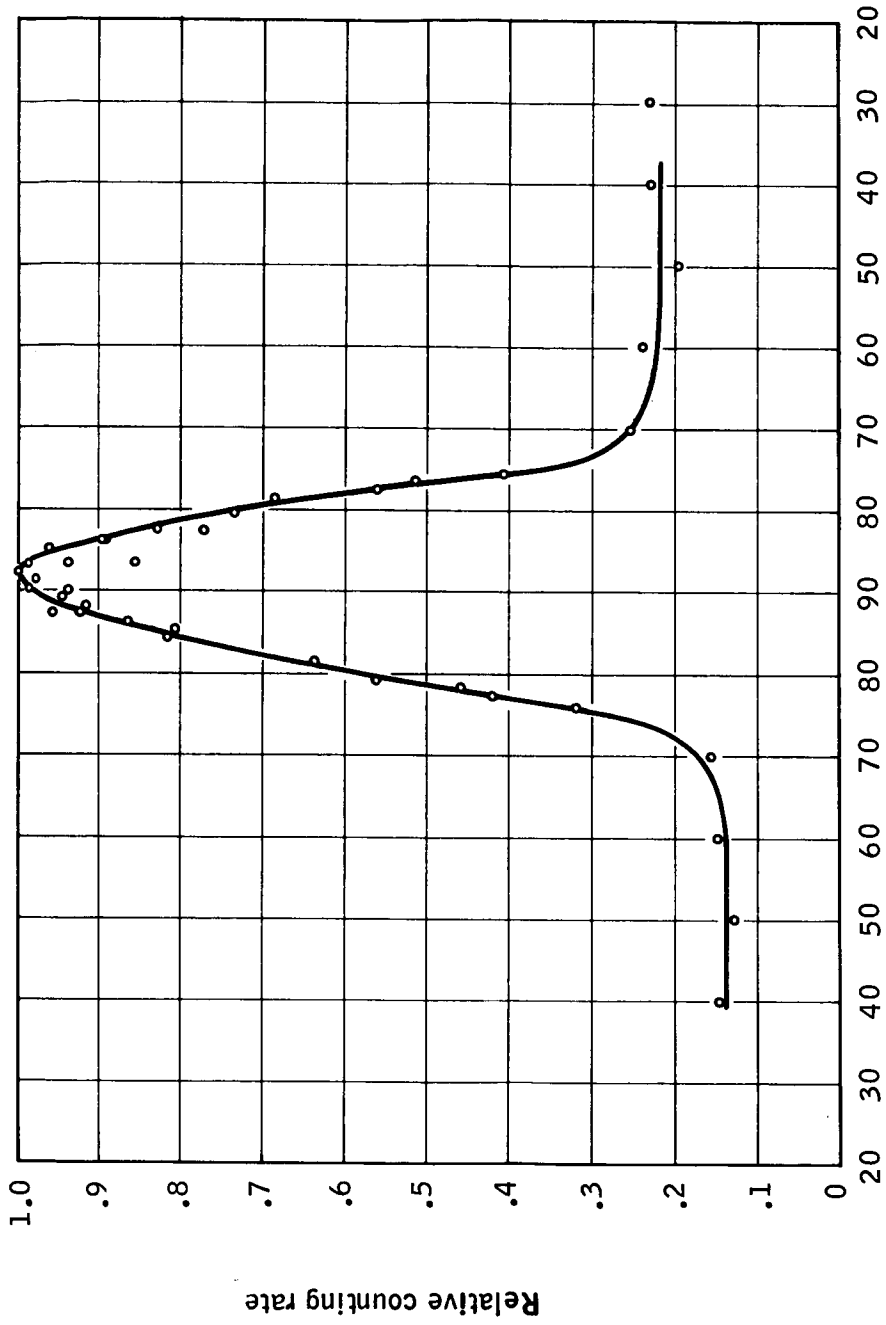


Figure 2-6. - Spectrometer view angle with magnetic field lines versus relative counting rate.

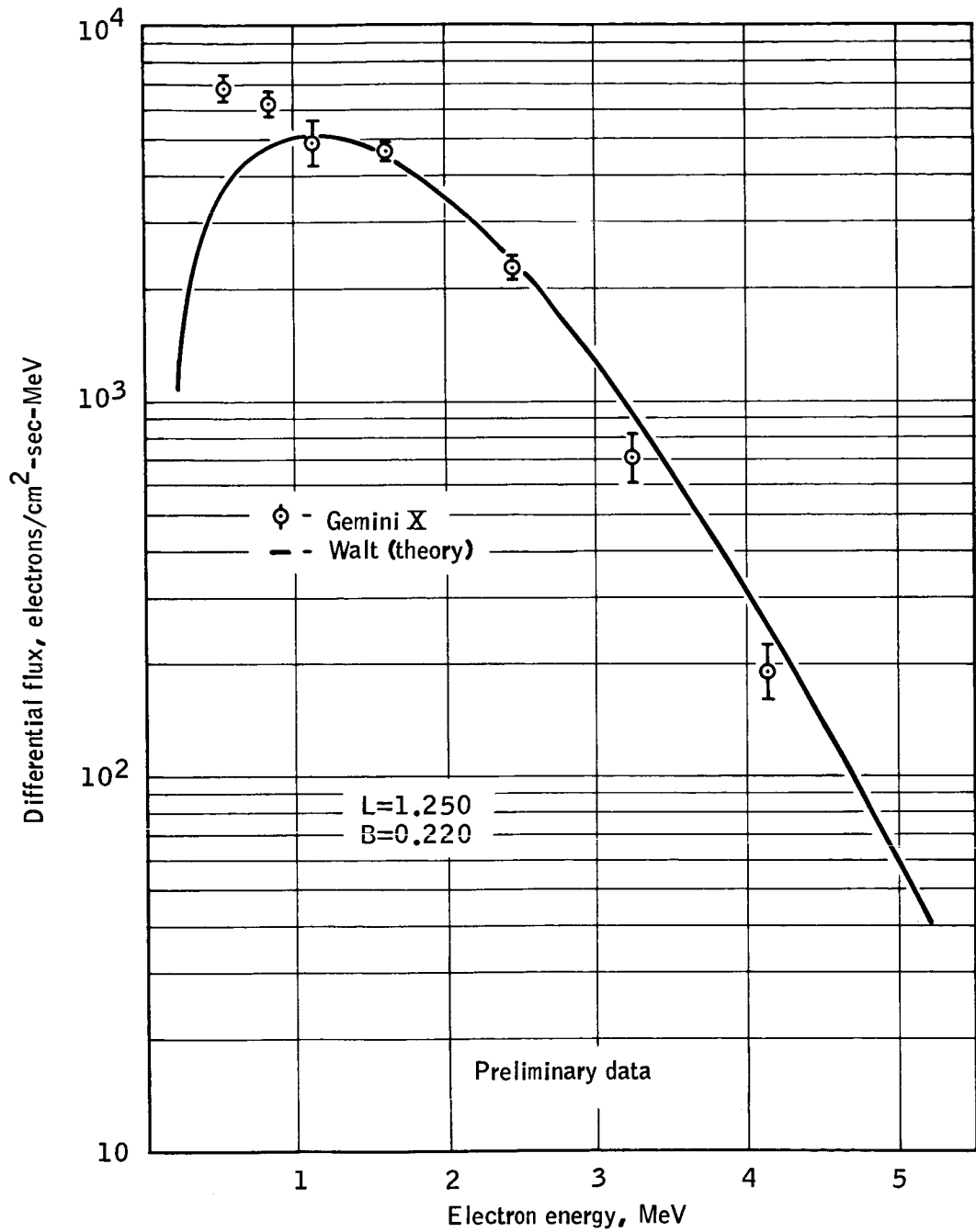


Figure 2-7. - Measured average electron spectrum.

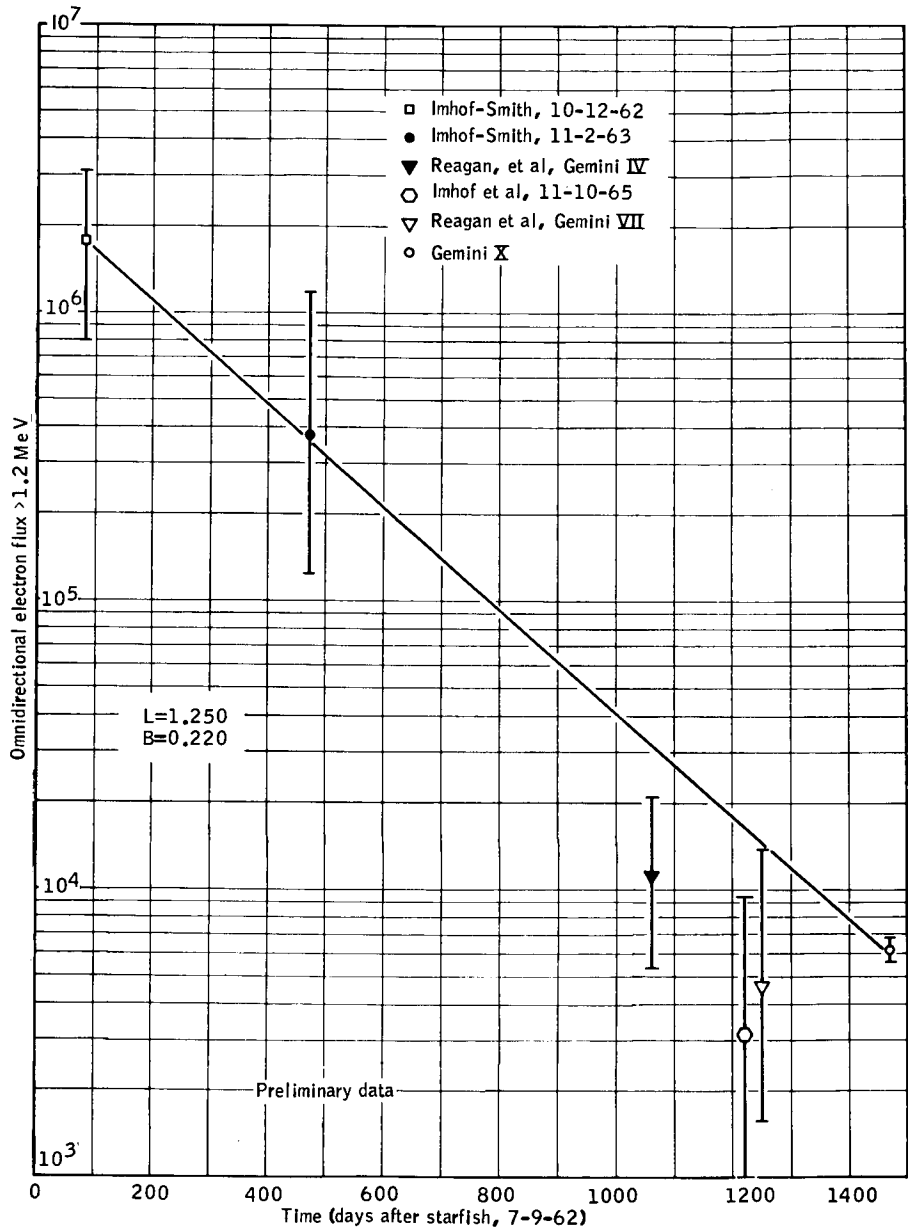


Figure 2-8. - Predicted decay of artificial electron belt based on Gemini X data.

Employing this output format the error due to compression is always positive and less than 5.9 percent so that the average error is approximately 3 percent.

Figure 3-3 shows the data processor circuit. The circuit is composed of 10 binary counters, a read matrix, a shift register, and control logic. Each of the 10 channels is sampled every 1 second. The decoder connects a particular binary counter with the shift register through the read matrix. The decoder is driven by a 10-per-second telemetry clock pulse. As soon as the information from the counter is shifted, it is free to accumulate again. This read time is about 30 microseconds. When the data have been transferred to the 13-bit shift register, a 50-kilocycle internal clock begins to shift the contents of the register to the right. This process continues until a significant digit appears at the 13th bit or seven shifts occur and stop. The number of shifts is recorded in the place counter. The last five bits of information in the shift register, which represent the five most significant bits of data, are then read out with the three bits of place information. The total is eight bits of information representing the contents of one channel. When the next 10-per-second clock pulse transfers the next information from the binary counter to the shift register, the cycle begins again. All 10 channels are read out in 1 second with the maximum dead time of 20 microseconds per channel.

PROCEDURE

The spectrometer, located behind the command pilot at about shoulder level, was controlled by an on/off switch through the experiment circuit breaker. It was turned on following orbit entry and turned off just prior to reentry, allowing data to be taken during the entire flight. No other operational procedures were required during the mission.

RESULTS

A few spectra were observed during post-pass telemetry dumps at the Hawaii ground station. These spectra indicated that the spectrometer functioned as expected. The computer data processing will consist of reconstruction of spectra as a function of spacecraft time and path. The reconstruction will involve decompressing transmitted numbers, adding sensor efficiency, dead time, and calibration factors, and correlating spacecraft attitude and position. The final results of the experiment will be determined after data from several complete revolutions are processed and analyzed.

where a is the area of a detector having diameter D . The bremsstrahlung production rate into this solid angle is

$$\frac{D^2}{16d^2} 4\pi d^2 \times 10^4 \text{ photons/sec} = 2.5\pi D^2 \times 10^3 \text{ photons/sec}$$

If the detector has a counting efficiency of 0.4, the count rate C is

$$C = \pi D^2 \times 10^3 \text{ photons/sec}$$

A 1-inch detector diameter would, therefore, produce a maximum count rate of

$$C = 2 \times 10^4 \text{ photons/sec}$$

The bremsstrahlung system block diagram is shown in figure 3-2. The basic sensor is a CsI(Tl) crystal surrounded by a plastic fluor of thickness necessary to give a usable pulse height output for electrons and protons in the anticipated energy regions. Photomultiplier-tube anode signals consist of two components: (1) a fast component due to charged particle interactions in the plastic fluor, and (2) a slow component representing energy deposition in the CsI(Tl) crystal. The fast component of the pulses is separated by means of a 10-nanosecond differentiator. If the fast component exceeds a threshold of approximately 100 keV, it will produce an output used to inhibit the analysis of the slow component of the pulse since such an output corresponds to a charged-particle event rather than a bremsstrahlung interaction in the CsI(Tl) crystal. To convert the tunnel-diode discriminators into a differential pulse-height analyzer, a strobe pulse is generated which serves to interrogate the tunnel-diode discriminators at a time just following the peak of the signal pulse. Suitable coincidence logic within the tunnel-diode discriminators produces an output pulse from the highest tunnel-diode discriminator. The pulses from the various channels of this differential pulse-height analyzer are accumulated in binary counters from the 10-cycles-per-second telemetry clock pulse. In order to accommodate the very wide dynamic range of count rate anticipated, a data compression system is employed. The compression system contains five bits of number information and three bits of place information. Since the five-bit number represents a binary number from 1 to 32, and the three-bit place information represents a multiplier from 1 to 2^8 , the largest number that can be transmitted is 2^{13} , or 8192, and the smallest number is 2^0 , or 1.

behind the command pilot's seat, about shoulder height. The telemetry complement consists of eight bilevel 10-per-second telemetry channels sampled in parallel, two 1.25-per-second analog channels, and one 10-per-second telemetry pulse synchronized with the bilevel word.

The bremsstrahlung spectrometer is designed to determine gamma flux and energy spectra with ± 5 -percent accuracy between 100 and 4000 keV. The data will be time-correlated with exterior electron measurements. Determination of bremsstrahlung fluxes with this accuracy is a considerable improvement over existing bremsstrahlung calculations. The flux of electrons with energies above 250 keV should be between 10^5 and 10^6 electrons/cm²/sec in the South Atlantic Magnetic Anomaly at an altitude of 300 kilometers.

The calculation of the anticipated bremsstrahlung count rate is, of course, crude due to lack of information concerning spacecraft shielding and orientation in the directional electron field. For purposes of obtaining a maximum count rate, the following assumptions are made:

- (a) The spacecraft is a uniform sphere of radius d .
- (b) The spacecraft is oriented such that approximately 100 percent of its area is producing bremsstrahlung photons.
- (c) The efficiency of the number of bremsstrahlung photons produced per electron per unit time is one percent.

The bremsstrahlung production rate R radiating into 4π steradians of solid angle will be the electron flux F times the spacecraft surface area A times the efficiency E , as follows:

$$R = F A E = 10^6 \times \pi d^2 \times 10^{-2} = 4\pi d^2 \times 10^4 \text{ photons/sec}$$

The solid angle subtended by a point on the spacecraft surface to the detector is

$$\frac{a}{A} = \frac{\pi D^2/4}{4\pi d^2} = \frac{D^2}{16d^2}$$

3. EXPERIMENT M409 (MSC-7), BREMSSTRAHLUNG SPECTROMETER

By Reed S. Lindsey
NASA Manned Spacecraft Center

N 6 8 - 1 4 1 5 3

SUMMARY

Preliminary analysis of data from the Gemini X mission indicates that the bremsstrahlung spectrometer functioned as planned. Bremsstrahlung relative countrate-time spectra are presented for revolutions 6, 20, 32, and 34. It will be possible to construct flux-energy spectra for comparison to theoretically predicted spectra to determine the validity of calculational techniques.

OBJECTIVE

The objective of the Bremsstrahlung Spectrometer (M409) experiment is to determine the bremsstrahlung flux-energy spectra inside the Gemini spacecraft while passing through the South Atlantic Magnetic Anomaly region. The spectra will be compared with computer-predicted bremsstrahlung spectra using data from the Beta Spectrometer (M408) experiment.

Secondary gamma rays produced in the Gemini spacecraft material by trapped electrons are not expected to reach biologically significant levels. On long-duration missions which may be flown in high trapped-electron flux environments, the problem attains considerably more importance. The calculations of bremsstrahlung radiation involve uncertainties due to the small amount of information available on cross-section interaction and the complex, heterogeneous makeup of the spacecraft. The bremsstrahlung detector was designed to give a time-differentiated measurement of the electron-induced gamma rays over a large section of the vehicle.

EQUIPMENT

The spectrometer (fig. 3-1) is of the standard phosphor-plastic design. It is a 10-channel spectrometer covering the energy range 0.1 MeV to 2.0 MeV. The spectrometer occupies less than 148 cubic inches, weighs less than 7.5 pounds and requires 2 watts at 28 volts dc. Location is

Although absolute bremsstrahlung flux-energy spectra resulting from the Gemini X mission have not as yet been deduced, some preliminary relative count-rate-time spectra are available. Figures 3-4 and 3-5 are relative count-time distributions for passages through the magnetic anomaly region on revolutions 20 and 32, respectively. The curve shape in figure 3-4 indicates that the spacecraft was changing altitude thereby modifying the bremsstrahlung flux at the location of the spectrometer. During the time figure 3-5 data were taken, no change in spacecraft altitude occurred resulting in a spectrum similar in shape to an electron flux-time spectrum for a similar traversal of the anomaly. Figures 3-6 and 3-7 are bremsstrahlung relative count-rate-time spectra for revolutions 6 and 34, and electron relative flux-time spectra for the same points as taken from the following publication: Models of the Trapped Radiation Environment, Volume I entitled "Inner Zone Proton and Electrons," by James I. Vette (NASA SP-3024, 1966). Unfortunately, no data were available from the Beta-Spectrometer Experiment M408 (MSC-6) for these passes. The figures show that it should be possible to draw a strong correlation between electron and bremsstrahlung fluxes to provide a means of monitoring bremsstrahlung calculational techniques. The rather strange behavior of the bremsstrahlung curve of figure 3-7 is not yet explained; however, one interesting fact is that the bremsstrahlung energy-flux spectral shape changed during the depressed portion of the curve. Detector efficiency corrections may result in a more regular shape.

It will be possible to construct bremsstrahlung flux-energy distributions for each traversal of the magnetic anomaly region and to complete the bremsstrahlung dose at the location of the detector for comparison to dose calculations resulting from theoretically produced bremsstrahlung spectra.

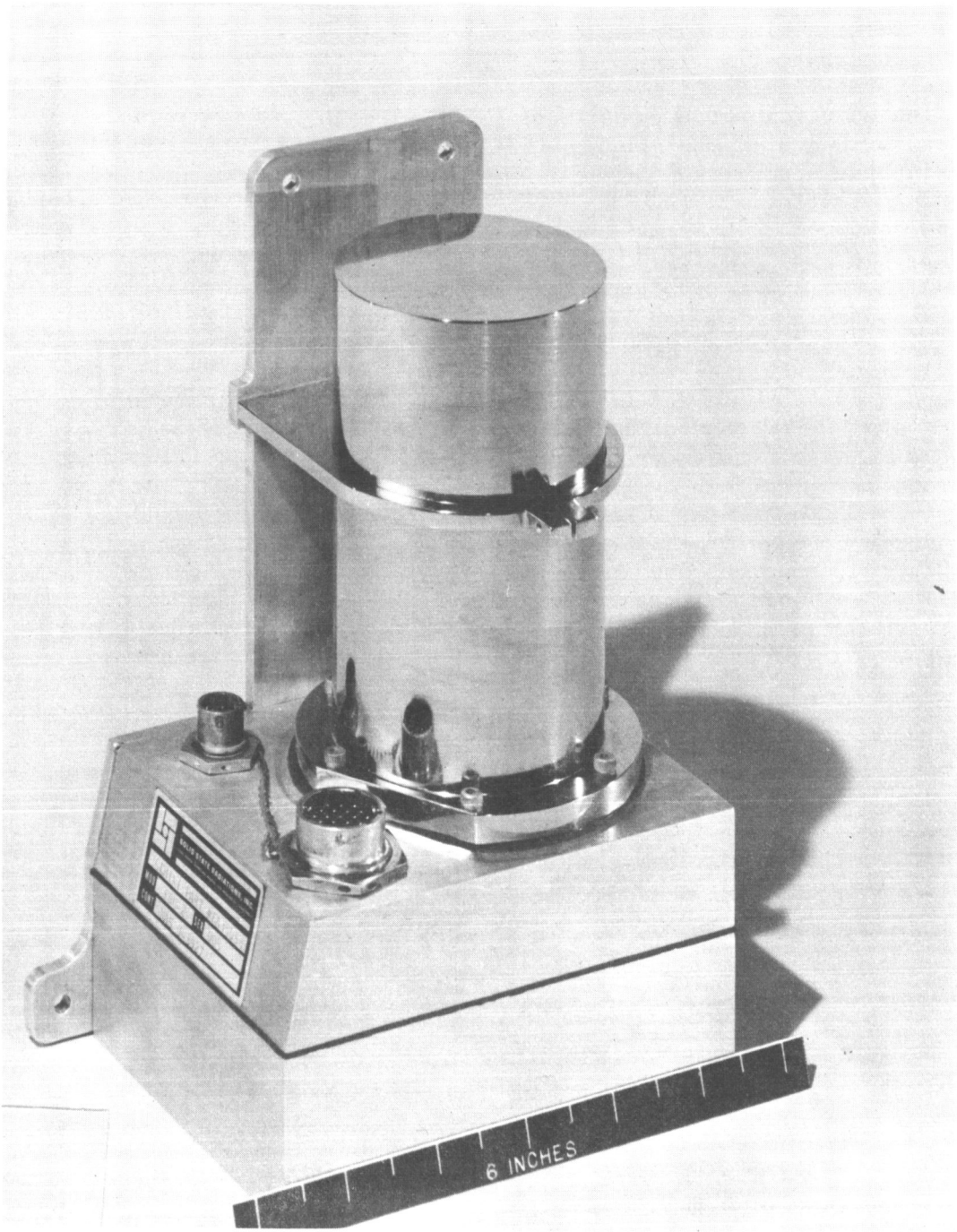


Figure 3-1. - Bremsstrahlung spectrometer.

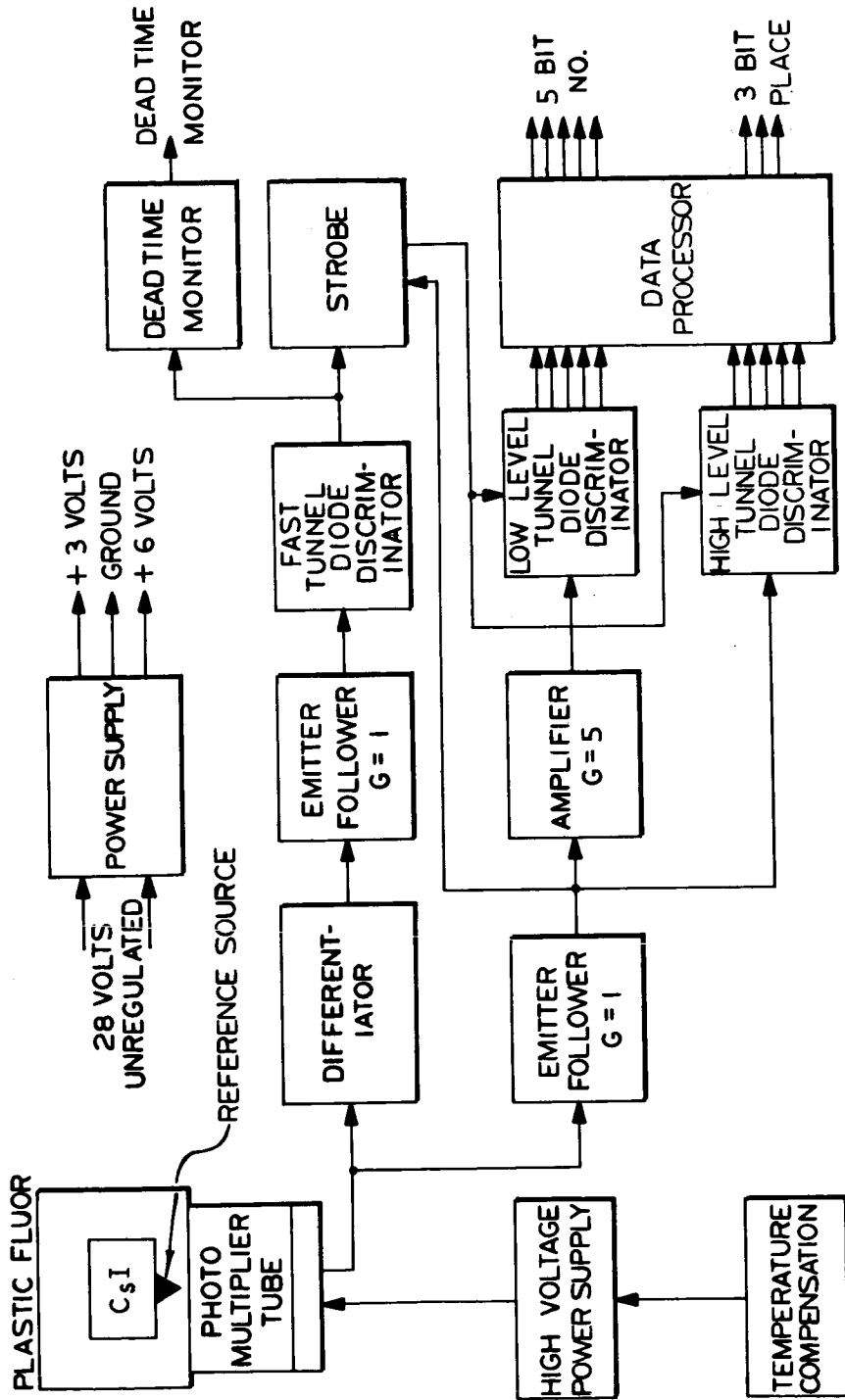


Figure 3-2. - Bremsstrahlung spectrometer block diagram.

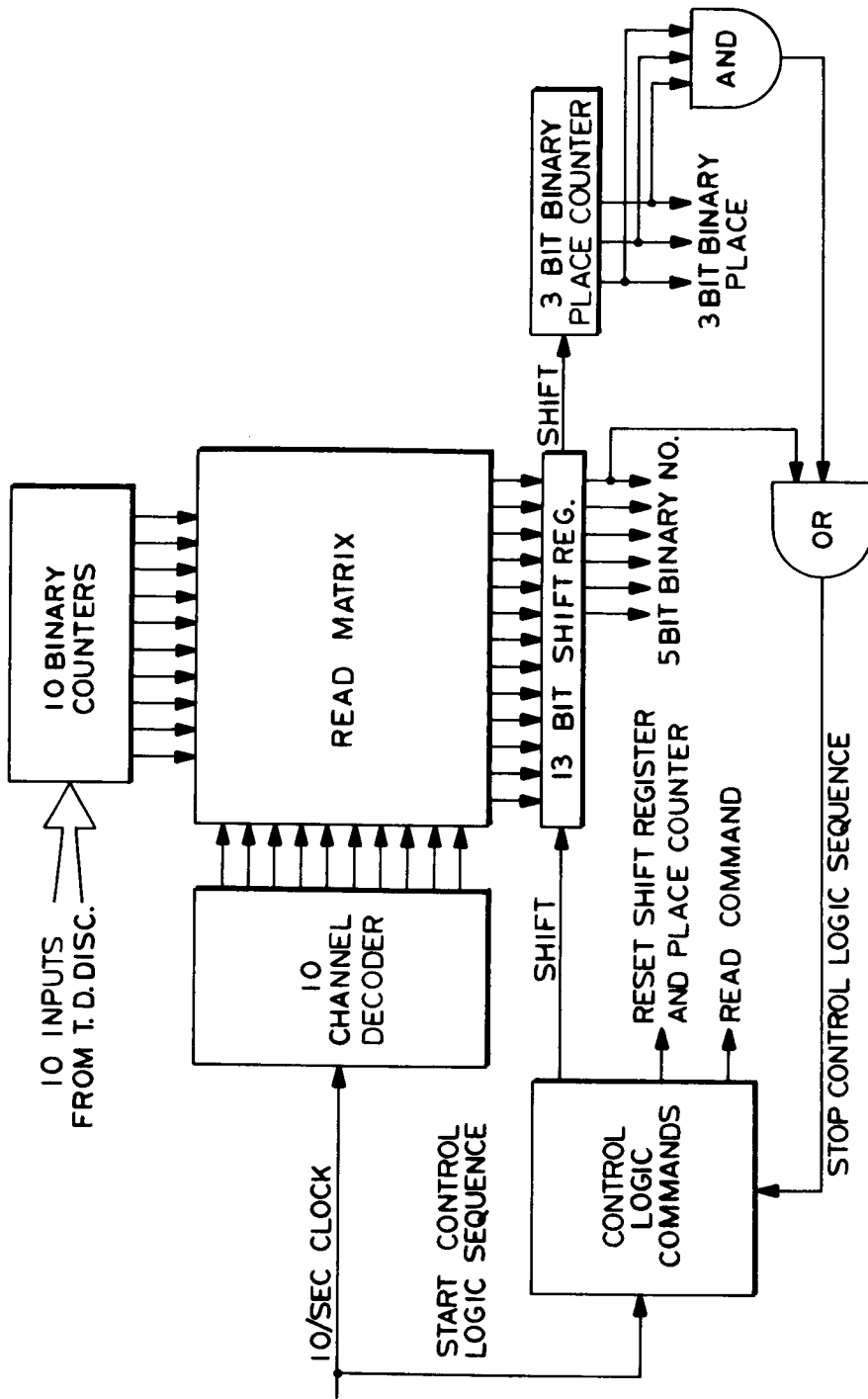


Figure 3-3. - Data processor circuit.

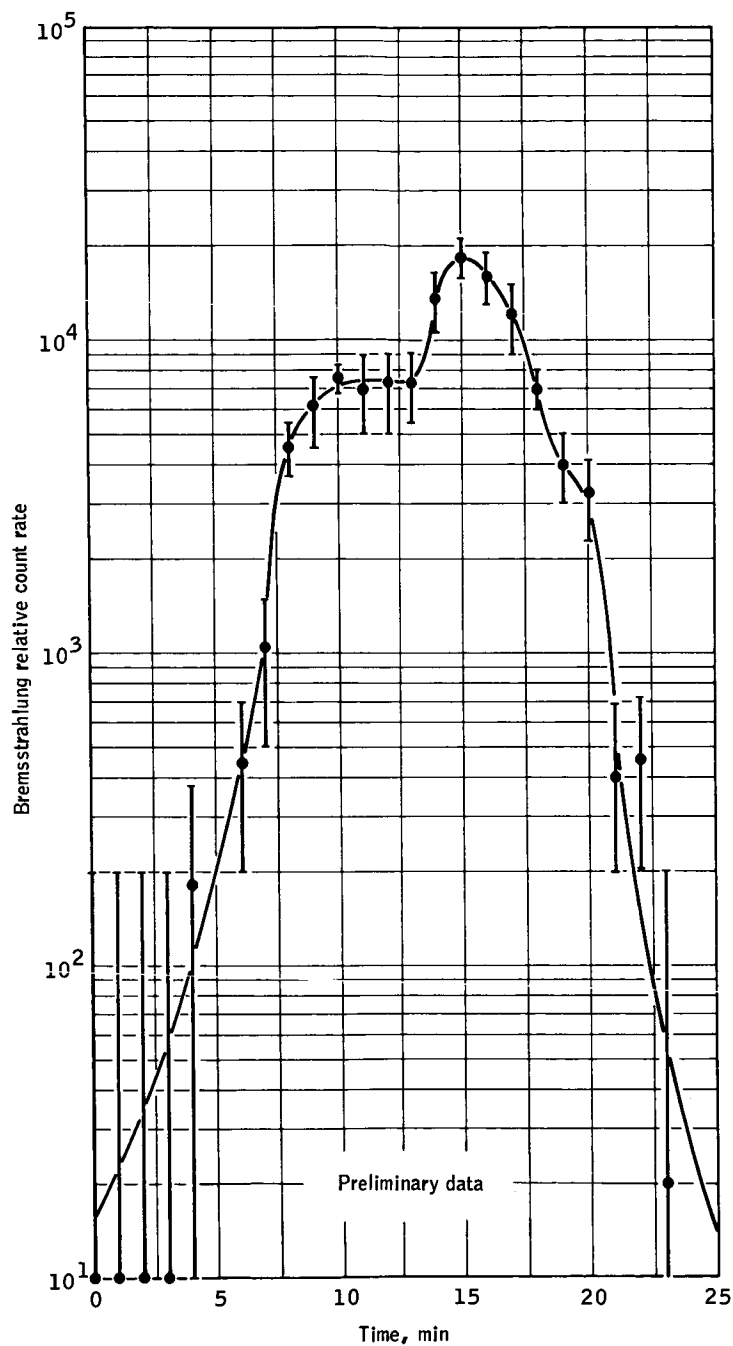


Figure 3-4. - Relative count-time distributions for revolution 20.

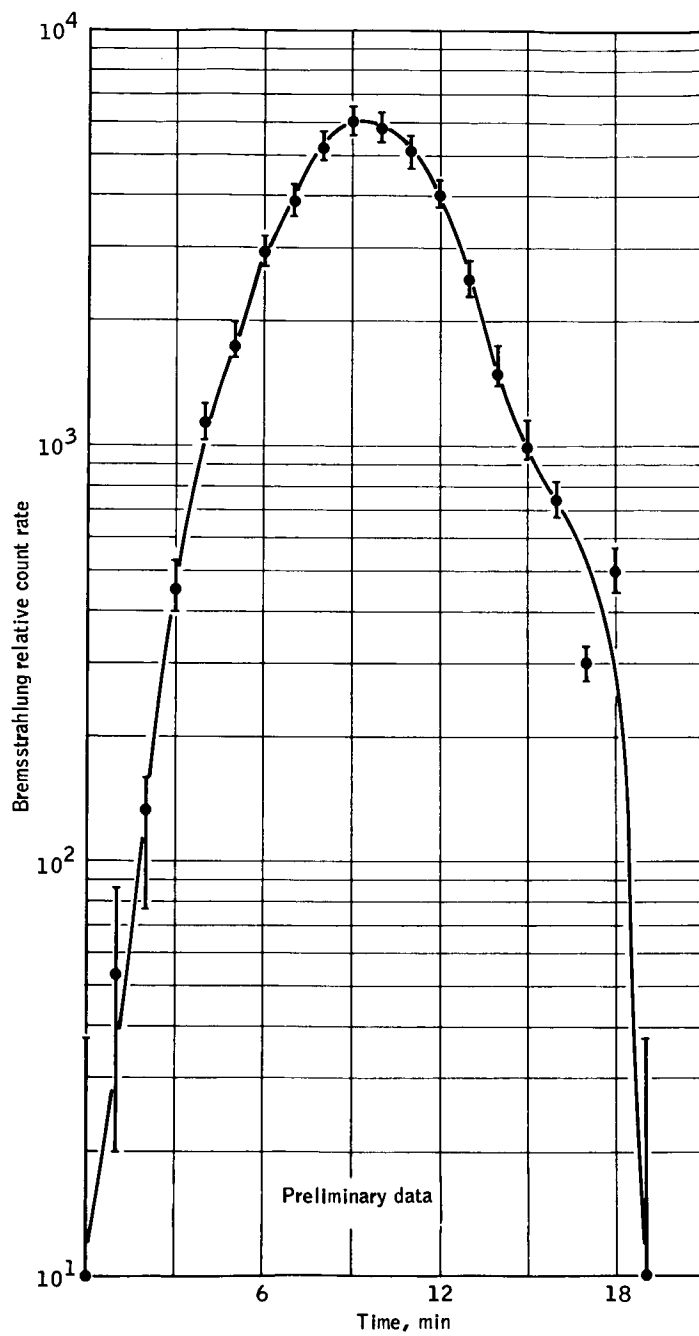


Figure 3-5. - Relative count-time distributions for revolution 32.

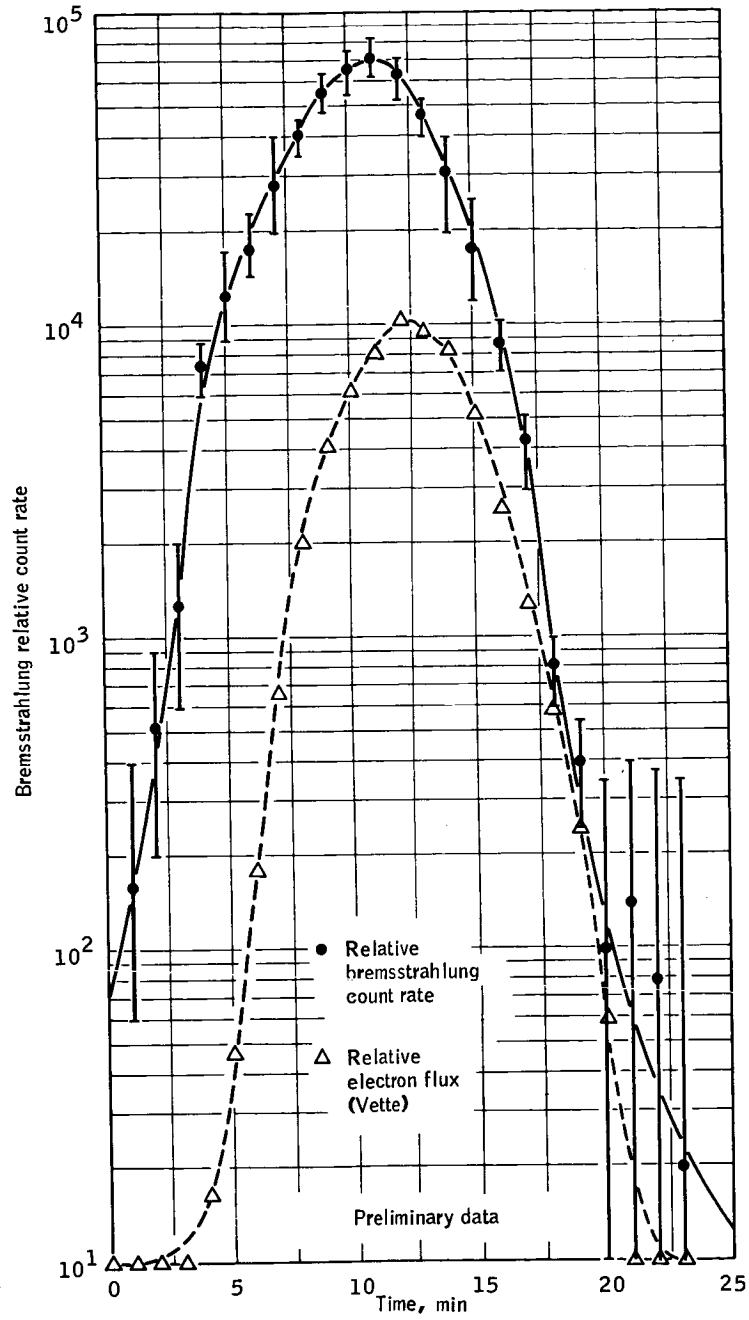


Figure 3-6. - Bremsstrahlung relative count-rate-time spectra for revolution 6.

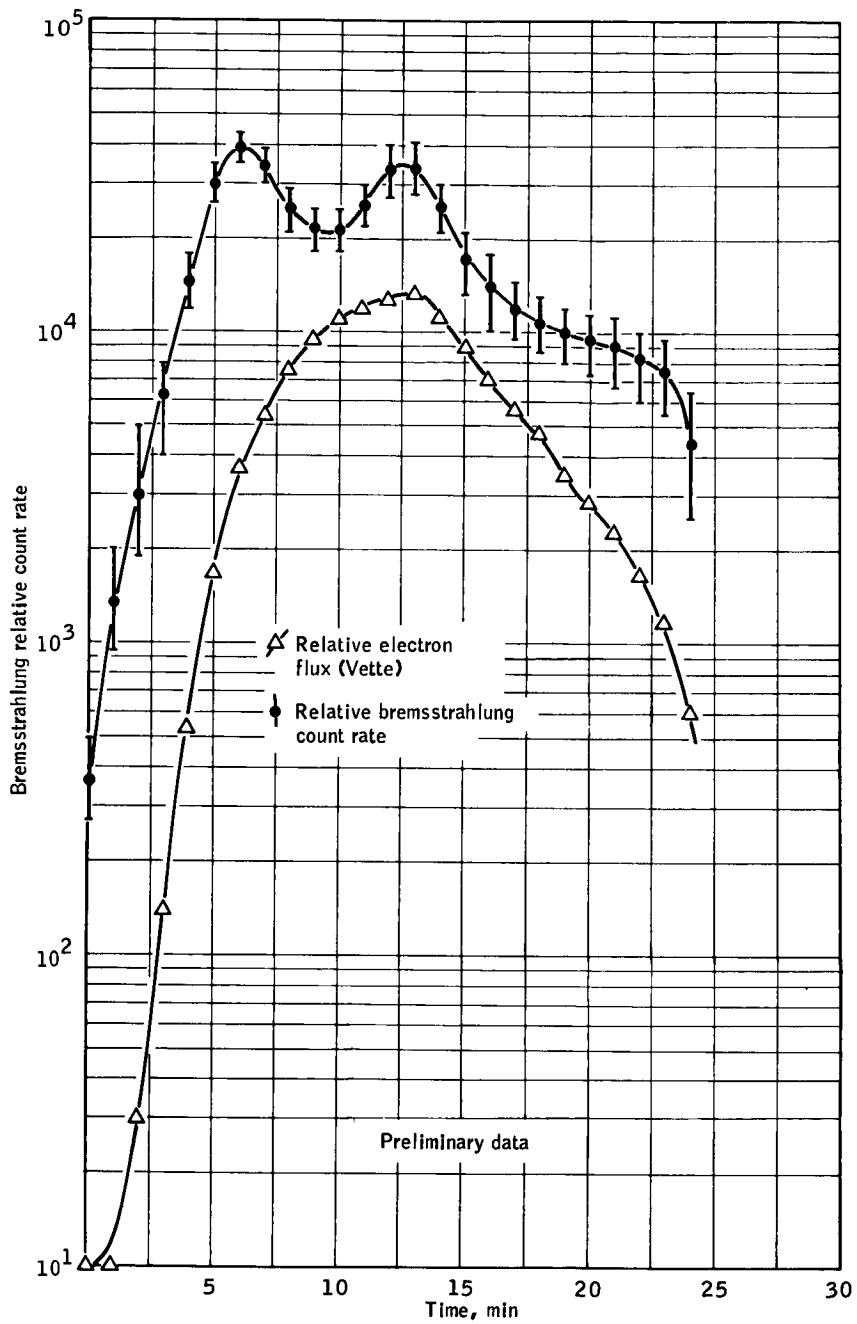


Figure 3-7.- Bremsstrahlung relative countrate-time spectra for revolution 34.

4. EXPERIMENT M410 (MSC-8), COLOR PATCH PHOTOGRAPHY

By John R. Brinkmann and Robert L. Jones
NASA Manned Spacecraft Center

SUMMARY

N 6 8 - 1 4 1 5 4

A slate supporting four calibrated color targets was photographed during Gemini X extravehicular activity (EVA) to determine if existing outdoor-type color films can accurately reproduce colored objects in the environment of space. The results indicate that color film can be used to obtain photographs in space with a high degree of color fidelity.

OBJECTIVE

In the Mercury and Gemini programs, the crew's interpretation of color rendition often did not agree with that shown in their flight films. Prior to the performance of the color patch experiment the reasons for the apparent color shifts were not understood. If Apollo photography, particularly that exposed on the lunar surface, is to be of scientific value, every effort must be made to insure true color fidelity in the resulting photography. Most geoscientific disciplines, such as photogeology, oceanography, the various agricultural sciences, hydrology, air and water pollution, meteorology, and many other possible applications, require a precise knowledge of the true color for interpretation of the results.

A preliminary analysis of the various factors which could cause the apparent false color rendition in space photography was conducted by personnel of the MSC Photographic Laboratory and Space Science Division. The results of the analysis indicated that the change could be due to the unattenuated solar spectrum for which the film may not be balanced. Normal outdoor color film is spectrally balanced for a combination of sunlight and blue skylight, which is not present in space. To determine if color film can accurately reproduce color when photographed in space-environment conditions, the color patch experiment was proposed for the Gemini Program.

EQUIPMENT

The experimental equipment shown in figure 4-1 consisted of a color patch slate, a 3-ft extension rod, and a 70-mm camera. The color patch slate, manufactured by the Erie Ceramic Company, was an 8 by 8 by 1/16-inch titanium plate, supporting four-color targets composed of a ceramic material in a matte finish. The four colors were National Bureau of Standards primary colors (red, blue, and yellow) and neutral gray.

To simplify the experiment, a 3-ft rod of four sections of 1/2-inch-diameter aluminum, 9-inches long, was provided to hold the color patch at a predesignated distance of 36 inches from the camera. The camera and color patch were attached to the rod by a dovetail fitting.

A 70-mm Maurer space camera, fitted with an f/2.8, 80-mm Xenotar lens was used. The camera was selected for its superior optical qualities suitable for a photographic experiment of this type. To reduce the effect of ultraviolet energy on the film, a 0-52 Corning glass filter with a cutoff at 3500 Å was used.

The camera used 70-mm film with a 2.5-mil base. This film had excellent color-reproducing qualities and had been used on previous Mercury and Gemini flights. Except for 2.5-mil base, the film is identical to Ektachrome MS commercial Kodak film.

PROCEDURE

Prior to the Gemini X mission, the flight color patch was photographed under controlled lighting conditions at Kennedy Space Center, utilizing the flight camera and film. A series of six exposures were made at 1/250 sec at f/8, 1/250 sec at f/11, and 1/250 sec at f/16. The purpose was to obtain photographs which could be compared to similar postflight photographs taken under the same controlled setup. This would determine if the film had undergone any changes during the mission.

During the flight the crew were to assemble the experiment and the pilot was to photograph the color patch nine times while standing in the spacecraft seat (fig. 4-2) and return the color patch slate to the spacecraft for postflight calibration and analysis. The exposures were to be made in groups of three, beginning with 1/250 sec at f/8, followed

by 1/250 sec at f/16, and ending with 1/250 sec at f/11. The solar illumination angle was to be within 30° of the patch nominal.

RESULTS

Due to unexpected trouble in the spacecraft environmental control system (ECS), the standup EVA was terminated prior to completion of the experiment. To facilitate spacecraft ingress, the color patch and rod were discarded. Before the ECS trouble, the crew obtained four color patch photographs at an exposure of 1/250 sec at f/8. The remaining film in the magazine was used to photograph the earth weather and terrain patterns.

Although the experiment was not fully completed, the pictures provided enough data from which certain conclusions can be drawn.

The results of a subjective comparison of the flight film and the backup color patch, which was identical to the flight hardware, confirm the suitability of existing film to record true colors in space.

Density measurements that were made from the gray section of the flight film exposures showed a difference of 10 percent between the first and third exposures, and a difference of 17 percent between the lightest of the two and the second exposure which is most dense. The density difference can either be attributed to variances in the shutter mechanism, slight changes in the incident illumination angle, or a combination of both.

Saturation of the four colors on the first and third exposures are almost identical, while the colors on the second exposure are richer because they more nearly approach the nominal exposures of 1/250 sec at f/11.

CONCLUSION

The experiment provided sufficient information to confirm that objects can be photographed in space with a high degree of color fidelity using existing materials. It can be generally stated that available color film is balanced to the solar spectrum in space, and the effect of ultraviolet energy appears to be negligible to film degradation.

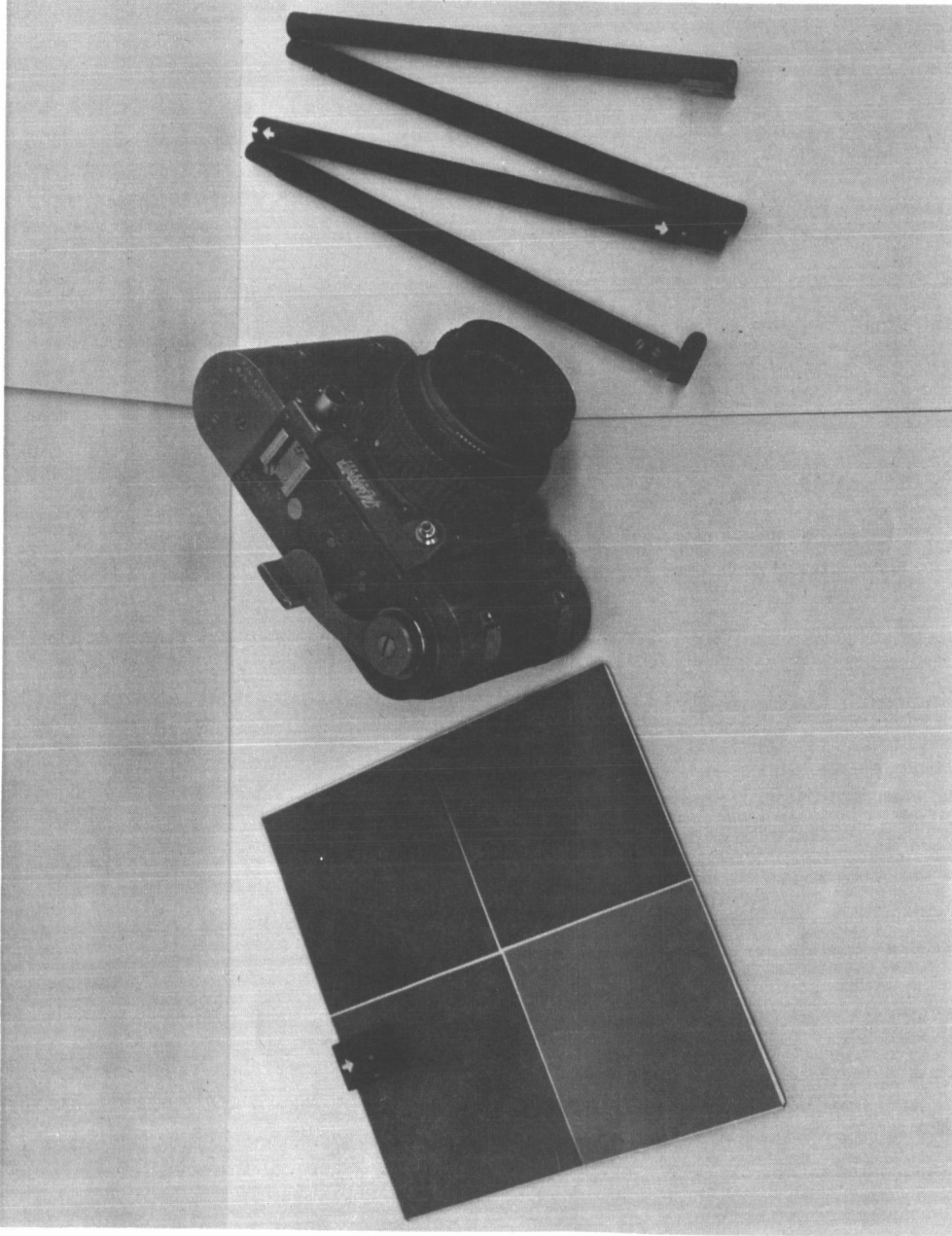
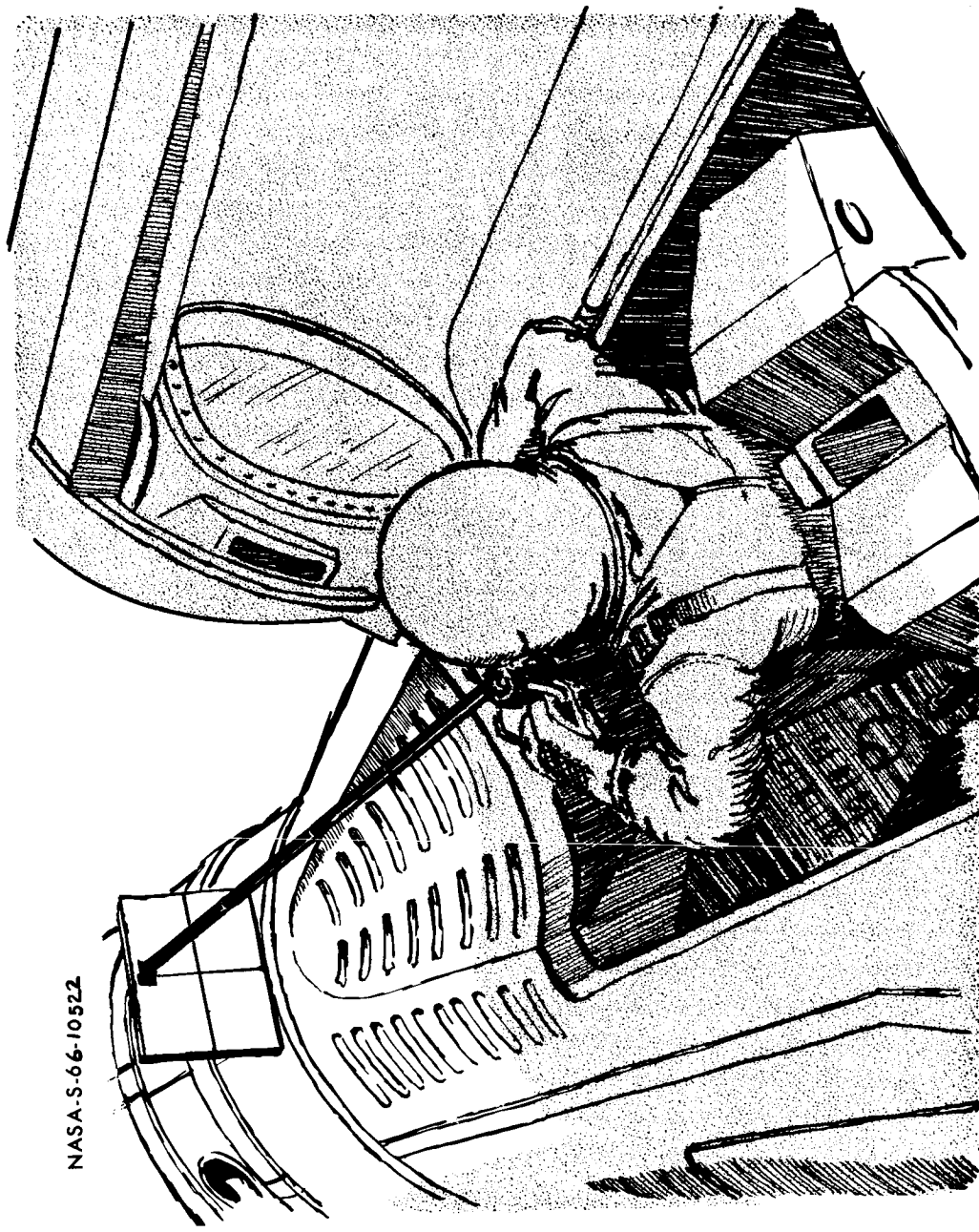


Figure 4-1.1. - Color patch photography experiment equipment.



NASA-S-66-10522

Figure 4-2. - Method of photography by spacecraft pilot.

5. EXPERIMENT M412 (MSC-12), LANDMARK CONTRAST MEASUREMENTS

By Charles E. Manry
NASA Manned Spacecraft Center

OBJECTIVE

N 6 8 - 1 4 1 5 5

The objective of the landmark contrast measurements experiment was to measure the visual contrast of landmarks against their surroundings to determine the relative visibility of terrestrial landmarks from outside the atmosphere. These landmarks would provide a source of navigational data for Apollo onboard guidance and navigation systems.

DESCRIPTION

The ability to perceive, identify, and align on landmarks is closely related to their luminance and contrast with the surrounding areas. The visual contrast of a terrestrial feature against its surroundings is reduced according to the amount of atmosphere between the feature and the eye of the observer. Therefore, the visual contrast of ground targets, as seen from outside the atmosphere, will be considerably reduced from that of the targets observed at close range.

The measured parameter required during the mission was the visual contrast of landmarks, where contrast is defined as

$$\text{Contrast} = \frac{\text{Luminance of landmark} - \text{Luminance of surroundings}}{\text{Luminance of surroundings}}$$

This value can be positive or negative. The measured contrast of a light-colored landmass viewed against a darker ocean might be more than 10. The contrast of a dark object viewed against lighter colored surroundings, however, can never exceed unity.

Visual contrast, as defined, is a useful criterion for target visibility because of the constancy of threshold values through several orders of magnitude of luminance levels. Because contrast is a ratio, the measurement is independent of long-term photometric equipment gain stability, a predominant source of error in those devices that use photomultiplier sensors. The effect of scattered light entering a photometer is also lessened because of the measured ratio.

EQUIPMENT

This experiment required the use of the photometer provided for Experiment D005 (D-5), with the addition of two optical filters which fit over the photometer lens. The instrument consisted of an objective lens which received landmark-reflected sunlight radiation and optically transferred it to a field stop and then to a photomultiplier sensor. The amplified output from the photomultiplier was sampled 10 times per second, and the resulting signal was recorded onboard the spacecraft by means of the standard Gemini telemetry system.

The linearity of the photomultiplier and its associated circuitry was typically better than 1 percent of full scale. The dynamic range of the instrument was designed to cover the expected luminance range of sunlit terrain as follows:

Maximum landmark	
luminance	2.4 candles/cm ² (7000 foot-lamberts)
Minimum landmark	
luminance	0.02 candles/cm ² (58 foot-lamberts)

The signal-to-noise ratio of the photometer was estimated to be in excess of 800:1 for the minimum landmark luminance using the sample rate of 10 per second.

The probable error of measurement was expected to be near 3 percent after adjustment for near-maximum signal level. Error due to scattered light in the photometer during an observation could not be assessed accurately, except that it would tend to reduce measured contrast.

Landmark contrast data for use in guidance and navigation design in Project Apollo have been calculated by extrapolation of airborne spectro-photometric measurements of photographs taken during Gemini and other orbital missions. A comparison of these data with direct measurements obtained in this experiment was expected to verify correctness of calculated contrasts as well as reduce the present uncertainty of landmark contrast variance with change-of-sun-aspect angle.

PROCEDURES

The photometer was to be handheld, and aimed through the right-hand window as it was for the Star Occultation Navigation D005 (D-5) experiment. Several minutes before the appearance of the target landmark, the observer was to turn on the photometer power source. The spacecraft was to be turned so that the photometer could be pointed at the landmark. The spacecraft was to be positioned so that the sun was behind the observer, thus shading the spacecraft window from direct sunlight.

It was anticipated that the landmark would be recognizable at about 60° from the nadir. This would have allowed the observer time to aim the photometer and adjust the instrument gain so that target area luminance would provide a strong signal level to the telemetry system. As the command pilot tracked the landmark, the pilot alternately directed the photometer at the land and water sides of the landmark. About 8 to 12 samples of each side were expected during each pass over a landmark.

The pilot was to have verbally described the landmark, cloud cover, weather, sun aspect, and filter used. If available, operational camera film was to be used to photograph a few landmarks to assist data validation.

RESULTS

This experiment was not performed by the flight crew because of fuel-usage constraints and time limitations. The experiment was attempted on a previous Gemini mission; but, because of equipment failure, no results were obtained. This experiment is not scheduled for either remaining Gemini mission. Consequently, there are no results or conclusions obtainable from the two attempts to perform this experiment.

6. EXPERIMENT S001 (S-1), ZODIACAL LIGHT PHOTOGRAPHY

By E. P. Ney, Ph. D. and W. F. Huch, Ph. D.
University of Minnesota

OBJECTIVE

N 6 8 - 1 4 1 5 6

The purpose of the zodiacal light photography S001 (S-1) experiment was to obtain exposures of several subjects of astronomical interest using a lens setting of f/1 and a speed of 30 seconds. These subjects included the airglow (viewed in profile from above), the zodiacal light, and the Milky Way.

EQUIPMENT

The camera was designed to view a wide-angle field of approximately 50° by 130° . Mechanically, it was the same kind of camera as that flown on the Gemini V, Gemini VIII, and Gemini IX-A missions. The exposure sequence was automatic and alternated 30-second exposures with 10-second off periods. During these off periods, thrusters could be fired for attitude-hold without exposing the film. The film used was 35-mm, high-speed, black and white.

PROCEDURES

The flight plan required that the camera be handheld on night passes, with the pilot taking photographs through his window. The pilot held the camera against the window during the exposure periods, sighting past the camera and directing the command pilot to maneuver to appropriate positions. Astronomical objects were not in the command pilot's field of view, and his role was to null the spacecraft rates. The planned procedure required that photographs be taken with the following camera orientations:

- (1) Horizontal toward the west
- (2) Alined along the Milky Way to include the southwest horizon
- (3) Alined along the Milky Way in the zenith

- (4) Alined along the Milky Way to include the northeast horizon
- (5) Horizontal toward the northeast
- (6) Horizontal toward the east
- (7) Horizontal toward the south

RESULTS

The 20 photographs obtained are listed in table 6-I. The spacecraft attitude held by the crew during the exposures was very adequate; however, a combination of the following three factors make the pictures obtained difficult to use quantitatively:

- (1) The film was only one-half as sensitive as the film used during the Gemini IX-A mission.
- (2) Observations of the same star field in various exposures show that light transmission through the dirty spacecraft window varied by a factor of at least six.
- (3) The earth horizon was not seen in all the pictures.

CONCLUSIONS

The results obtained from these pictures will be of qualitative or geometrical value only. For example, the airglow heights are measurable in two pictures showing the earth horizon. One picture confirms the existence of a higher airglow layer at 200 to 300 kilometers. This layer was also seen in the Gemini IX-A photography. One picture shows the presence of wisps extending upward from the lower airglow layer. These wisps had been seen for the first time in the Gemini IX-A S001 (S-1) experiment photographs. Complete analysis and interpretation will continue for several more months.

TABLE 6-I.- PHOTOGRAPHS TAKEN DURING EXPERIMENT S001 (S-1)

Exposure number	Camera orientation	Object
1, 2, 3	Horizontal toward the west	--
4	--	Spacecraft thruster plumes
5, 6	Along the Milky Way	α and β Centaurus centered in the field of view
7, 8, 9	Along the Milky Way	Galactic center in the upper right
10, 11, 12	Along the Milky Way	Northeastern sectors
13, 14	Along the Milky Way	From stars Vega to Cassiopeia
15, 16, 17, 18, 19, 20	Horizontal toward the east	Orion's star field centered

7. EXPERIMENT S005 (S-5), SYNOPTIC TERRAIN PHOTOGRAPHY

By Paul D. Lowman, Jr., Ph. D., and Herbert A. Tiedemann
NASA Goddard Space Flight Center

SUMMARY

{ Approximately 75 pictures useful for the purposes of the synoptic terrain photography experiment S005 (S-5) were taken on the Gemini X flight. Areas covered include North Africa, parts of South America, China, Formosa, and various oceanic areas. Despite various operational difficulties, the experiment can be considered successful. Specific applications of the pictures obtained are apparent in geology, geography, and oceanography. }

OBJECTIVE

The objective of experiment S005 (S-5) on the Gemini X mission was essentially the same as on previous missions: to obtain high-quality color photographs of selected areas for geologic, geographic, and oceanographic study. The last two categories represent the expansion of scope of experiment S005 (S-5) to nongeological areas which began with the Gemini VII flight. Strip photography, with overlapping coverage, was requested for the following areas (in order of priority): Red Sea-Arabian Peninsula, central and southern Mexico, West Pakistan, North Africa (Anti-Atlas, Hoggar, and Tibesti Mountains), and northwestern South America and adjacent coastal waters. Individual photographs or pairs of photographs were requested for the following areas: Mississippi River mouth, Ganges River mouth, Bahama Islands and adjacent shelf, Philippine Islands, and the Mekong delta.

EQUIPMENT

Two cameras were used: the 70-mm Maurer space camera, with Xenotar f/2.8 lens (80-mm focal length), and the 70-mm Hasselblad super side-angle camera, with Zeiss Biogon f/45 lens (38-mm focal length). Haze filters were used. Film used in both cameras was Eastman Ektachrome MS (SO 217), with a 55- by 55-mm format. The medium-speed color-reversal film is on a 2.5-mil polyester base.

PROCEDURE

The requested procedure was to take, subject to operational restrictions, vertically oriented photographs of the areas previously listed. For strip photography, 5-second intervals between pictures were requested. For individual photographs or pairs of photographs, the same time interval was suggested but the actual interval used was left to the crew's judgment. Photography of relatively cloud-free areas was stressed. It was stressed to the crew that good pictures of any land area would be of value if the experiment plan could not be carried out precisely.

RESULTS

Approximately 75 pictures of use for the S005 (S-5) experiment were taken, most of which are of good quality although cloud cover was extensive over several areas. Window obscuration apparently affected some pictures. Areas covered include northwestern South America, northwestern and north-central Africa, the Formosa Straits, and numerous islands in the Indian and Pacific Oceans. Detailed evaluation of the photographs is in progress; however, typical pictures will be discussed briefly.

Figures 7-1 and 7-2 were taken as the spacecraft approached Africa; the view is to the northeast over the Spanish Sahara and Morocco. Although they are obliques, these photographs are of considerable value. They will be useful for precisely locating other, more nearly vertical photographs taken of the same area, a task which has been difficult in some cases. Geologically, they are potentially useful because of the extremely large area covered. The broad plateau at the left in figure 7-2 is the Hamada du Dra, which overlies the Tindouf Basin, a large synclinal structure. The pronounced curvature to the south is of interest in relation to continental drift, in that it demonstrates that not all pre-Mesozoic structures are truncated by the continental margins, as might be implied by some maps such as those presented by Holmes (ref. 1).

Figure 7-3 was taken over Niger looking to the southwest. The Air Mountains, previously photographed on Gemini missions (ref. 2), are visible on the horizon. Visible in the foreground are poorly understood arcuate or linear features which evidently consist of fractures and dune chains. These were first photographed on the Gemini IV mission east of the Tibesti Mountains. It is hoped that synoptic photography of this sort will throw light on their origin.

Figure 7-4, which was taken over the Rio Grande delta, shows the Gulf coast of Texas and Mexico from Baffin Bay almost to Laguna del Barril.

Despite the window obscuration, considerable terrain detail is visible. Of particular interest are the features of Laguna Madre, the prominent coastal lagoon at center, and Padre Island and the barrier island bounding it. Numerous units can be distinguished in the lagoon which presumably reflect sedimentation. The effects of man-made structures, such as the Intracoastal Waterway, on normal sedimentation can be seen in the photograph. This area has been the subject of extensive study (ref. 3) in connection with sedimentation.

Figure 7-5 is a nearly vertical view of the coast of China in Fukien Province. It is of interest because of the considerable detail in the bottom topography in coastal areas. Although not a primary area for the experiment, the picture further suggests the oceanographic value, first indicated on the Gemini IV pictures, of such photography.

Figure 7-6 shows the southern end of Formosa. In addition to the detail visible in land areas, most of which reflects vegetation and cultivation, considerable structure is apparent in the glitter pattern at the southern tip of the island. Possible elements in this structure include internal waves, slicks, near-surface ocean currents, and currents of fresh water from the numerous rivers.

Figure 7-7 shows several atolls in the Maldive Islands, with the view to the southwest over the Indian Ocean. This picture, although not taken at the optimum angle, suggests the value of orbital photography in correcting map positions of widely separated ocean islands.

REFERENCES

1. Holmes, A.: Principles of Physical Geology. Ronald Press (London), 1965.
2. Lowman, P. D.: Synoptic terrain photography (Experiment S-5) during Gemini 6 and Gemini 7, in Gemini Midprogram Conference. NASA SP-121, 1966.
3. Shepard, F. P., Phleger, F. B., and van Andel, T. H.: Recent Sediments, Northwest Gulf of Mexico. Am. Assoc. Petroleum Geologists, Tulsa, Oklahoma, 1960.



Figure 7-1. - View to the northeast over the Spanish Sahara and Morocco.

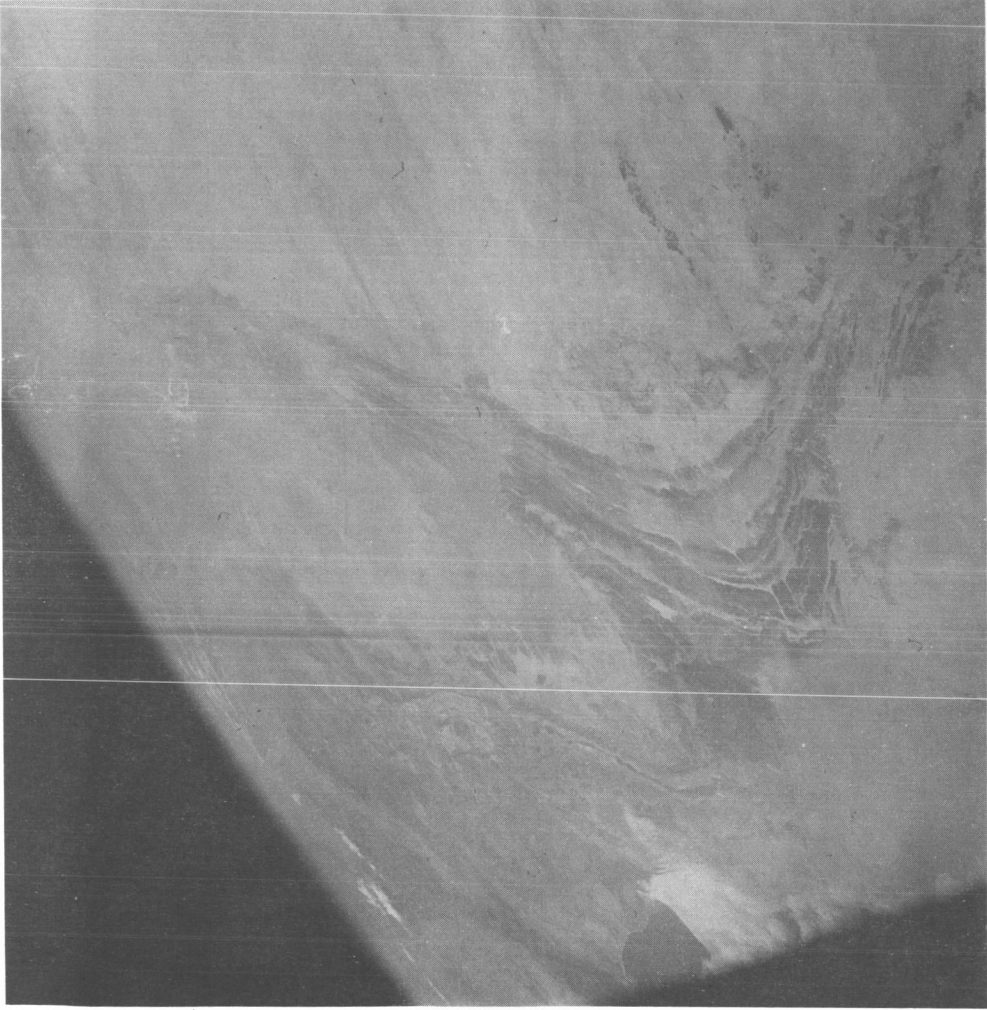


Figure 7-2. - A second view over the Sahara with Hamada du Dra to the left.



Figure 7-3. - View to the southeast over Niger.

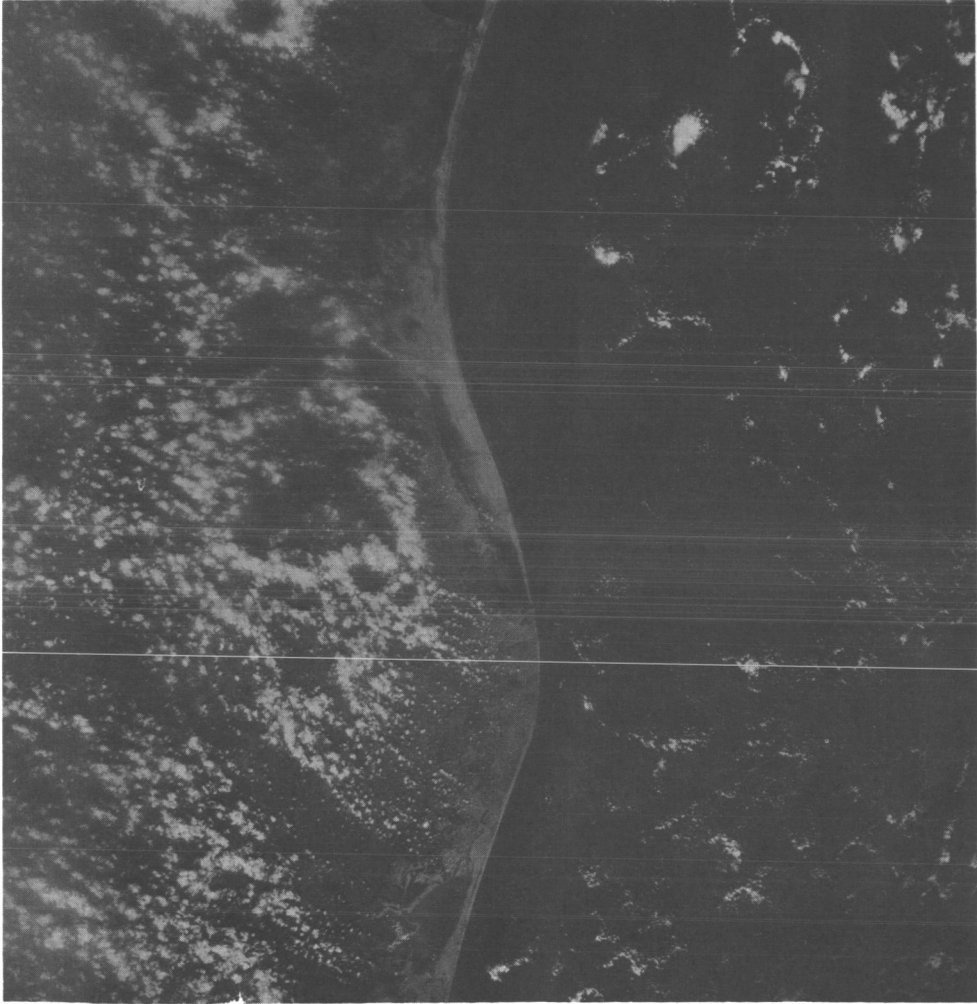


Figure 7-4. - The Rio Grande Delta.

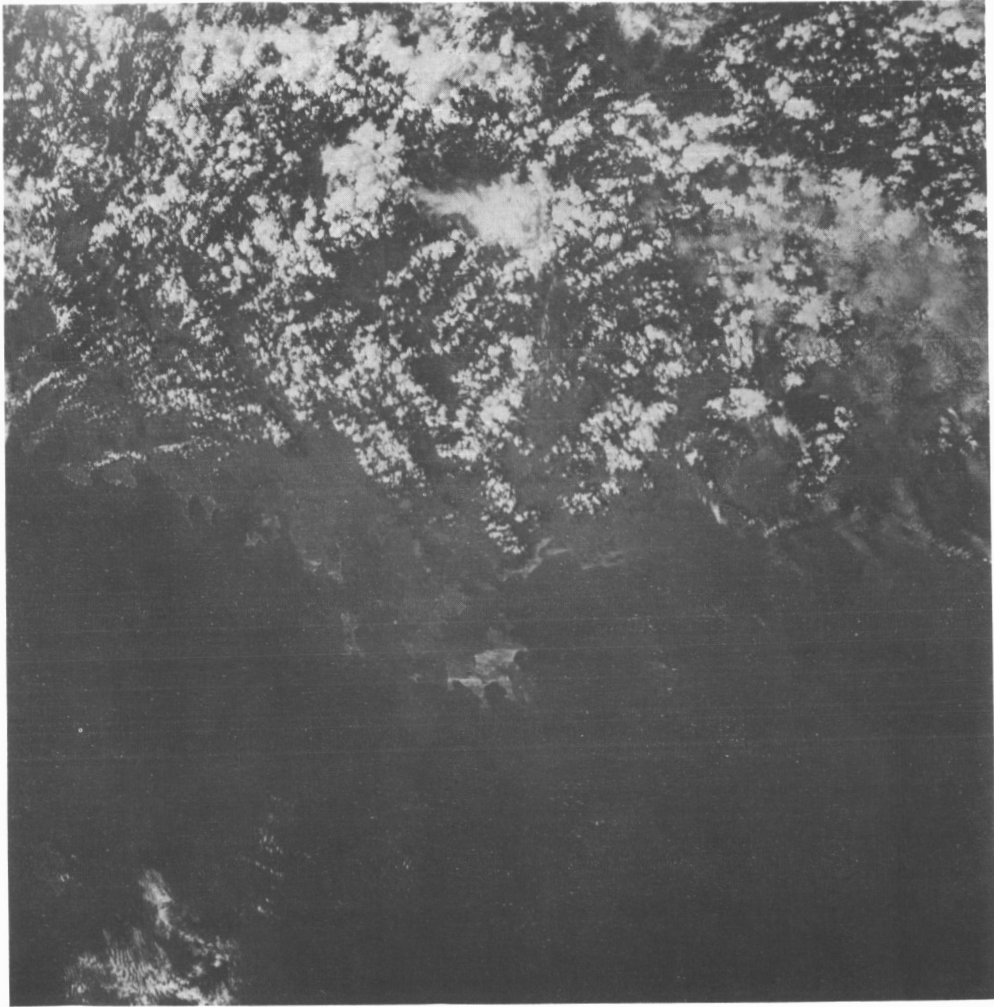


Figure 7-5. - The China coast.

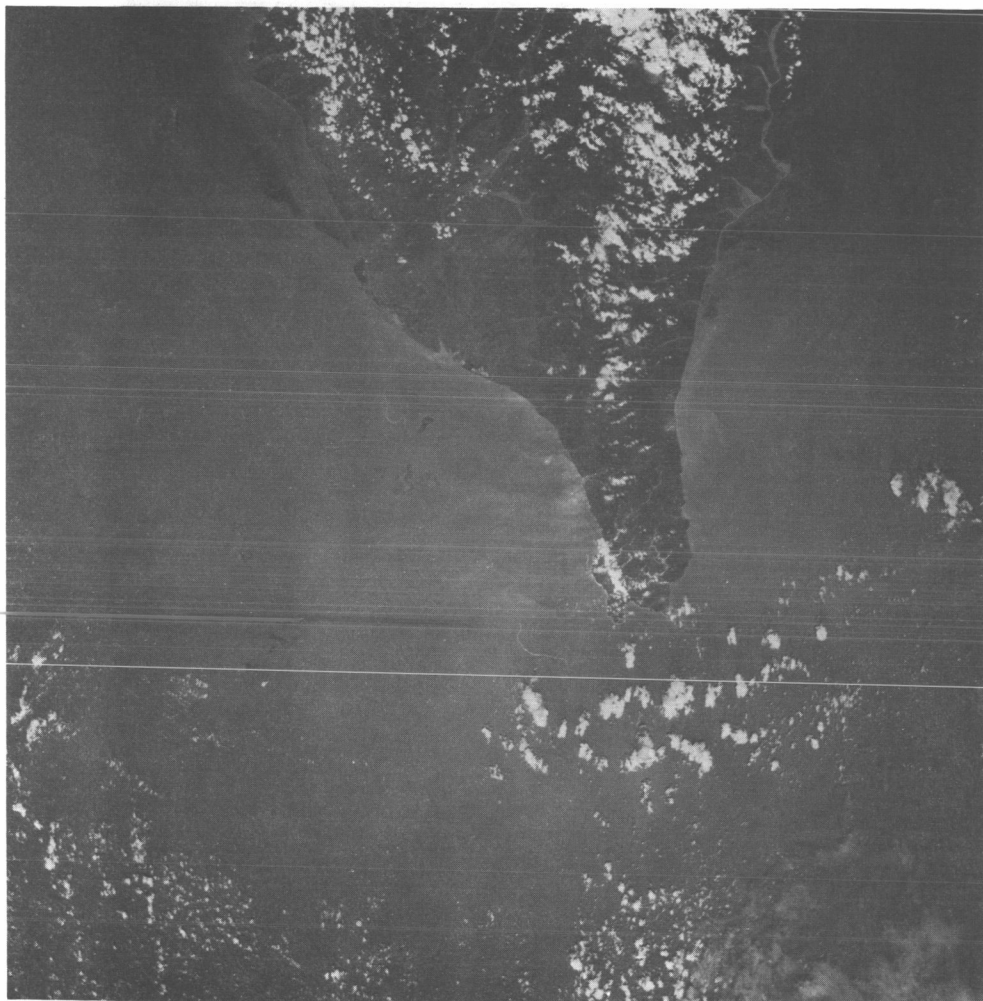


Figure 7-6. - Southern Formosa.

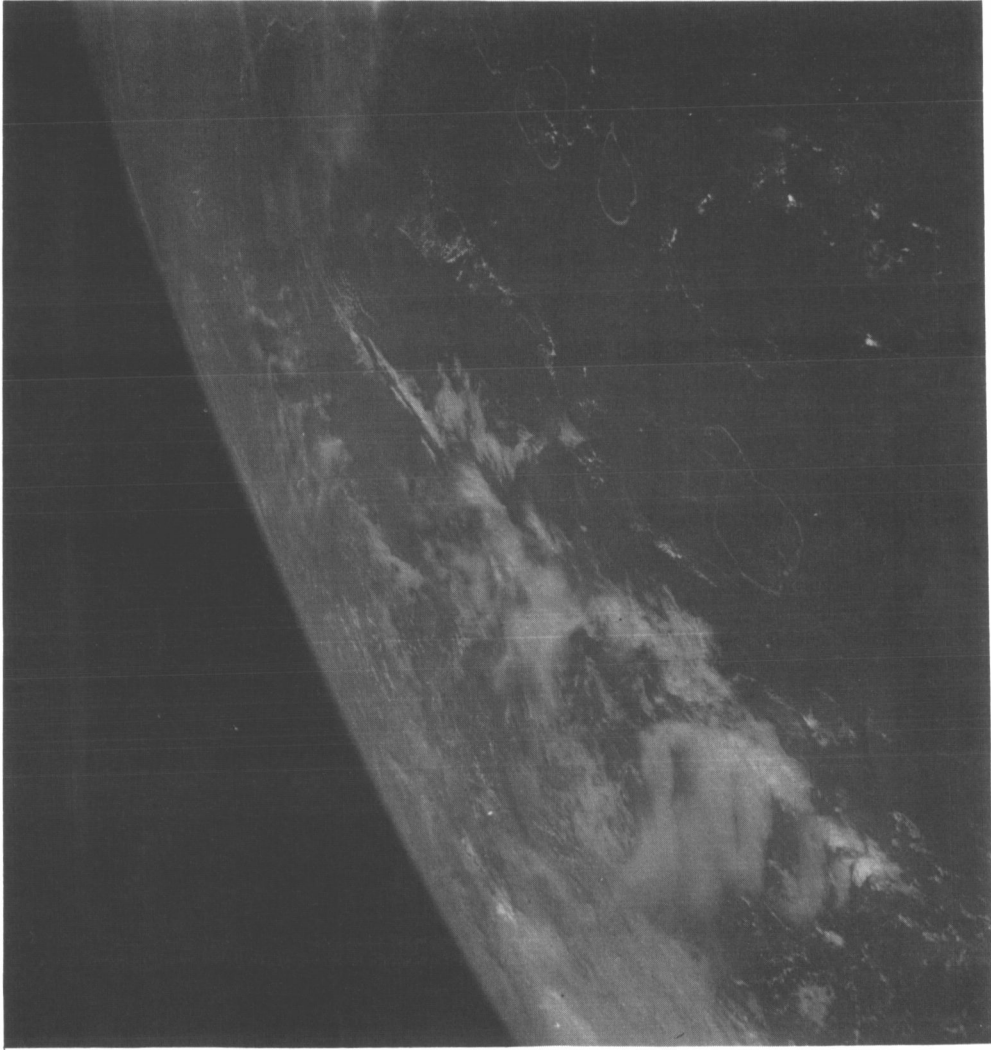


Figure 7-7.- Atolls in the Maldine Islands.

8. EXPERIMENT S006 (S-6), SYNOPTIC WEATHER PHOTOGRAPHY

By Kenneth M. Nagler, Weather Bureau
Environmental Science Services Administration, N 6 8 - 1 4 1 5 8

and

Stanley D. Soules, National Environmental Satellite Center
Environmental Science Services Administration

SUMMARY

The weather photography experiment conducted in the Gemini X mission resulted in over 200 color pictures showing clouds. Southeast Asia was photographed twice during successive revolutions. Convective cloud patterns appear over South America, the Indian Ocean, the Gulf of Mexico, and the Pacific Ocean. Cloud eddies are pictured near the northwest African coast and Guadeloupe Island. Considerable cirrus cloudiness was found near Sumatra and southwest of India. A number of overlapping picture frames have permitted stereoscopic viewing of several cloud levels.

OBJECTIVE

The objective of the Synoptic Weather Photography (S006) experiment was to obtain detailed selective color photographs of the earth's cloud cover in order to amplify and verify the information obtained from weather satellite pictures and to provide new evidence for studies of atmospheric behavior.

EQUIPMENT

The experimental equipment consisted of a 70-mm film magazine and a Maurer 70-mm space camera. It contained sufficient Kodak Ektachrome MS (S0-217) film for approximately 50 exposures. The camera had an f/2.8 lens with an 80-mm focal length. An ultraviolet haze filter was used. Five film magazines were onboard for all experiments.

PROCEDURE

The flight crew was briefed prior to the flight on the types of weather systems of interest for the experiment. During the mission, meteorologists used pictures from the ESSA weather satellites and world weather maps to select specific regions likely to contain cloud patterns of interest. This information was relayed to the crew so that they could photograph these patterns. Views also were taken of clouds which the crew observed and had time to photograph.

RESULTS

Over 200 high-quality pictures showing cloud patterns were obtained. A number of the frames have sufficient overlap in the areas photographed for stereoscopic viewing. Cloud layers can be resolved quite readily by this method, to provide important information on the relative altitude of the cloud tops.

Cumulus cloud lines are prominent features in the convective cloud patterns (fig. 8-1) of northern South America. Here, the Essequibo River system, in Guyana, with its relatively cool waters, has suppressed the development of clouds above it. The flow of the sediment-laden waters can be traced into the Atlantic.

Over the oceans, convective cloud lines can form open, polygonal cells (fig. 8-2), 3 to 6 miles in diameter. These cells are undetected by weather satellite television pictures because the cloud walls are too thin and the cell diameter is very small. The cell configuration is an indicator of the motion of the atmosphere in its lower level.

The crew took a series of pictures on two successive revolutions over southeast Asia and the adjacent Pacific. Cloud motion and changes in cloud growth that occurred during the 90-minute period can be studied from these pictures.

Frequently, large cloudy areas, 300 to 400 miles in diameter, appear in weather satellite photographs of the equatorial convergence zone. These cloud masses sometimes grow into tropical storms. A cloudy area such as this was photographed over the Indian Ocean by the crew, and a detailed view showed a great amount of convective activity in the cloud mass (fig. 8-3). The cirrus plumes from the thunderstorm tops are carried downwind from the northeast, and low-level cumulus cloud lines are oriented southeast to northwest. Figure 8-4 is one of a series of photographs taken over Sumatra and Malaya, depicting equatorial cloud conditions at various altitudes in the atmosphere.

Another series of photographs depicted the cloud cover over the Gulf of Mexico and the Caribbean. Part of tropical storm Celia, which was then southeast of Florida, appeared in several frames, permitting stereoscopic viewing. Among other subjects photographed were cirrus cloud bands over northern Africa, and cloud eddies off the northwest coast of Africa, the Canary Islands, and Guadeloupe Island. A sun-glitter pattern formed by reflected sunlight from the ocean surface was photographed several times. An analysis of the brightness of the pattern may provide information concerning the surface roughness. Considerable cirrus cloudiness, forming lengthy bands, was found near Sumatra and southwest of India.

CONCLUSIONS

Experiment S006 (S-6) was successful, and the many photographs obtained are being analyzed and evaluated for new information that may be useful in understanding the behavior of the atmosphere.

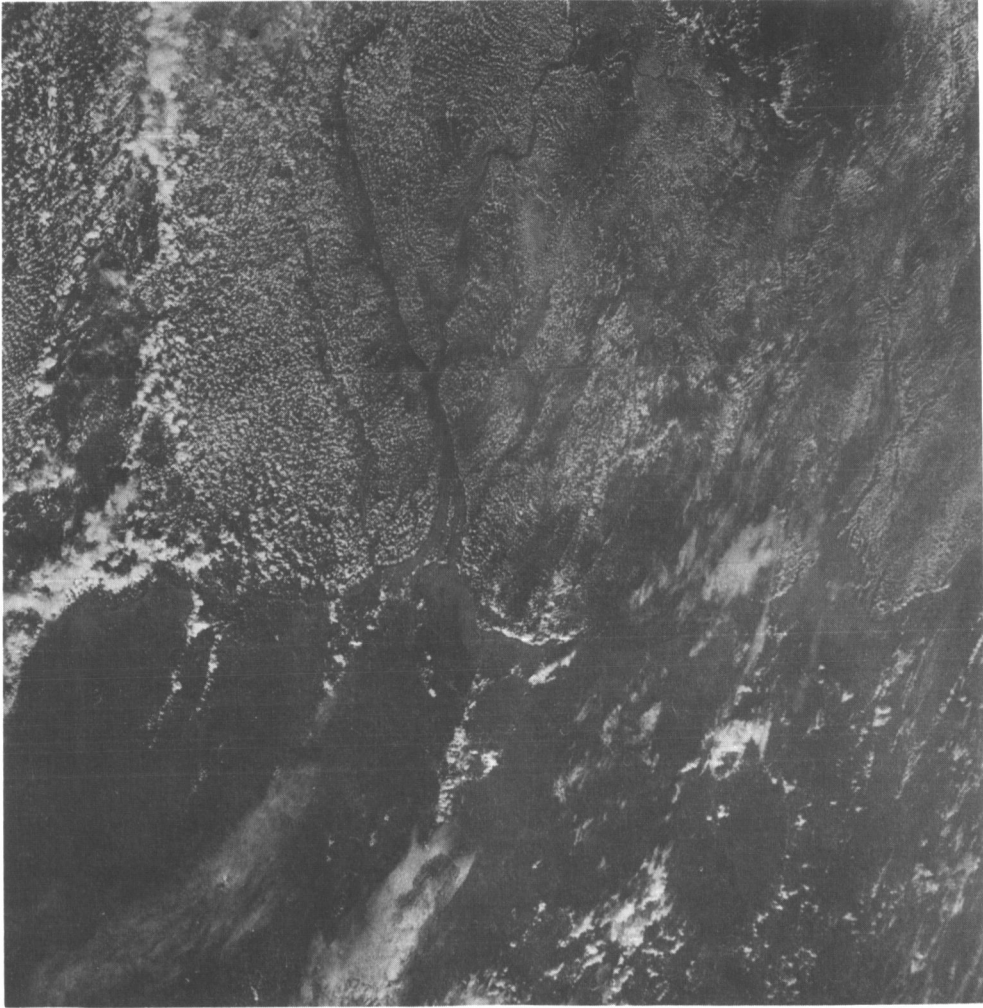


Figure 8-1-1. - Convective cloud patterns of northern South America.

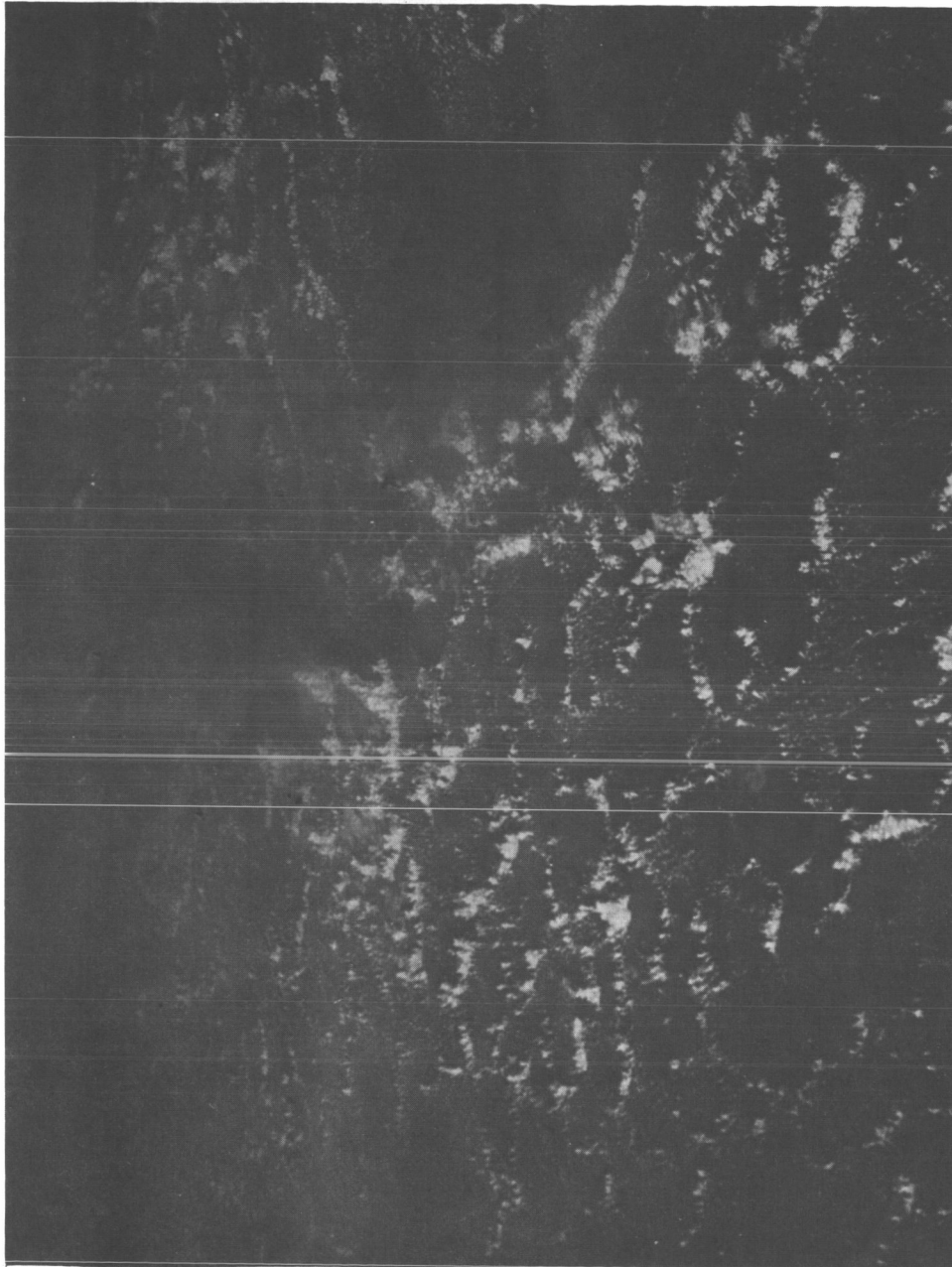


Figure 8-2. - Open polygonal cells, 3 to 6 miles in diameter, formed over the oceans.



Figure 8-3. - Convective activity in a cloud mass over Indian Ocean.

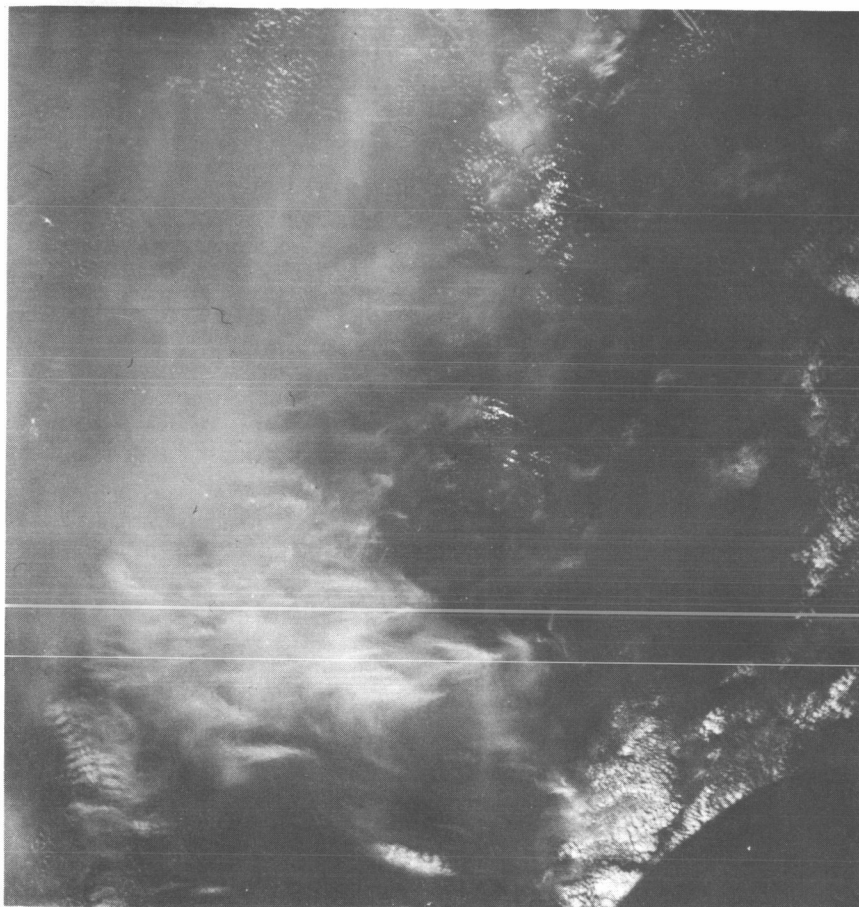


Figure 8-4. - Equatorial cloud condition taken over Sumatra and Malaya.

9. EXPERIMENT S010 (S-10), AGENA MICROMETEORITE COLLECTION

By Curtis L. Hemenway, Ph. D.
The Dudley Observatory

SUMMARY

N 6 8 - 1 4 1 5 9

Micrometeoroid impacts have been recorded during the 4-month exposure of experiment S010 (S-10) equipment. A partial examination revealed two macroscopic craters; two microscopic craters were found as a result of scanning one-quarter of the total area. Further work has been delayed to make use of a recently installed scanning electron microscope.

With the number of impacts located, the flux values found from the satellite microphone experiments are approximately confirmed.

OBJECTIVE

The object of this experiment was to obtain a large area-time product exposure of micrometeoroid detection plates to confirm the flux values obtained with shorter exposures from sounding rockets, balloons, and experiment S010 (S-10) equipment flown aboard the GT-9 spacecraft. Accomplishment of the objective was attempted by (1) exposing polished metal and plastic surfaces to the particle flux for later study of the resulting impact craters, (2) exposing highly polished sections of meteorite material to the particle flux to obtain direct measurement of meteor erosion rates, (3) exposing optically polished glass surfaces to the particle flux for determining the deterioration of optical surface properties, (4) exposing thin films to the particle flux to observe thin-film penetration, (5) exposing extremely clean surfaces to the particle environment in an attempt to collect ultrasmall particles, and (6) exposing biological specimens to the space environment. Experiment data include the particulate material collected, holes and craters in the specially prepared surfaces, and numbers of viable micro-organisms remaining on the biological exposure plates. The micro-organisms used were ubiquitous agents which are absolutely harmless to man. Two of the organisms used were:

- (1) T-bacteriophage (an E. coliphage).
- (2) Penicillium roquefort mode spores.

EQUIPMENT

The hardware configuration consisted of an aluminum structure designed to provide a mounting platform for the polished plates and collection surfaces. The device was interfaced with the Target Docking Adapter (TDA) of the Gemini VIII target vehicle by a mounting plate which allowed detachment of the experiment hardware from the vehicle. Cratering samples were installed on the outside surface of the aluminum structure. During launch and the insertion of the target vehicle into orbit, these external surfaces were protected from direct impact of airborne particles by a fairing which directed airflow over the mounting. The pilot was to remove this fairing cover during extravehicular activity (EVA).

The loaded collector box is shown (fig. 9-1) as it appeared prior to flight. The plates on the outside are highly polished stainless steel. The interior of the box contained other collection and detection samples which were not exposed because there was no extravehicular activity during the Gemini VIII mission.

The six circular depressions along the edge of one of the plates contain micro-organisms which were exposed to test their ability to survive in the environment of space.

PROCEDURE

The loaded experiment hardware was hand-carried to KSC and mounted to the target docking adapter (TDA) at approximately T-24 hours. The protective cover was removed at T-6 hours. In addition, a fully loaded unit was stowed in the spacecraft. It was hoped that the pilot would deploy this unit on the GT-8 Agena target-vehicle and recover the experiment S010 (S-10) unit launched aboard this Agena. Upon completion of the double rendezvous, the pilot was able to retrieve the experimental hardware from the TDA of the Agena VIII vehicle. He was unable to deploy the "carry-up" unit and was forced to jettison it in space. Deployment of the experiment S010 (S-10) unit aboard the Agena target-vehicle for the GT-10 was not included in the flight plan.

RESULTS AND CONCLUSIONS

The pilot recovered the S010 experiment package from the Gemini VIII target vehicle and handed it to the command pilot at approximately

49 hours 5 minutes g.e.t. The hardware was in a closed position; only the outer four test panels had been exposed to the space environment. Additional S010 hardware was not placed on the target vehicle because the pilot was concerned that the umbilical might become entangled in the various projections on the vehicle.

A photograph of the flight package retrieved from the Gemini VIII GATV by the extravehicular pilot is shown in figure 9-2. The photograph clearly shows the various erosions incurred by the collection surfaces during a 4-month period in a space environment. Two macroscopic craters (figs. 9-3 and 9-4) were found by partially scanning the surface of one plate. Large quantity of debris on the surface makes light microscopic scanning very difficult. According to current plans, the surfaces will not be cleaned until all possible data are obtained from the debris. Until the surfaces are cleaned, only craters larger than 50 microns will probably be found. Figure 9-5 shows the same crater that is shown in figure 9-4 as seen in the scanning electron microscope. The greater definition and depth of focus of the electron microscope provide an image of three-dimensional craters that could not be produced by light microscopy. The electron microscope has just been installed; and when this instrument is performing routinely, further data on impact sites are expected to be available.

The data obtained thus far are in general agreement with the micro-meteorite flux values obtained from the satellite microphone experiments and balloon collections.

The biological micro-organisms on the outside surfaces did not survive the 4-month period of exposure. However, the same kinds of specimens inside the hardware package showed good survival rates. The shielding offered by the closed covers contributed directly to the protection and survival of these micro-organisms. Continuing analysis of the S010 hardware is expected to provide additional and more conclusive results.

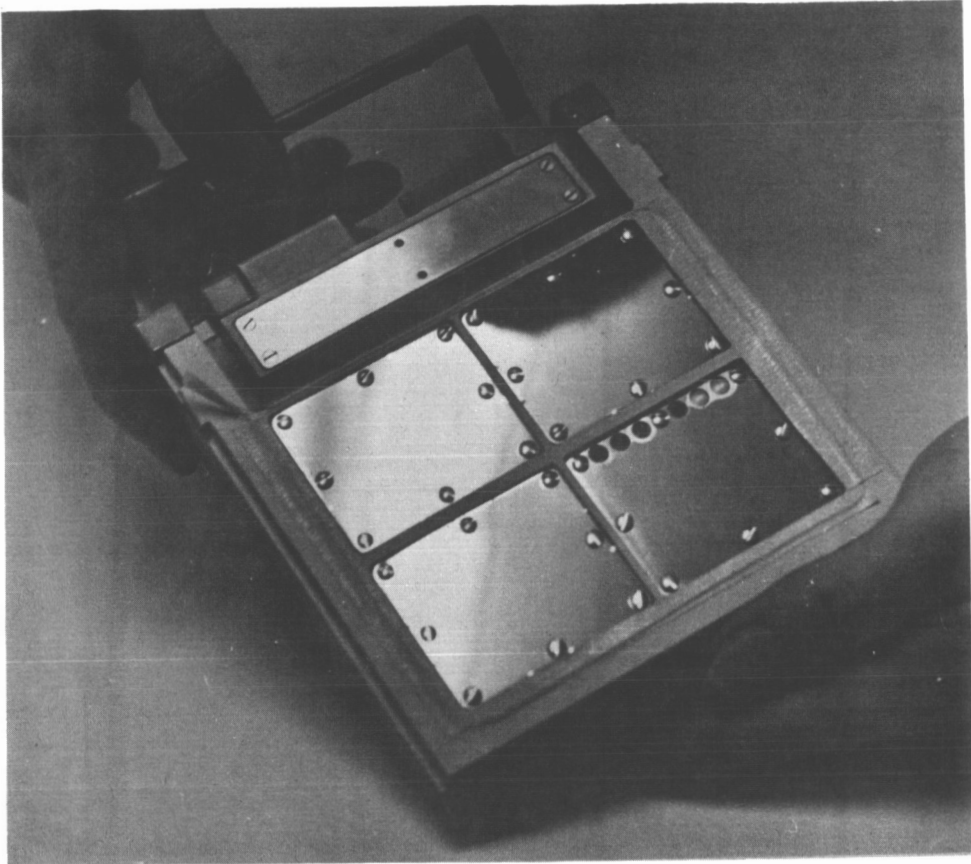


Figure 9-1. - Agena micrometeorite collection unit before flight.

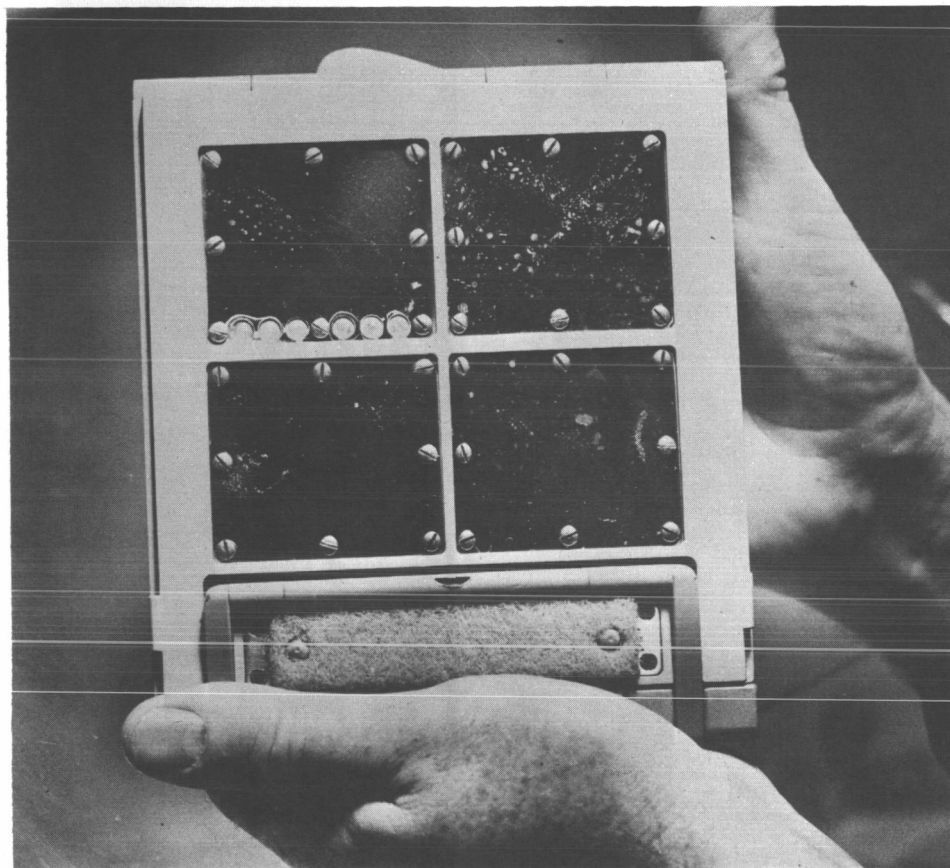


Figure 9-2. - Collection unit after 4-months exposure.

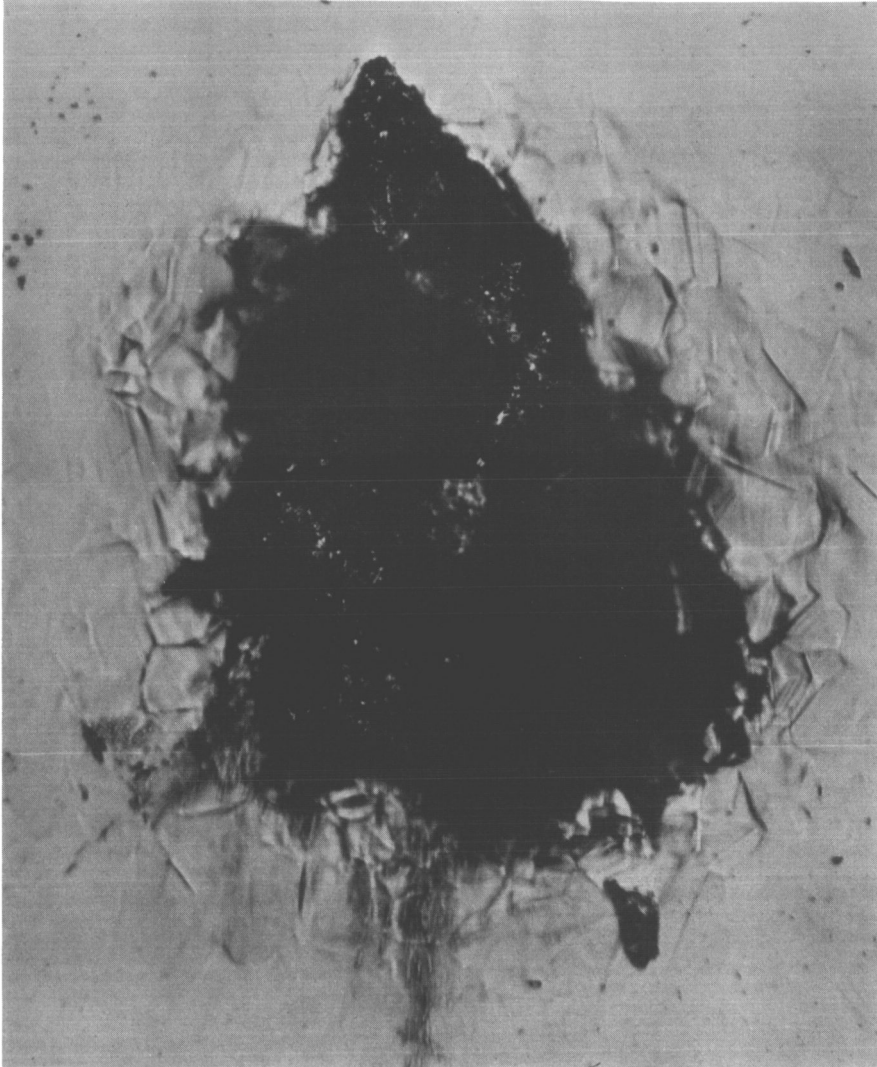


Figure 9-3. - Macroscopic crater in stainless steel plate
(light micrograph - 500X).

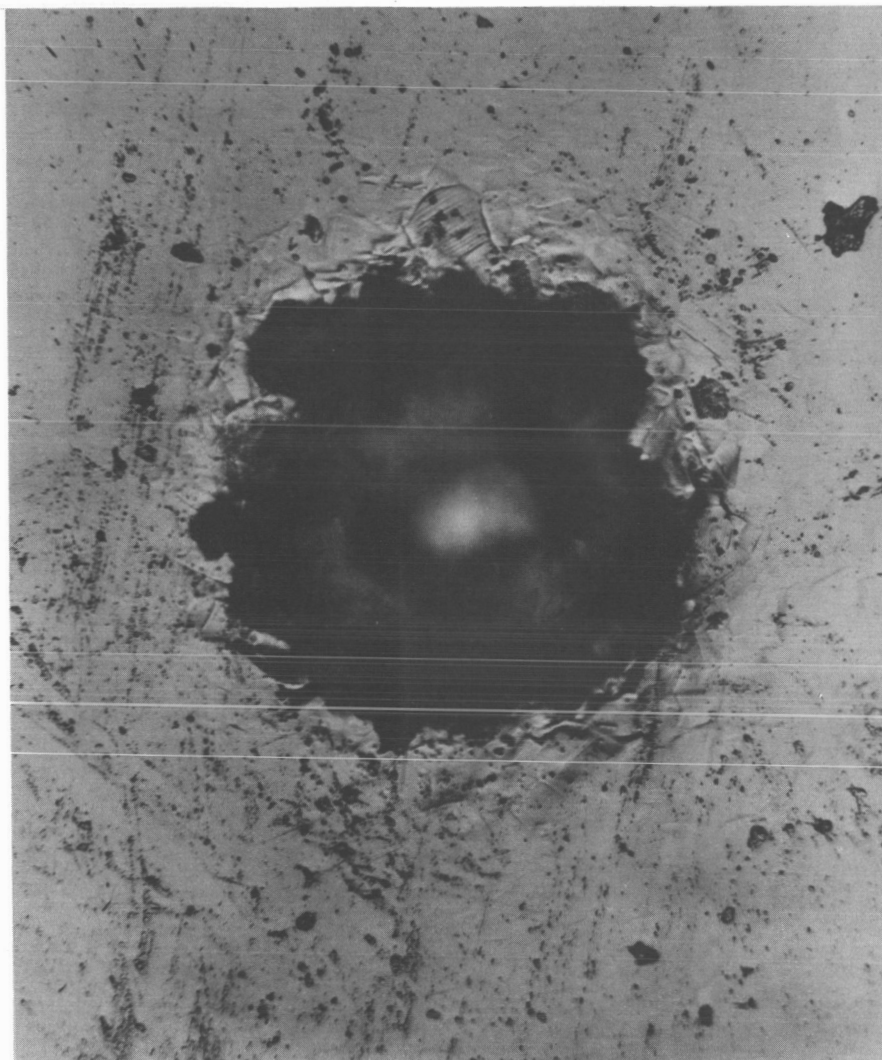


Figure 9-4. - Second macroscopic crater in stainless steel plate (light micrograph - 500X).

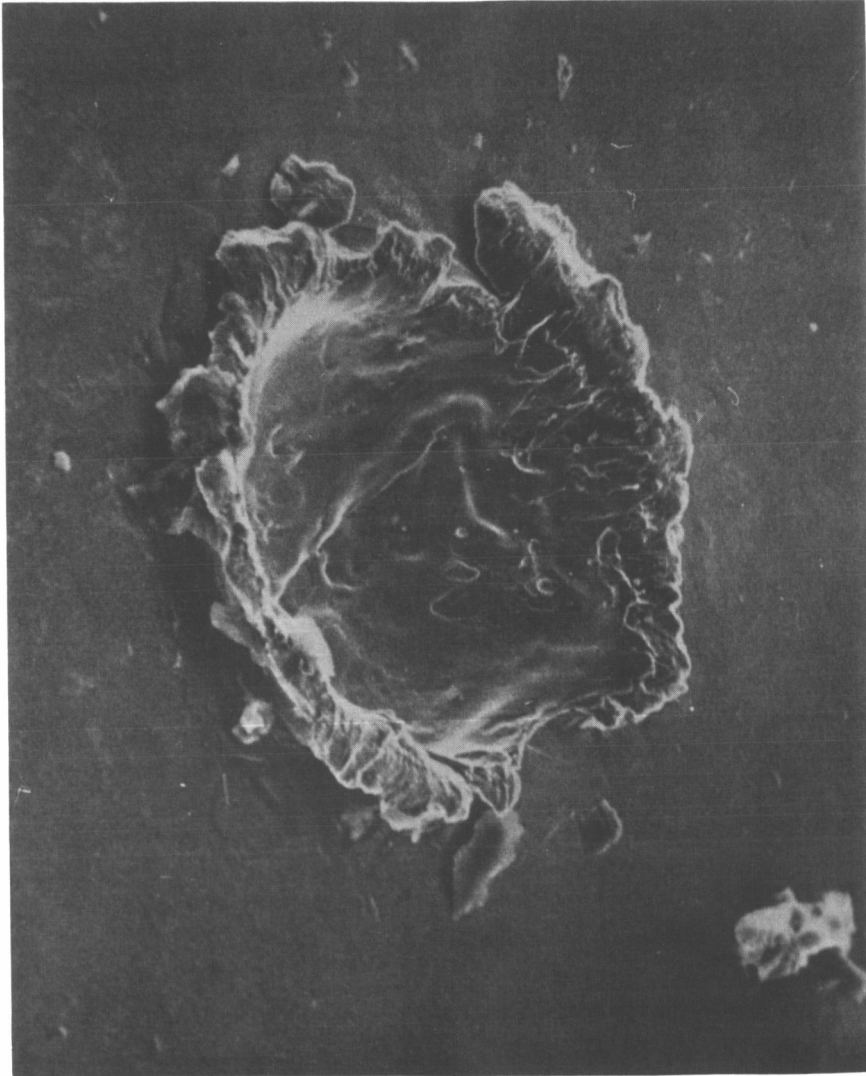


Figure 9-5. - The second macroscopic crater in stainless steel plate (scanning electron micrograph - 500X).

10. EXPERIMENT S012 (S-12), MICROMETEORITE COLLECTION

By Curtis L. Hemenway, Ph. D.
Dudley Observatory

OBJECTIVES

N 6 8 - 1 4 1 6 0

The micrometeorite collection S012 (S-12) experiment was to determine the micrometeorite activity in a near-earth environment and to study the effect of the environment on biological micro-organisms. The basic objectives were to be accomplished by exposing polished metal and plastic surfaces to the environment outside the Gemini spacecraft. The environmental data to be acquired included the particulate material collected, holes and craters in the specially prepared surfaces, the penetration characteristics of micrometeorites on thin films, the surviving fractions of viable micro-organisms remaining on the biological exposure plates, and a search for viable micro-organisms in the particle flux in the spacecraft vicinity. The micro-organisms used were ubiquitous agents which are absolutely harmless to man. Laboratory tests have shown these organisms to be resistant to adverse conditions, hence their selection for space studies. All material specimens were to be returned to earth by stowage in the Gemini reentry assembly for postflight examination and analysis at special laboratories.

In addition, through a guest experimenter program, scientists from various institutions were invited to provide samples within the context of the above areas. Guest experimenters for Gemini X were Robert Skrivanek, Air Force Cambridge Research Laboratory; Hugo Fetchig, Max Planck Institute; Neil Farlow, NASA Ames Research Center; Uri Shafrir, University of Tel-Aviv; John Kerridge, Birkbeck College; H. Fernandez-Moran, University of Chicago; Paige Burbank, NASA-MSC; Michael Carr, U. S. Geological Survey; Otto Berg, Goddard Spaceflight Center; Francis Wright, Smithsonian Observatory; and Paul Hodge, University of Washington.

EQUIPMENT

The S012 (S-12) micrometeorite collection hardware consisted of an aluminum structure mounted on the spacecraft adapter retrograde section (fig. 10-1). The equipment measures 5-1/2 by 11 by 1-1/4 inches and weighs approximately 6-1/2 pounds flight-loaded. It utilizes a dual internal battery package, cover drive motor and gear train, cover limit switches, and squib-actuated unlatching and locking devices. Mounting

spaces were designed for 24 surfaces, materials, or specimens. The collector cover door was remotely controlled by the flight crew, thereby allowing the cover to be opened or closed, as required, to expose the experiment samples.

Figure 10-2 shows the unit with one cover open and illustrates the 12 sample slides contained in one compartment of the device. The dual cover arrangement was provided to allow the inclusion of sterile samples in one area and live micro-organisms in the other. Figure 10-3 shows the sample slides in the second compartment. Figure 10-4 is a diagram showing sample locations and giving a brief description of the nature and source of the sample.

PROCEDURES

The final loading procedures were begun approximately 10 days before scheduled launch with a thorough cleaning of the entire S012 (S-12) unit. The compartment to be sterilized was loaded in a dust-free hood and the cover closed. The entire unit was then placed in a clean stainless steel box, the covers of the S012 (S-12) unit were partially opened, and ethylene oxide introduced for sterilization. After sterilization, the covers were closed and secured. The unit was removed to a dust-free hood and the nonsterile compartment opened manually for loading of its sample slides. After completion of loading and final mechanical adjustments the unit was wrapped in protective wrapping, placed in a special container, and hand-carried to KSC at T-3 days. Two units were loaded in this way and designated as flight and backup units.

After prelaunch tests designed to verify operational readiness, the flight unit (SN 006) was installed on the spacecraft retroadapter at T-17 hours. As part of the final countdown, three sterile swabs were used to take samples of the microbiological environment of three selected areas inside the spacecraft.

The cover door of the micrometeorite collection device remained in the closed position until just prior to the first crew sleep period, a period of drifting flight. This activation time was chosen to prevent exposing the sample surfaces to particles caused by thruster firing, fuel-cell purging, or dumping of liquids overboard. The collector door was left open for one period of 8 hours. The S012 (S-12) hardware was retrieved during the egress part of the extravehicular activity (EVA) at 49 hours 50 minutes ground elapsed time (g.e.t.) and then stowed in the spacecraft.

RESULTS

The flight crew reported at 64 hours 15 minutes g.e.t. that the SO12 (S-12) hardware could not be located in the spacecraft. They believed that the experiment hardware floated through the open hatch during EVA. A subsequent crew compartment check, after spacecraft retrieval, verified that the collection device had been lost. Since no data samples were recovered for analysis, no results can be reported.

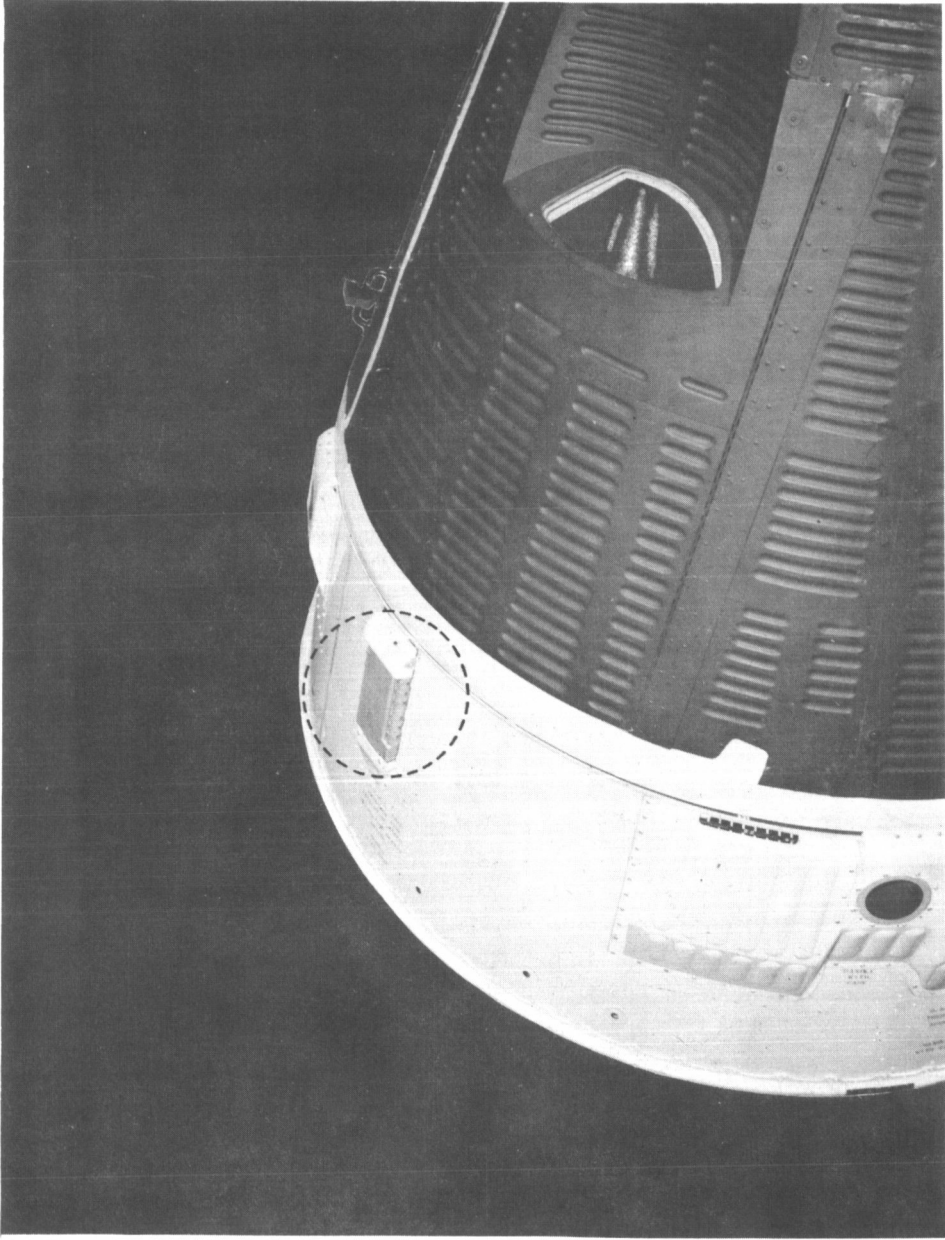


Figure 10-1.- Mounted micrometeorite collection hardware.

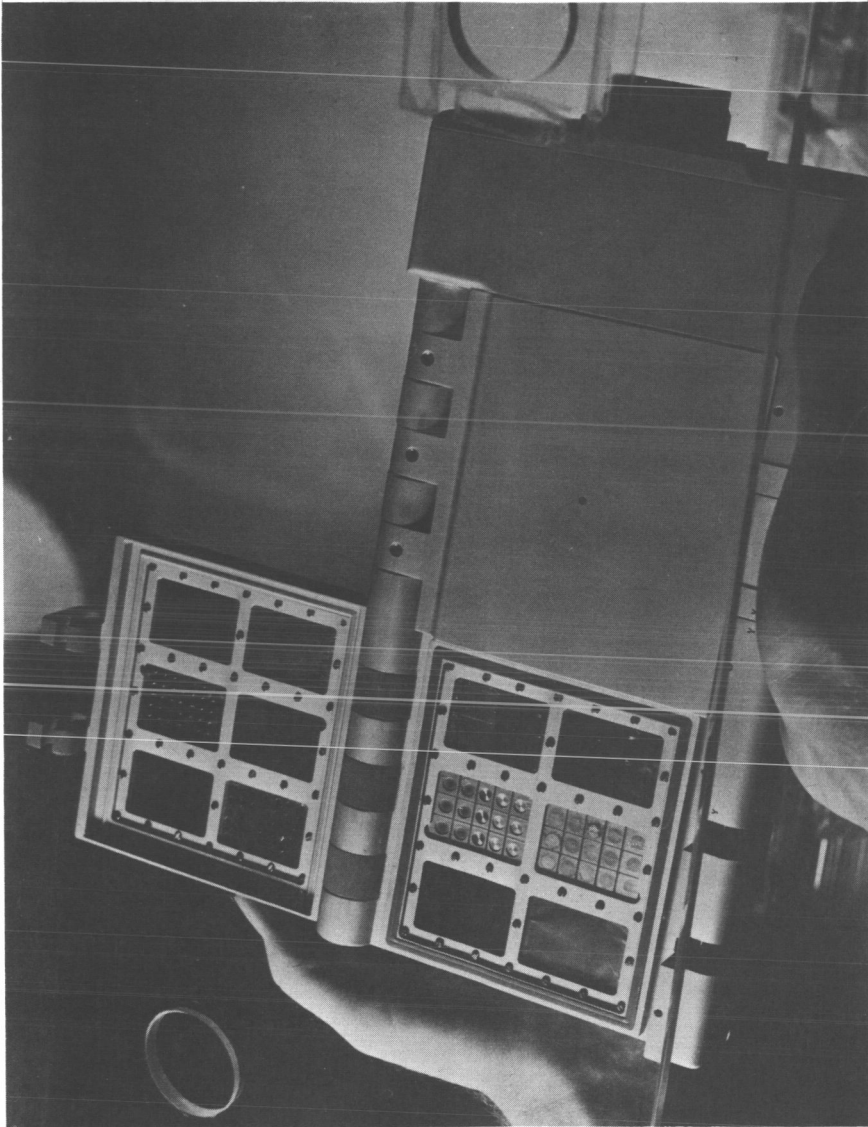


Figure 10-2.- Micrometeorite collection unit with one cover open.

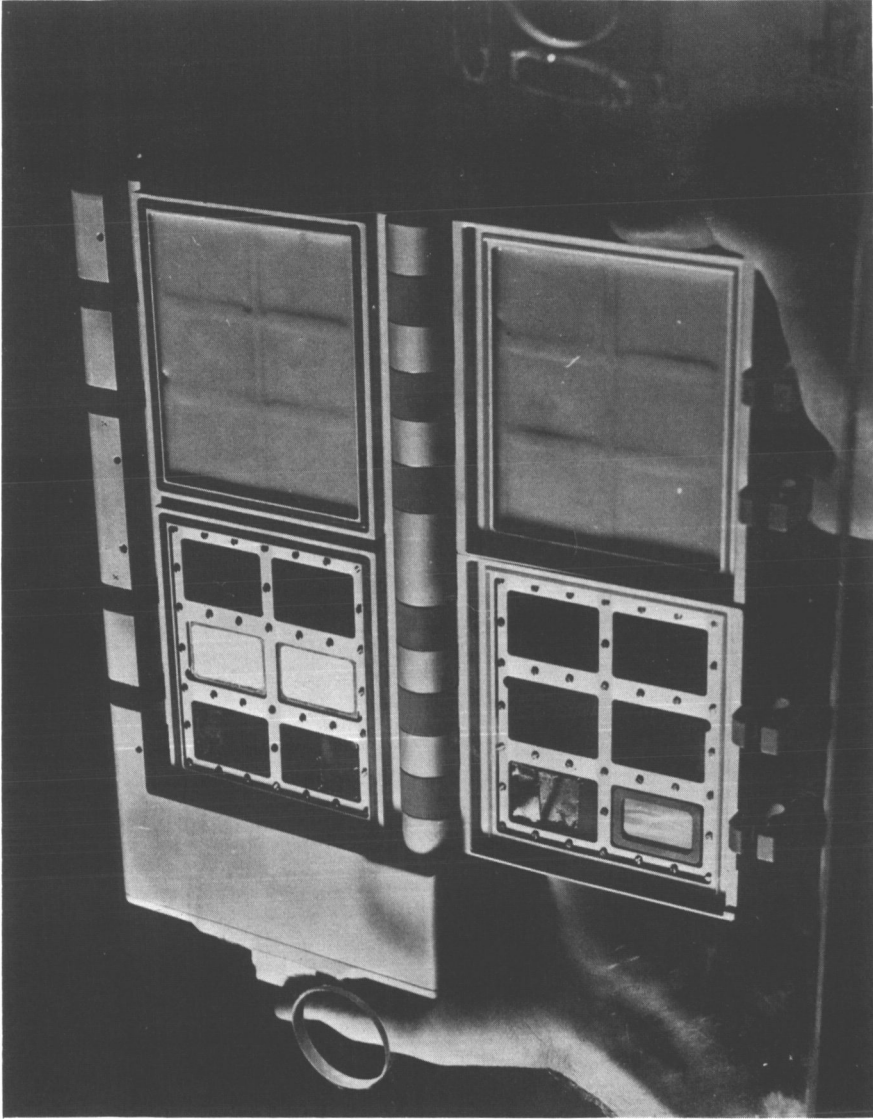
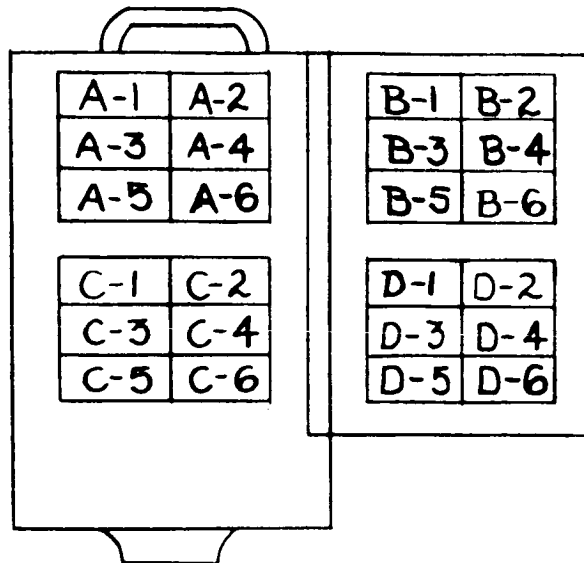


Figure 10-3. - Sample slides in second compartment in micrometeorite collection unit.



A-1 Dudley - Nitrocellulose film over glass
 A-2 Dudley - Gold coated glass
 A-3 Dudley - Biological exposure
 A-4 Dudley - Biological exposure
 A-5 Air Force Cambridge Res. Lab. - Nitrocellulose on Copper
 A-6 Max Planck Institute - Coated metal plates

B-1 Dudley - Penetration experiment
 B-2 Dudley - Stainless steel
 B-3 Ames Research Lab. - Copper film on plastic
 B-4 Tel Aviv University - Penetration through film
 B-5 Birkbeck College - Aluminum film on stainless steel
 B-6 University of Chicago - Carbon on Mica

C-1 Dudley - Nitrocellulose over glass
 C-2 Manned Spacecraft Center - Silver on lucite
 C-3 Dudley - Sterile plate
 C-4 Dudley - Sterile plate
 C-5 U. S. Geological Survey - Beryllium on aluminum
 C-6 Max Planck Institute - Coated metal plate

D-1 Goddard Space Flight Center - Titanium coated glass
 D-2 Dudley - Stainless steel
 D-3 Ames Research Lab. - Gold film on plastic
 D-4 Dudley - Gold coated glass
 D-5 Air Force Cambridge Res. Lab. - Nitrocellulose on copper
 D-6 Smithsonian Observatory and University of Washington - Gold coated plastic

Figure 10-4. - Locations and descriptions of samples.

N 6 8 1 4 1 6 1'

97

11. EXPERIMENT S013 (S-13), ULTRAVIOLET ASTRONOMICAL CAMERA

By Karl G. Henize, Ph. D., and Lloyd R. Wakerling
Dearborn Observatory, Northwestern University

OBJECTIVE

The purpose of this photography was to obtain data on the ultraviolet radiation (2200 to 3000 Å) of hot stars and to develop and evaluate basic techniques for the photography of celestial objects from manned spacecraft. Twenty-two frames were exposed on the southern Milky Way as the spacecraft's orbital motion caused the camera to scan from Crux to Vela.

EQUIPMENT

The Maurer 70-mm camera, designed and manufactured under the supervision of scientists at the NASA Manned Spacecraft Center, was used to obtain these spectra. The ultraviolet lens has a 22-mm aperture, 73-mm focal length, and a field of 30° diameter. A 10-degree objective prism in a cell provides attachment to the ultraviolet lens. The film magazine carries 50 frames of Kodak spectroscopic I-0 emulsion on an Estar base. Combined with a 600-line/mm objective grating, it produces spectra with a dispersion of 180 angstroms per millimeter. Figure 11-1 shows the camera and prism assembly mounted to the spacecraft in the position used during flight.

PROCEDURE

Since the Gemini windows do not transmit ultraviolet light, the observations were made through the opened hatch. The camera was fastened on a bracket pointing 5° above the roll axis of the spacecraft.

The original operating plan called for the command pilot to point the undocked Gemini at the desired star field, and to nullify the angular motions of the spacecraft by using the pulse control system. With the craft stabilized, the pilot was to make 10 exposures on each field, ranging in length from 10 to 60 seconds, for three separate fields.

During the Gemini X mission, this plan was altered due to shortage of fuel for maneuvering. The observations were made while Gemini was

docked with the Agena, in order that the Agena stabilization system could be used. Since the Agena could not be reoriented once the hatch was opened, it was decided to point at the Southern Cross, which lay near the pole of the orbit and would remain in the camera field all night. However, by mischance, during assembly of the equipment, the grating was turned 17° counterclockwise, causing the orbital motion of the horizon-stabilized spacecraft to produce a migration of the field center from near β Crucis to near γ Velorum. After the basic pointing had been accomplished and the Agena stabilization had been activated, the pilot opened the hatch, mounted the camera on its bracket, and took 22 exposures. All exposures were about 20 seconds in length.

RESULTS

One of the most interesting regions of the entire Milky Way was scanned, and spectra were obtained for many more stars than was expected. However, the displacement of the grating caused trailing in the direction of dispersion for most stars, thus degrading wavelength resolution. This prevented the possible resolution of line spectra but did not interfere with the measurement of ultraviolet energy curves.

In preliminary examinations of the film, the spectra of 57 stars have been identified. These are listed in table 11-I. About one-half are bright enough to permit quantitative analysis of the ultraviolet energy curves. The only absorption feature visible in the spectra is the Balmer continuum. The limiting ultraviolet magnitude (effective wavelength 2200 \AA) for unwidened spectra is about +3.5 or a little fainter. An illustration of one of the better frames is given in figure 11-2. Figure 11-3 is a key chart for figure 11-2.

Four separate equipment problems occurred during the mission.

(a) Twelve of the frames were marred by a vertical streak which does not appear to be caused by ordinary light leaks. Static electricity rising from camera operation under vacuum conditions could cause this effect.

(b) Preflight and postflight calibration exposures with the flight camera showed images of good quality at the center of the field. The inflight exposures showed poor image quality at the center of the field and good image quality away from the center. The shape of the images indicates the film was too close to the lens, apparently caused by film bowing towards the lens in vacuum conditions.

(c) The cable release was broken during assembly of the camera. A more suitable cable release has been provided for the Gemini XI mission.

(d) One of the screws in the bracket assembly backed out preventing proper insertion in the ways. According to the pilot, difficulty was encountered during bracket insertion.

About 10 percent of the field of first-order star spectra was obscured by the GATV when in the docked configuration. About 40 percent of the field of zero-order star images was obscured. The masking of zero-order images prevented interference with most of the first-order spectra.

Extraneous light was not observed either originating in or reflected from the GATV. GATV stabilization which was achieved during the second half of the night exposure period appears to have been adequate for the purpose of this experiment. The experiment operation while in a docked configuration is now recommended in order to use the greater inertia of the combined masses of the two vehicles. This provides increased sensitivity of the pulse control mode in attitude-hold.

CONCLUSIONS

In addition to gathering basic astrophysical data about hot, young stars, the Gemini experiment aims at clarifying the problems and techniques of ultraviolet photography of stars from manned spacecraft. It is vital that such problems and techniques be explored in order to lay the technical foundation for the large manned orbiting telescopes, currently under discussion by NASA and the National Academy of Sciences. The amount of data gathered by the crew of Gemini X with very simple equipment and in the face of unexpected difficulties clearly indicates the value of man in such research programs.

This experiment can be considered successful in that it achieved useful scientific data and established needs for better equipment and procedures on additional flights.

TABLE 11-I.- REVISED CENSUS OF STARS ON GEMINI X SOL3 (S-13) FILM

Star	Frames	Maximum intensity (a)	Spectral type	V (b)	B-V (c)	Predicted 2200 Å magnitude	BS (d)	HD (e)
β Cru	5	3	B0.5 IV	1.50	-0.24	-0.82	4853	111123
α Cru	8	4	B1 IV + B3m	1.05	-0.26	-1.14	4730/1	108248/9
β Mus	11	3	B2.5 V	3.26	-0.19	1.45	4844	110879
α Mus	14	4	B3 IV	2.94	-0.20	1.12	4798	109668
β Cen	7	3	B1 II	0.86	-0.22	-1.42	5267	122451
α Cen	6	1	G2 V + dK1	0.06	-----	-----	5459/60	128620/1
ε Cen?	1	1	B1 V	2.56	-0.23	0.33	5132	118716
γ Mus	4	2	B5 V	4.04	-0.16	2.76	4773	209026
ζ Cru	3	1	B3 IV	4.26	-0.18	2.54	4679	106983
β Cha	3	1	B6 V	4.38	-0.13	3.41	4674	106911
δ ² Cha	3	1	B3 V	4.62	-0.19	2.85	4234	93845
ω Car	11	2	B7 IV	3.56	-0.08	3.00	4037	89080
β Car	13	3	A1 IV	1.80	0.00	2.04	3685	80007
E Car	8	1	B2 Ve	4.86	-0.16	3.16	3642	78764
θ Car	13	4	O9.5 V	3.03	-0.22	0.62	4199	93030
HR 4205+	7	2	B5 Vn	5.09	-0.14	3.91	4205	93194
HR 4222			B3 IV	5.10	-0.15	3.53	4222	93607
M Car	1	1	Am	5.15	+0.22	5.60:	4025	88981
v Car	2	1	A9 II	3.15	-----	4.95:	3890/1	85123/4
i Car	8	2	B3 IV	4.18	-0.19	2.41	3663	79447
κ Vol?	1	1	B9 + Ap	4.74	-0.06	4.49	3301/2	71046/66
p Car	8	3	B5 Ve	3.58	-0.12	2.50	4140	91465
c Car	7	2	B8 II	3.98	-0.11	3.48	3571	76728
d Car	5	2	B1 III	4.42	-0.12	2.74	3457	74375
e Car	3	2	KO II + B	1.85	+1.30	-----	3307	71129
γ Vel	8	4	WC7 + O	2.22	-0.26	-0.16	3207	68273
z Car	7	2	F0 Ib	2.24	+0.18	4.04	3699	80404
a Car	7	3	B2 IV	3.56	-0.19	1.71	3659	79351
δ Vel	7	3	A0 V	2.01	+0.04	2.21	3485	74956
o Vel	6	3	B3 III	3.68	-0.19	1.91	3447	74195
χ Car	4	2	B2 IV	3.60	-0.19	1.75	3117	65575
HR 4188+	4	1	WN7	6.48	+0.08	5.82	4188	92740
HR 4198			B3 Ia	5.44	+0.24	5.47	4198	92964
κ Vel	5	4	B2 IV	2.63	-0.20	0.73	3734	81188

^a1 = barely visible, 2 = weak, 3 = medium, 4 = strong, 5 = overexposed.

^bPhotoelectric visual magnitude (yellow).

^cPhotoelectric visual magnitude (blue) minus photoelectric visual magnitude (yellow).

^dSerial numbers for stars from the Yale Catalogue of Bright Stars.

^eSerial numbers for stars from the Henry Draper Catalogue of Stellar Spectra.

TABLE 11-I.- REVISED CENSUS OF STARS ON GEMINI X S013 (S-13) FILM - Concluded

Star	Frames	Maximum intensity (a)	Spectral type	V (b)	B-V (c)	Predicted 2200 Å magnitude	BS (d)	HD (e)
NGC 3293	2	1	B0 Ib ^f	6.51	+0.01	4.24	----	91969
J Vel	3	2	B3 IV	4.65	-0.13	3.18	4074	89890
φ Vel	4	3	B5 II	3.70	-0.09	2.67	3930	86440
f Car	3	1	B2 Vne	4.63	-0.17	2.87	3498	75311
L Vel	3	2	B3 n	5.16	-0.20	3.34	3819	83058
H Vel	1	1	B5 V	4.77	-0.13	3.64	3574	76805
I Vel	2	2	B5 n	5.22	-0.12	4.14	3753	81848
HR 3467	2	2	B4 IV	5.04	-0.18	3.49	3467	74560
D Vel	4	1	B0 Vn	5.19	-0.22	2.93	3476	74753
E Vel?	1	1	B9 si	5.79	-0.14	5.54	3413	73340
f Vel	4	1	B0 III	4.89	-0.22	2.63	3527	75821
n Vel	3	1	A5 II	4.76	+0.13	5.93	3452	74272
B Vel	3	1	B1 V	4.90	-0.16	3.02	3294	70930
J Pup	3	2	B1 Ib	4.32	-0.15	2.14	3090	64760
h Car	2	1	B5 II	4.20	+0.01	3.67	3825	83183
HR 3453?	1	1	B2 Vn	6.14	-0.22	4.14	3453	74253
V Pup	2	1	B2 n	4.40	-0.18	2.60	3129	65818
HR 3142/3?	2	1	B5	6.43	-----	4.50:	3142/3	66005/6
b ² Car	1	1	B3 IV	5.08	-----	3.26:	3582	77002
e ² Car	1	1	B3 Vn	5.40	-0.15	3.83	3415	73390
HR 3330	1	1	B3 n	5.23	-----	3.41:	3330	71510
A Vel	1	1	B4	6.50	-----	4.50:	3375	72485
P Pup	1	2	B0.5 III	4.25	-0.20	2.13	3055	63922

^a1 = barely visible, 2 = weak, 3 = medium, 4 = strong, 5 = overexposed.

^bPhotoelectric visual magnitude (yellow).

^cPhotoelectric visual magnitude (blue) minus photoelectric visual magnitude (yellow).

^dSerial numbers for stars from the Yale Catalogue of Bright Stars.

^eSerial numbers for stars from the Henry Draper Catalogue of Stellar Spectra.

^fThe data given are for the brightest star in the cluster.

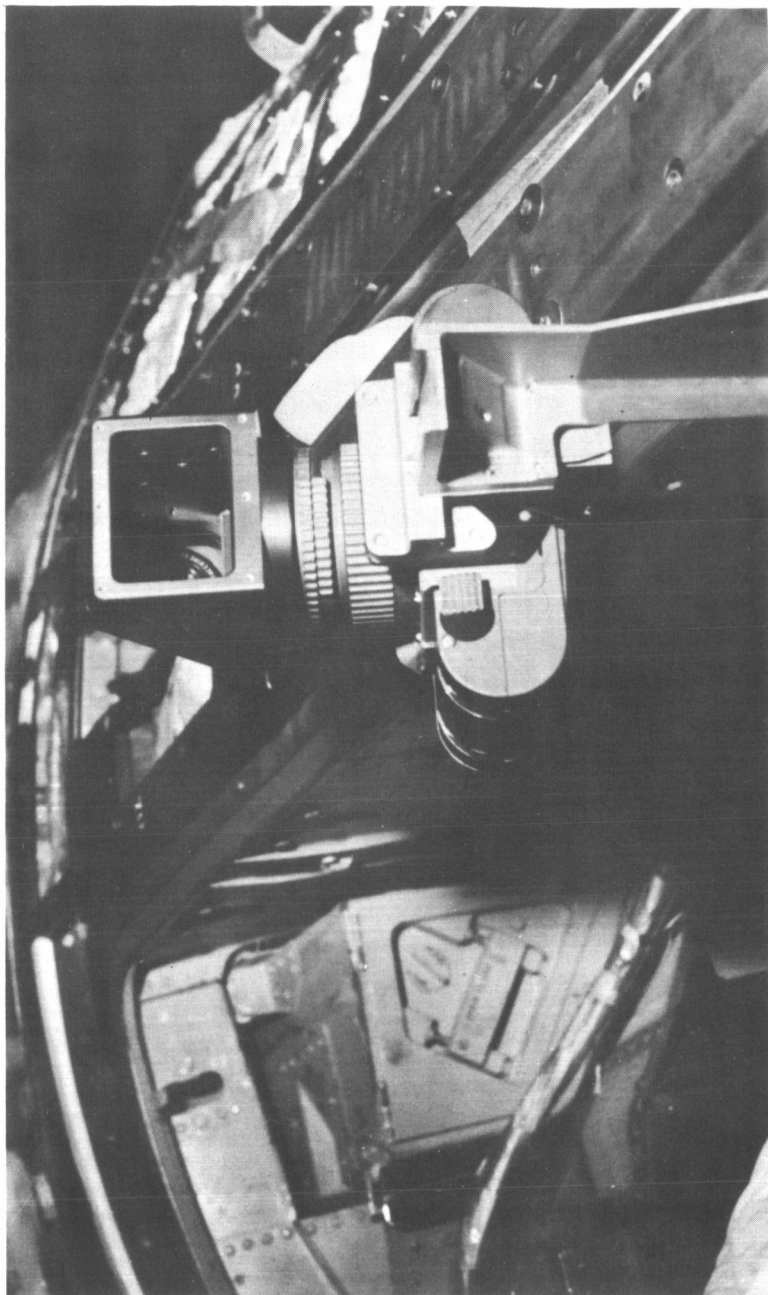


Figure 11-1. - Ultraviolet Astronomical Camera assembly mounted to spacecraft.

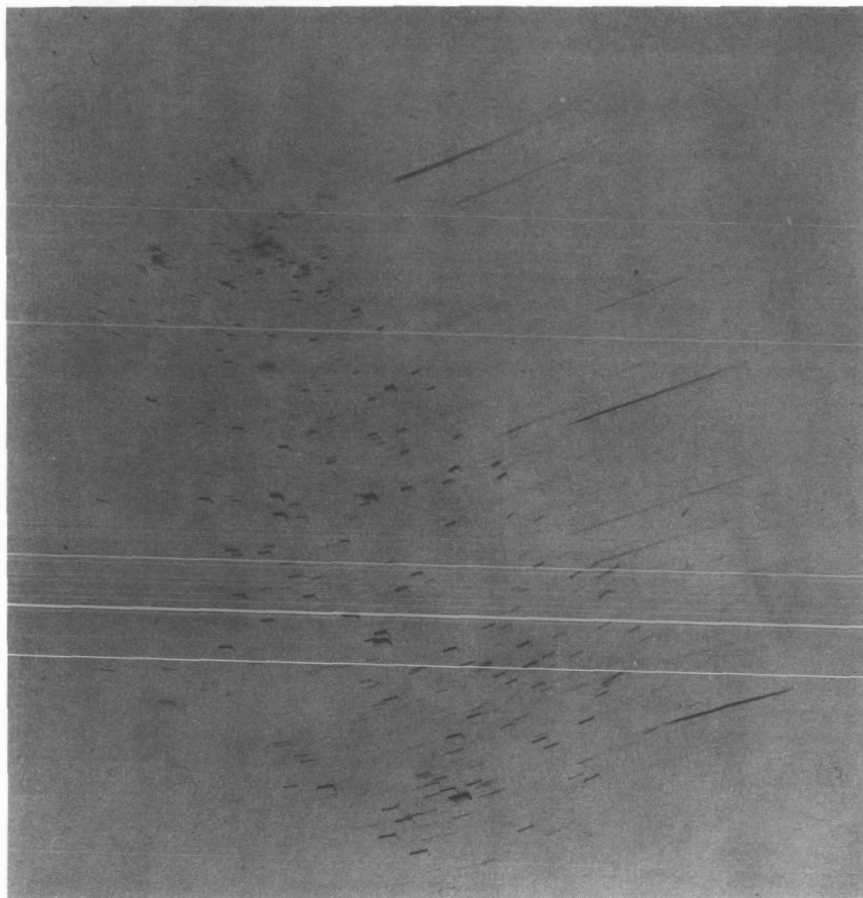
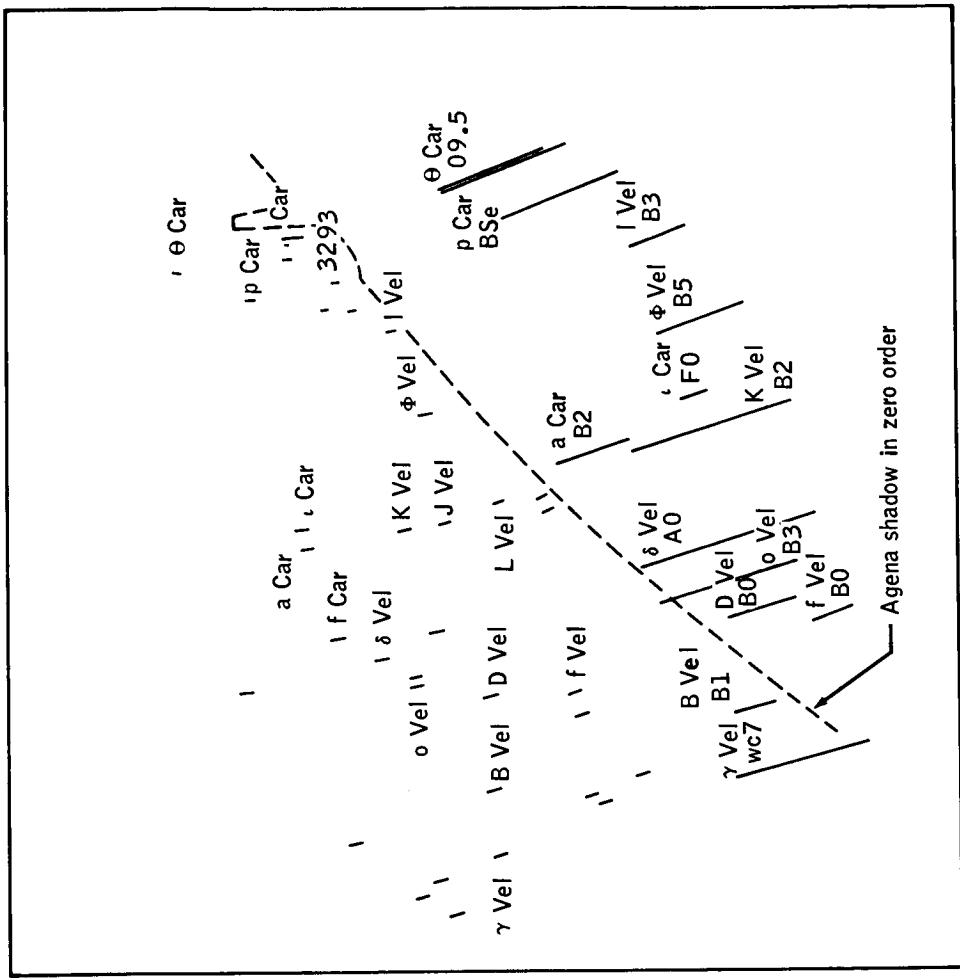


Figure 11-2. - Ultraviolet spectra of stars in the Carina-Vela region of the southern Milky Way.



UV STELLAR SPECTRA

Experiment S-13 Gemini 10 Frame 28
Dearborn Observatory, Northwestern University

Figure 11-3. - Key chart for figure 11-2.

12. EXPERIMENT S026 (S-26), ION-WAKE MEASUREMENT

By David B. Medved, Ph. D.
Electro-Optical Systems, Inc.

N68-14162

OBJECTIVES

The objective of the Ion-Wake Measurement (S026) experiment is to measure and confirm the ion and electron wake structure and perturbation of the ambient medium produced by the orbiting Gemini spacecraft. The experiment is designed to obtain the following:

- (a) A mapping of the spacecraft ion density wake as a function of position coordinates relative to the reference frame of the spacecraft
- (b) A contour mapping of the spacecraft electron density wake as a function of the same position coordinates
- (c) Determination of electron temperature as a function of the position coordinates
- (d) Detailed information on ambient ion and electron densities and electron temperature as a function of altitude and diurnal variations from the Gemini Agena Target Vehicle (GATV)
- (e) Ionization transients caused by spacecraft thruster firings

INTRODUCTION

The Gemini spacecraft moves through the ionospheric medium with a velocity that is high compared with the random thermal velocities of the ions but small compared with the random thermal motions of the electrons. The vehicle motion is supersonic with respect to the ions and subsonic with respect to the electrons. Electrons, therefore, approach the vehicle from all directions as if it were standing still, whereas the ions are swept up by the vehicle motion.

To an observer on the spacecraft, there is a ram ion flux to the vehicle along the direction of the vehicle velocity vector. The motion of the vehicle results in a sweeping out of the ions and neutral particles in its path. If the constituents of the ionosphere were completely

at rest, a shadow zone would extend an indefinite distance behind the spacecraft.

As a result of the random thermal motions, the shadow or hole region is filled in by a sequence of interacting mechanisms, with the region behind the orbiting vehicle actually being a plasma rather than an ion wake. Because the electrons approach the spacecraft from all directions, it would be expected that these would rapidly fill the shadow region. The electrostatic forces between these charged particles prevent substantial imbalances in the local space charge from occurring. The electrons are thus constrained by electric fields from moving too far away from their positive-ion counterparts.

EQUIPMENT

The electron detector (fig. 12-1) is located on the GATV Target Docking Adapter (TDA) and operates continuously during the experiment. Operation of the inboard and outboard ion detectors depends upon the angular relationship of the GATV with respect to the orbital velocity vector. The inboard ion detector provides useful data whenever the GATV moves TDA-forward with its axis parallel to the orbital path; the outboard detector is operative whenever the GATV yaws at right angles to the orbital path. The placement of the equipment on the GATV is shown in figure 12-1, and figure 12-2 shows a general ion-wake profile.

The sensors, shown in figures 12-3 and 12-4, are five-elevent retarding potential analyzers with ac modulation for low-threshold operation. They are designed to measure ion and electron densities over a range from 5×10^6 per cm^3 to 50 per cm^3 , with electron temperature measurements in a range from 3 electron volts down to zero. For contour mapping, position resolution to approximately 1 foot in accuracy is obtained from a 16-mm general-purpose sequence camera.

The sensor-electrometer systems each collect and modulate plasma current in a faraday cup containing four grids followed by a collector plate. The voltage bias placed on the front grid limits the minimum energy plasma particle which can enter the sensor. The second grid accelerates the properly charged particles which passed the first grid.

A third grid is driven by a 3840-hertz square wave which modulates the plasma current by alternately blocking and accelerating the particles passing through the second grid. A fourth grid actually consists of three screens connected together to act as a capacitive shield between the modulation grid (grid three) and the final collector. The third

screen in the final grid also serves as a collector for secondary photo electrons produced in the sensor.

The sensor output current is designed to swing from zero to the dc value of the input plasma current and back within 1 microsecond, with a 50-percent duty cycle at a frequency of 3840 hertz. This square-wave current is amplified by an ac electrometer located behind the sensor. Electrometer signals are synchronously demodulated and averaged by an analog signal processor carried aboard the GATV. A resulting voltage proportional to the logarithmic average is generated and buffered, then input to the analog-to-digital converter in the GATV telemetry system for transmission to the network tracking stations.

PROCEDURES

Two distinct modes are used during flight. These modes have been designed to obtain a maximum amount of information on the wake structure with minimal consumption of spacecraft fuel. Mode-A constitutes a direct axial mapping of the wake, which is accomplished by linear separation of the spacecraft from the GATV. This type of maneuver is accomplished during final departure of the spacecraft from the GATV. In this mode, ion data are obtained by the inboard ion sensor.

The primary data mode of the S026 experiment is mode-B, illustrated in figure 12-5. The maneuvers are intended to map the spacecraft wake using in-plane maneuvers. Mapping commences with docked spacecraft/GATV configuration in a TDA-south orientation. The spacecraft separates from the target vehicle and performs a maneuver to a specific position. This position is on an axis along the orbital velocity vector of both the spacecraft and target vehicle and passing through the outboard sensors, with the spacecraft nose approximately 1 to 3 feet away from the target vehicle. The spacecraft then translates downward, maintaining the axial separation as constant as possible for a distance of approximately 15 feet. The spacecraft stops and then proceeds to carry out the portions of the trajectory described in figure 12-5. The distances off-axis corresponding to the transverse motion of the spacecraft were purposely chosen in excess of the anticipated wake dimensions in order that all thruster firings required to change direction in the manner shown will occur in regions where plasma-wake data are not of critical interest.

RESULTS

The objectives of the experiment were met to only a limited degree due to fuel constraints encountered during the mission. The sensors were operative immediately after GATV shroud removal (6 minutes from Gemini Atlas-Agena Target Vehicle lift-off) until GATV power depletion several days after spacecraft landing. Measurement of local electron and ion concentrations and electron temperatures was carried out during all phases of the mission. During the Gemini X mission, there were two distinct measurements of wake and/or bow shock effects. These occurred during the docking and undocking maneuvers of the spacecraft. The bow shock effects are assumed to result from reflection of positive ions from the Gemini spacecraft and their subsequent measurement on ion sensors of the target vehicle.

A large amount of ambient data over the altitude band covered by the GATV from 160 to 750 nautical miles were obtained. These data will be of considerable interest to those engaged in studies of the ionosphere and also to those concerned with the effects of charges and the relaxation of charges on space vehicles during and following power propulsion in the ionosphere.

Real-time telemetry data were obtained from all three sensors during passes over the Air Force Eastern Test Range. Real-time telemetry data from the Canary Islands were transmitted over the aeromedical lines during the crucial undocking maneuvers. This real-time information was essential, because the GATV delayed-time tape recorder was inadvertently turned off during part of the undocking.

Photographs obtained with the 16-mm general-purpose sequential camera during the undocking and separation maneuver indicate that a considerable effort will be required to determine the effects of an apparent nonlinear separation which may have caused wake structure oscillations. In attempting a frame-to-frame reduction of the relative position coordinates of the two vehicles, a problem exists because of poor GATV definition and total loss of the GATV image during most of the departure after the separation distance had become approximately 100 feet. Other data were obtained during docking and station keeping and during the GATV primary propulsion system posigrade and retrograde firings.

CONCLUSIONS

Quick-look analysis of the data from the GATV orbits indicates that electron and ion temperatures were higher than estimated. The high

electron temperature accounts for the sensor saturation observed during the mission. This temperature measurement was 0.3 of an electron-volt at a 200-nautical-mile altitude during daytime conditions.

Spacecraft wake structure has been observed out to a distance of 100 feet from the vehicle. Some oscillatory behavior in the wake structure was observed. Wake data over a period of 10 minutes may be available from this mission. The theory of Gurevich and other Soviet scientists (ref. 1) predicted an oscillatory wake structure. It is not clear at this point whether these S026 observations are the result of spacecraft motion in and out of the wake or represent a confirmation of the Gurevich theory.

REFERENCE

1. Gurevich, A. V.; Al'pert, Ya. L.; and Pitaevskii, L. P.:
(H. H. Nickle, trans.): Space Physics With Artificial Satellites.
1965.

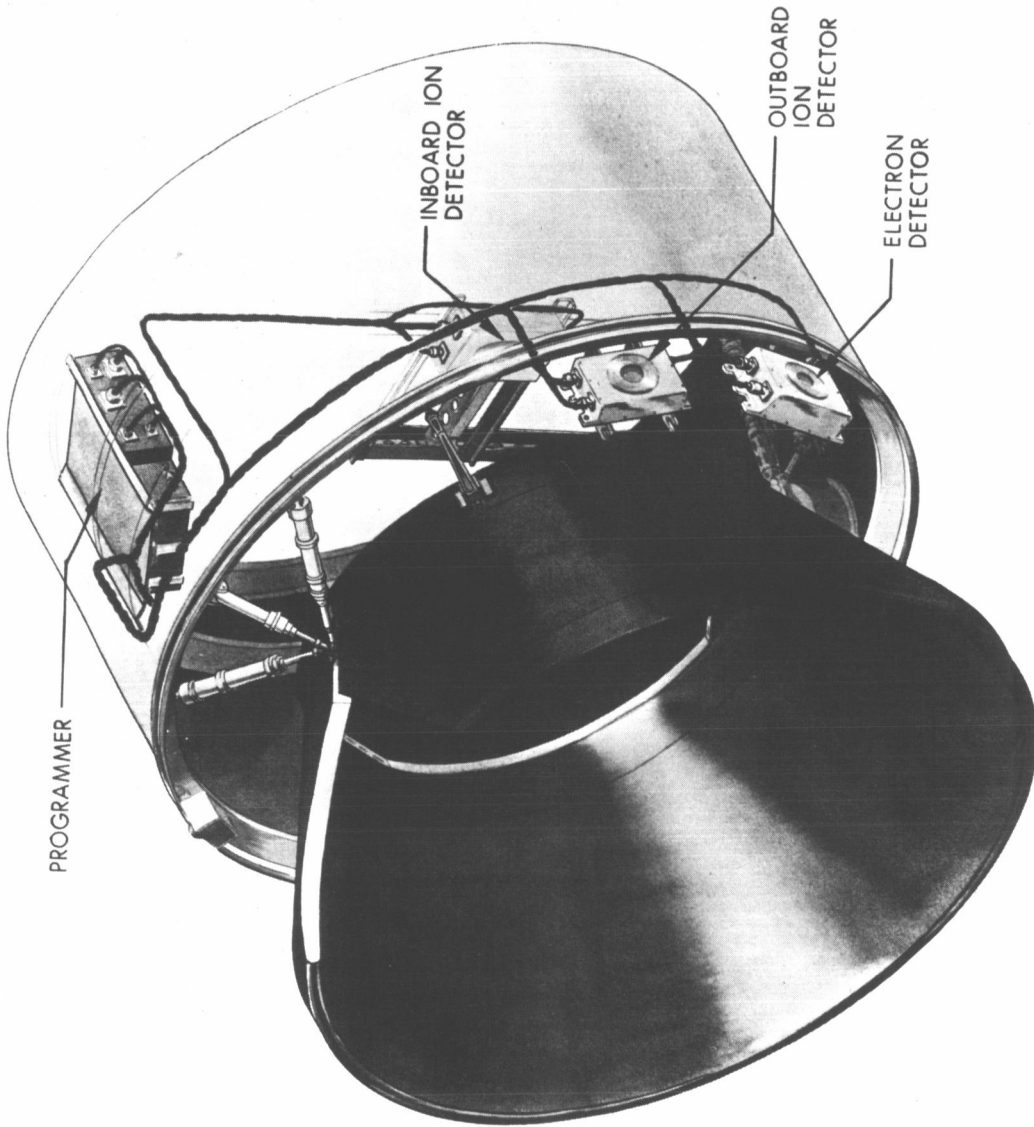


Figure 12-1.- Placement of ion-wake measurement equipment on GATV.

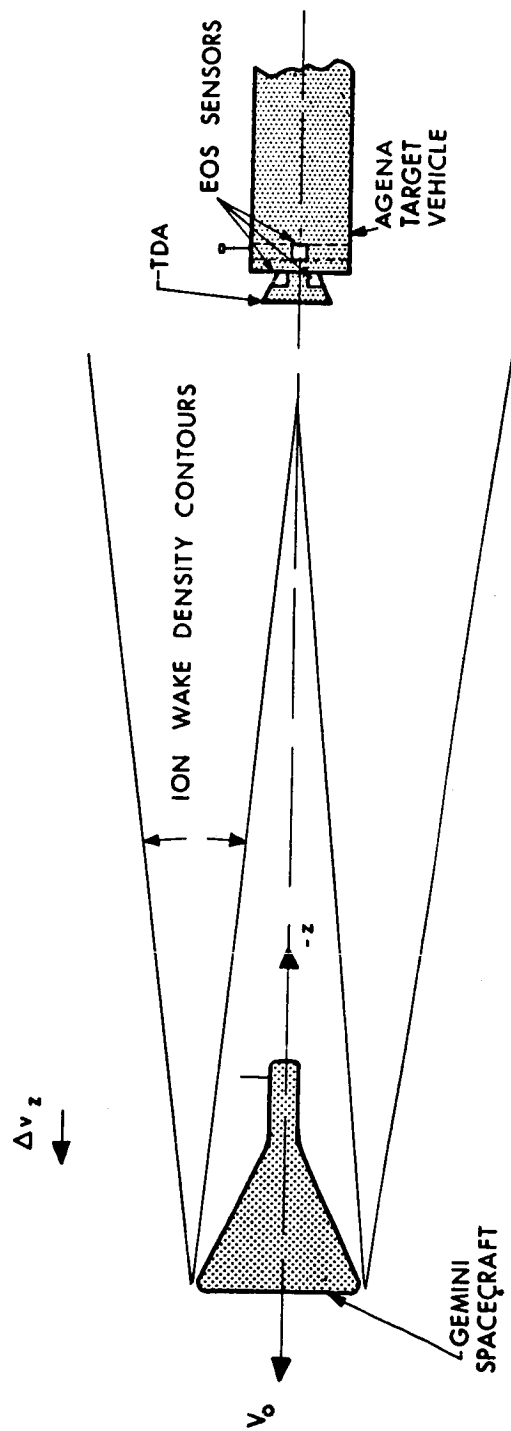


Figure 12-2.- General ion-wake profile.

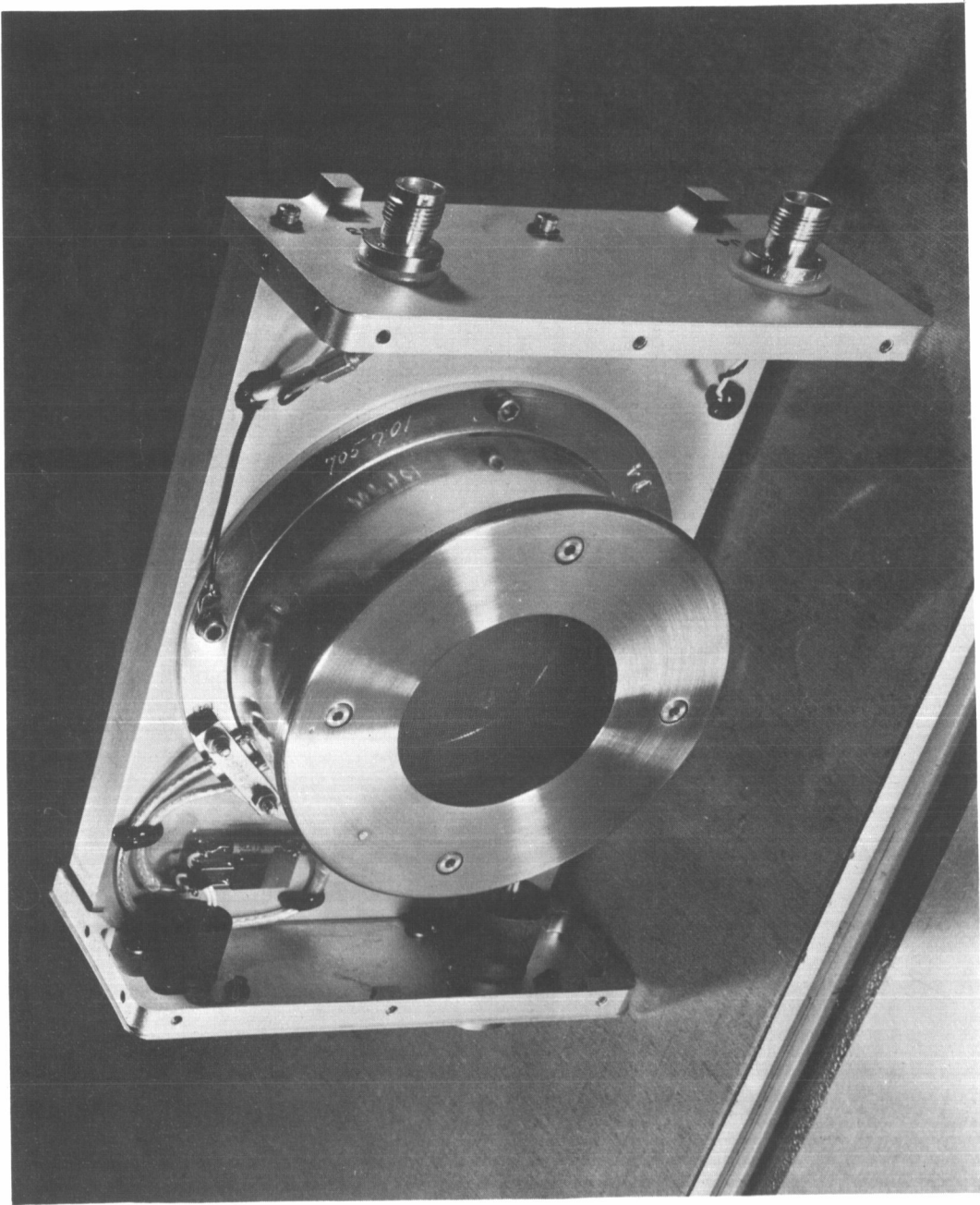


Figure 12-3. - An electron detector sensor.

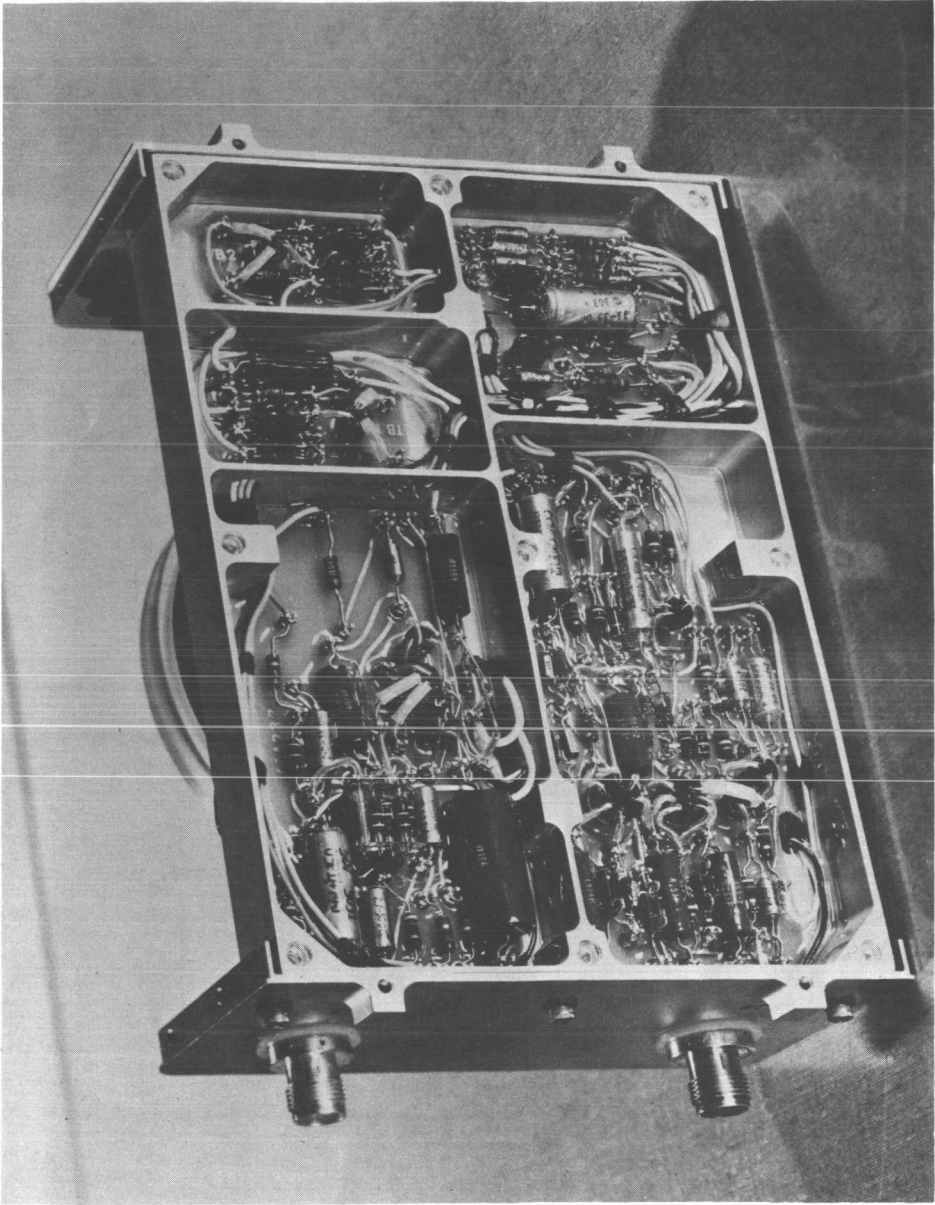
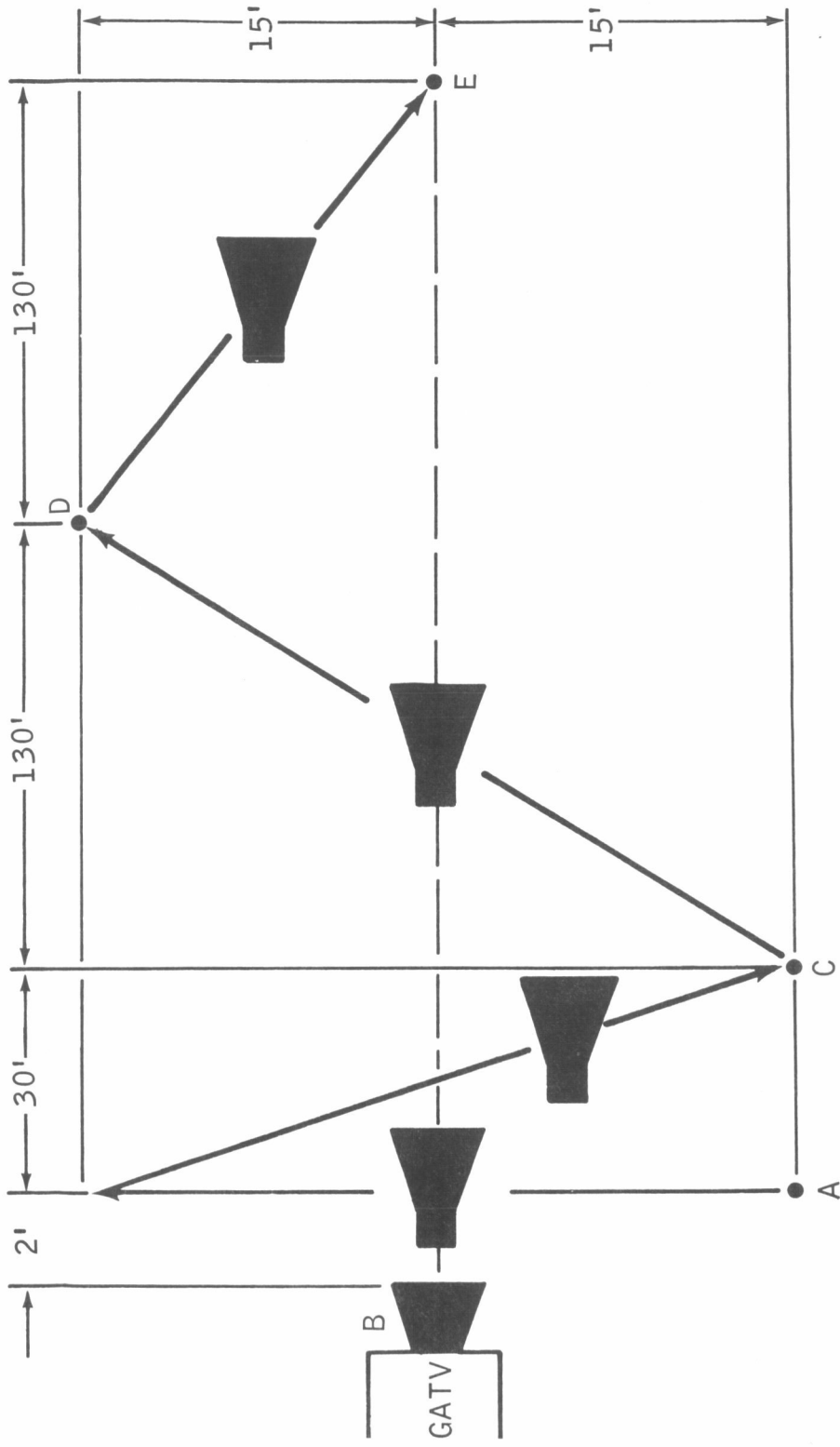


Figure 12-4. - View of sensor circuitry.



Total time of maneuvers = 10 min

Figure 12-5. - Gemini undocking maneuvers for ion-wake measurements.

13. EXPERIMENT D005 (D-5), STAR OCCULTATION NAVIGATION

By Robert M. Silva and Terry R. Jorris
Air Force Avionics Laboratory
Wright Patterson AFB

And

Eugene M. Vallerie, III
NASA Manned Spacecraft Center

OBJECTIVES

The purpose of experiment D005 (D-5), Star Occultation Navigation was to provide information on equipment and procedures to determine the usefulness of star occultation measurements for space navigation and to determine a horizon density profile.

This experiment was designed to make maximum use of man's capabilities in orbit in order to provide the simplest and most reliable systems. In this experiment, the astronauts had to accomplish the task of star acquisition, identification, calibration, and tracking. Instrumentation was required only to measure the relative intensity of the star as it set into the atmosphere.

The instrumentation designed for this experiment was designed to gather experimental data on star occultations over the entire attenuation phenomena.

EQUIPMENT

The star occultation photometer is a single-unit, dual-mode, hand-held externally powered instrument for electronically determining the extent to which the sight line to a selected star penetrates a planetary atmosphere. It also measures the contrast of a sun-illuminated ground target. Data from the instrument, when calibrated and plotted against time, provide the attenuation curve of a star passing through the earth's atmosphere relative to an unattenuated intensity. General characteristics of the instrument are as presented in the following table.

Size, in.	5 by 5 by 3
Weight, lb	2.5
Volume, cu in.	30

The star occultation photometer optical system is a dual-path type, separated on a wavelength basis by a dichroic reflector. One path carries the short-wavelength star spectrum (0.4 to 0.5 micron) to the photo multiplier cathode; the remainder of the star light continues along a second path into the operator's eye. The instrument's optical characteristics are summarized as follows:

<u>Lens system</u>	<u>Aperature</u>	<u>Focal length,</u> <u>in.</u>	<u>Wavelength,</u> <u>Å</u>	<u>Magnification</u>
Objective	32 mm	4.6	3500-7000	--
Eyepiece	0.788 in.	0.73	5000-7000	6X
Path no. 1	0.2 in.	0.33	3500-5000	1/16
Path no. 2	0.4 in.	0.277	--	--

The electronic system consists of a photomultiplier detector, pre-amplifier, active bandpass-filter amplifier, and postfilter amplifier-demodulator in the carrier signal section. The dc-signal section contains an active low-pass filter, calibration level detector, and indicator lights. A unijunction oscillator and three flip-flops are used to generate two-phase, 100-cps power for the size-5 hysteresis-synchronous modulator motor. Input power to the motor is regulated. Additional voltage regulators supply isolated low voltage to the signal circuitry and high voltage to the photomultiplier. The output of the low-pass filter is conducted to the input of the Schmitt trigger level detector biased at approximately one volt. Depressing the calibrate pushbutton inserts a nominal 5-to-1 attenuator in both day and night signal paths, lowering the full signal amplitude from 5 volts to 1 volt for calibration. The photometer is readied for use by plugging in one cable for power and one for high-level telemetry and by placing the mode switch to NIGHT. The photometer is shown in figure 13-1.

The Gemini X photometer was a instrument which had been refurbished and recalibrated after its inflight failure during the Gemini VII mission. The failure was caused by loose particles in the photomultiplier tube. A stringent quality control program designed to identify and count all loose particles was instituted in preparation for the Gemini X flight. Each photomultiplier tube considered for use was examined under a microscope, and all particles were sized to assure that the aggregate was not

larger than the smallest element spacing in the photomultiplier tube. Since the equipment worked as designed on the Gemini X mission, these quality control measures apparently had the desired effect.

PROCEDURES

Knowledge of the time of occultation of a known star by a celestial body, as seen by an orbiting observer, determines a cylinder of position whose axis is the line through the star and the body center and whose radius is equal to the occulting body radius. The times of six occultations provide information to uniquely determine all orbital parameters of the body. Determination of these times of occultation from the earth is difficult due to atmospheric attenuation of the star light. The star does not arbitrarily disappear but dims gradually into the horizon. Measurement of the percentage of dimming with respect to the altitude of this grazing ray from the star to the observer provides a percentage altitude for occultation. In other words, a star can be assumed to be occulted when it reaches a predetermined percentage of its unattenuated value.

The D005 experiment procedures provide the means of measuring this attenuation with respect to time to determine the usefulness of the measurements for autonomous space navigation. In addition, the measurements provide a density profile of the atmosphere to update the atmospheric model for use in star occultation navigation as well as other forms of horizon-based navigation and orbit prediction.

Star occultation measurements are made by identifying, acquiring, and tracking a selected star in the 1/2-degree reticle of the 10-degree field of view of the photometer. The light intensity of the star is normalized to the 5-volt telemetry output by depressing a calibrate button and adjusting the gain to drive the reticle light to an alternating red-green condition. Thus normalized, the button is released and the star is tracked as it disappears into the horizon. The star intensity is measured, recorded, and time-correlated on the onboard telemetry tape for postflight analysis. On any night pass, four to six stars are acquired, calibrated, and tracked to occultation, and the star and approximate time of occultation are recorded in the flight log for postflight correlation with tape-recorded data and ground-track information. Timing marks are recorded on the telemetry (using the calibrate button) on some runs to identify special selected observations such as time of star passage through the top of the airglow. Postflight data reduction and analysis include the following operations.

(a) Occultation measurements are inserted into the navigation equations to determine orbital parameters. Results are then compared with ephemeris data to determine the accuracy of the calculations.

(b) Ground track position data are used to determine the altitude of the grazing rays with respect to atmospheric attenuation to provide an atmospheric density profile.

(c) The newly determined atmospheric model is used to recompute navigation parameters from star occultation measurements. These are compared with ephemeris data and the previous navigation measurements to evaluate the degree of improvement.

A mode-D procedure was established shortly before printing of the Gemini X final flight plan. This mode required the use of the spacecraft computer and photometer data for real-time orbit navigation determination. Ground analysis will compare this solution with ground-track data to determine how well the orbit was established by the onboard technique.

RESULTS

The photometer was used twice during the mission. It was used the first time at 26 hours 30 minutes ground elapsed time (g.e.t.), while the spacecraft was docked with the Gemini Agena Target Vehicle (GATV), and the second time at 64 hours 46 minutes g.e.t. after the spacecraft and GATV had separated.

During the first attempt to perform the experiment in mode-A (calibration), difficulty was encountered in vehicle-attitude control because of the docked configuration. Due to the control problems, only five stars were tracked to total occultation. Since a minimum of six stars are required for complete computation, a total solution was not obtained.

A problem was encountered in tracking stars through the airglow. As the stars passed through the green glow layer, they disappeared momentarily. When acquisition was lost, the pilot discontinued sighting through the photometer until the stars reappeared below the green glow, and then he resumed tracking the stars through the photometer until they disappeared into the lower, dark horizon. Excessive attitude control gas expenditure during this procedure led to cancellation of further runs until after undocking.

The second experiment run was a mode-D sequence using the undocked configuration. No difficulties were encountered on this run with regard to the acquisition and tracking of seven stars to occultation; however,

procedural difficulties were encountered in entering the visual occultation data into the computer. Computation of an orbit solution was precluded because of improper entry of the right ascension and declination of the last star, and computer workload problems encountered after the measurement taken on the fourth star.

A calibration check on three stars in Cygus was not properly accomplished on either run. An attempt was made to calibrate on each star independently rather than to retain one gain setting. This does not affect the use of the occultation technique for navigation but was included to aid in data analysis and reduction.

Visual occultations through the photometer reported by the pilot were somewhat different from those reported by the command pilot. The command pilot could still observe some stars visually after the pilot had reported their disappearance. The phenomenon was probably caused by the selective reflection within the instrument which is designed to allow maximum blue light to fall on the photomultiplier tube.

Representative telemetry plots of normalized star light intensity from Gemini X, with time in seconds horizontally and normalized star intensity in volts vertically, are given in figures 13-2 to 13-4. A considerable amount of information can be derived from a visual analysis. In figure 13-2, the constant output portion of the Vega star curve can be clearly seen; this flat portion of the curve corresponds to the time the star remains well above the earth's atmosphere. As the line of sight to the star begins to pass through the upper portion of the atmosphere, the apparent intensity of the star begins to diminish (point A). In the lower portions of the atmosphere the downward slope approaches a straight line (point B to C) until the star seems to disappear into the background. In the straight-line portion, a time of percentage attenuation, with accuracy to within approximately one-half second, can be picked off by eye. The visual method of occultation time-determination would then limit the accuracy of the navigation solution to 2-1/2 nautical miles; however, if computer smoothing were used, as is anticipated for operational use, greater accuracies are achievable. Initial results of entering the occultation voltages into a computer for smoothing prior to calculation indicate time determination accurate to 0.1 to 0.2 seconds of time.

Orbit solutions based on these Gemini X timing accuracies and star occultation sequences as outlined in Gemini X flight plan would have provided navigation accuracies of approximately 1 nautical mile rms.

Procedures for occultation measurements are visible in traces from Arcturus shown in figure 13-3. At point 1 the photometer was turned on; calibration began at point 2 by depressing the calibration button; between 2 and 3 calibration is being accomplished; when complete at point 3,

the button is released and the photometer output jumps to the normalized 5-volt level. Sixty seconds later the intensity begins its rapid drop.

The noise apparent on the intensity signal is greater for the measurements to Arcturus than Vega, even though both stars are of the same approximate magnitude. This effect was anticipated because the photometer is constructed to be sensitive only to the 0.4 to 0.5 micron or blue visual light, and Arcturus is a more predominantly red star.

With the present photometer, stars down to and slightly below second magnitude can easily be used as shown in figure 13-4. The trace from Denebola is still well defined and shows a clear slope for time of occultation determination.

CONCLUSIONS

The experiment equipment appeared to function nominally, indicating that the stringent quality control procedures effected after the failure of the photomultiplier tube on a previous mission were justified. The compact design of the equipment allowed the equipment to exhibit its versatility when used during the docked configuration. The possibility of using the photometer, suitably modified to provide direct inputs into the spacecraft computer, for onboard orbit determination was verified. The use of direct inputs into the spacecraft offers advantages of simpler programming, no analog-to-digital conversion in the computer, and simpler system integration, but would sacrifice some accuracy.

The star occultation technique has both accuracy and flexibility and is a useful technique for automatic (for example, incorporation with star trackers), semi-automatic, or aided-manual navigation applications.

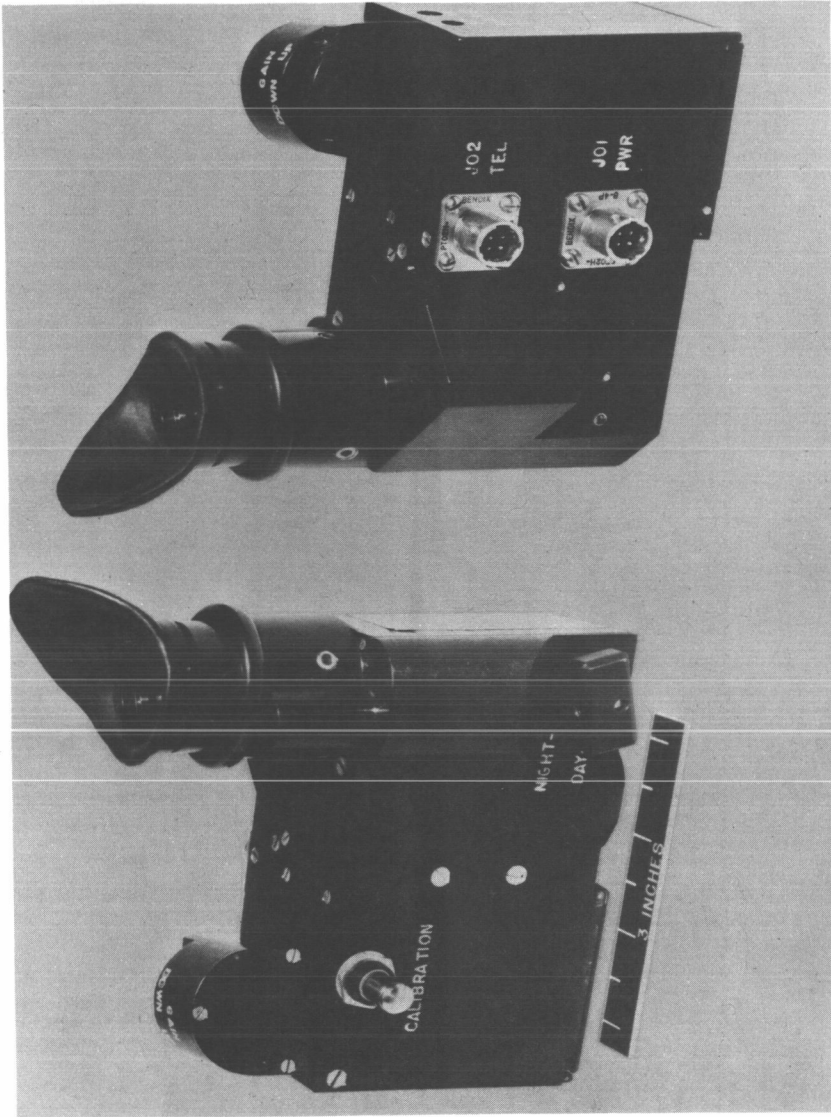


Figure 13-1.- Star occultation photometer.

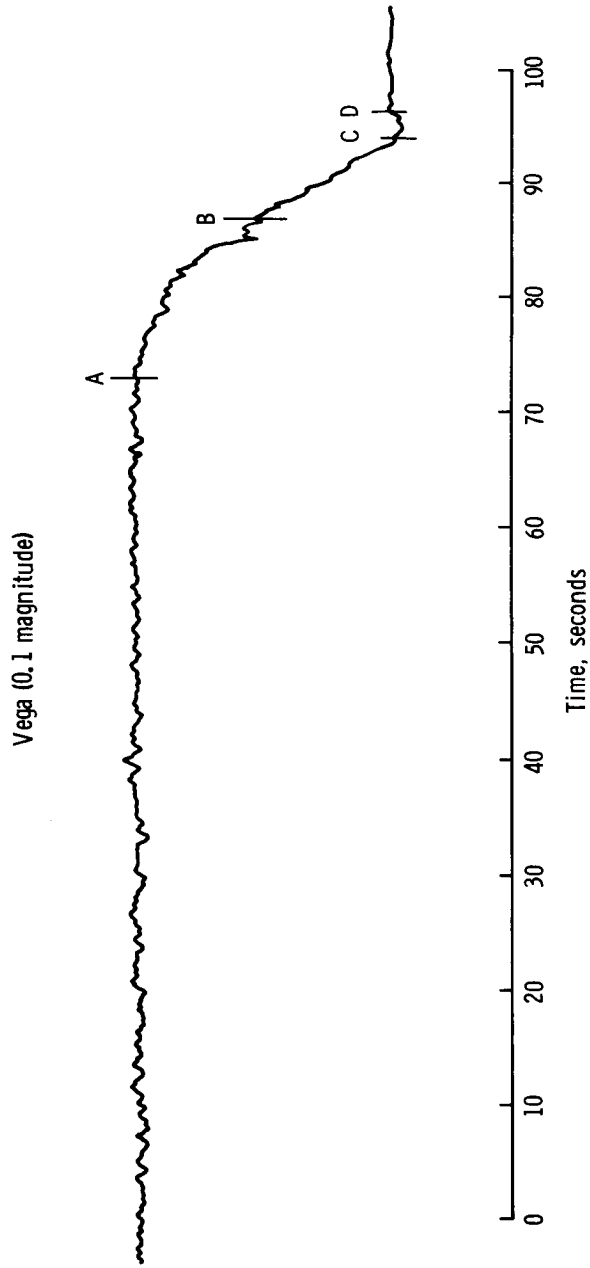


Figure 13-2.- Telemetry intensity profile of star Vega.

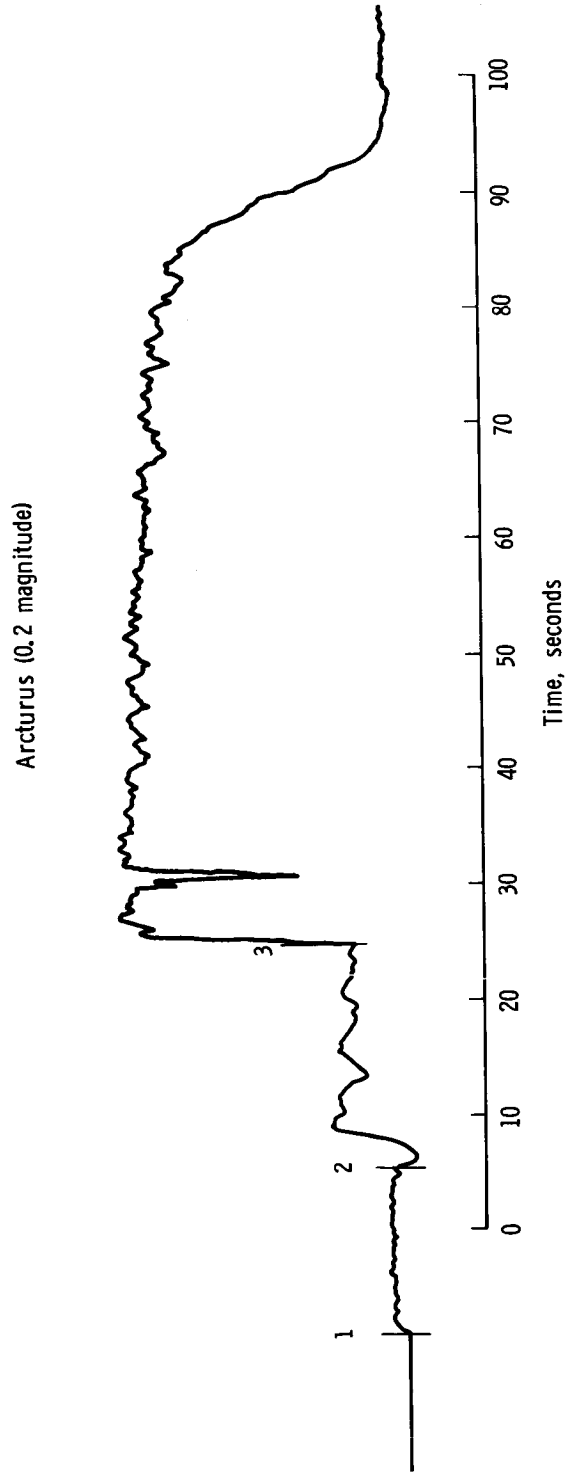


Figure 13-3. - Telemetry intensity profile of star Arcturus.

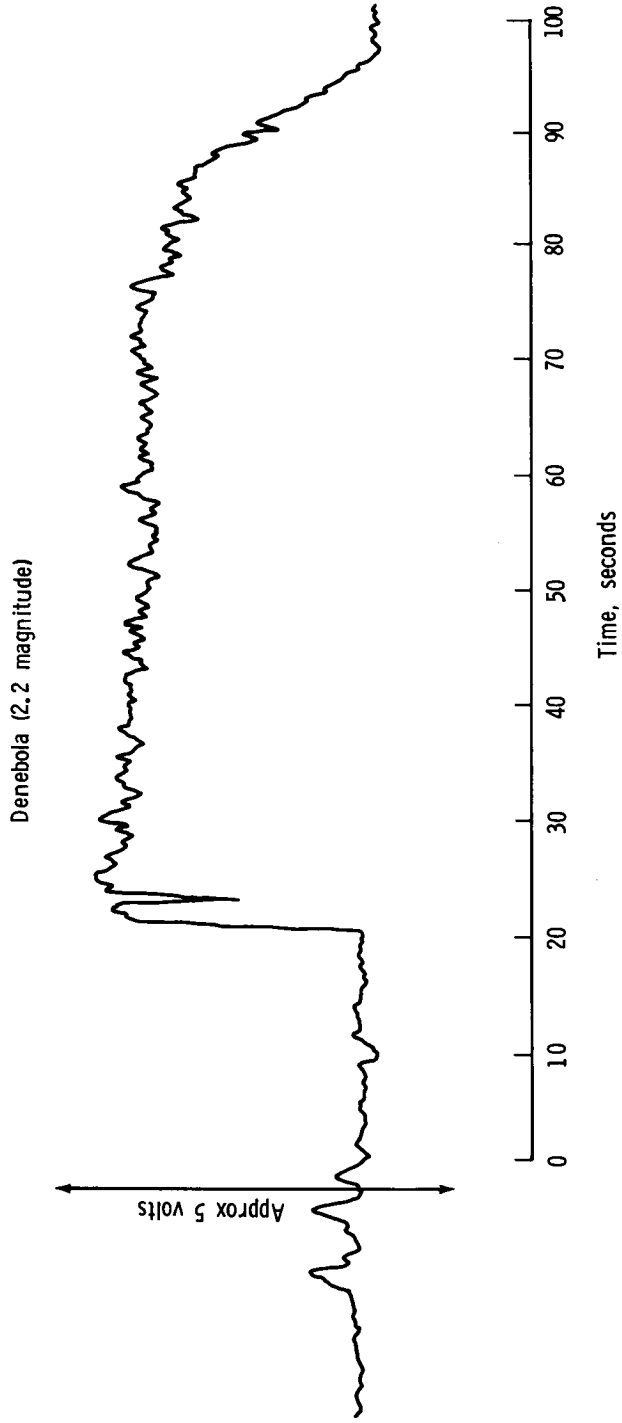


Figure 13-4. - Telemetry intensity profile of star Denebola.

14. EXPERIMENT DO10 (D-10), ION-SENSING ATTITUDE CONTROL

By Rita C. Sagalyn
Air Force Cambridge Research Laboratories
L. G. Hanscom Field

OBJECTIVES

The principal objective of the Ion-Sensing Attitude Control experiment was to investigate the feasibility of an attitude control system using environmental positive ions and an electrostatic detection system to measure spacecraft pitch and yaw. A secondary objective was to measure the spatial and temporal variations of ambient positively-charged particles along the orbital path of the Gemini spacecraft.

EQUIPMENT

The onboard spacecraft equipment consisted of two independent systems for the measurement of pitch and yaw attitudes. Dimensionally and electrically, each system was identical, except for placement of the sensor about the pitch and yaw axis. Each sensor configuration was mounted on a boom approximately three feet in length. The boom was extended by crew command after spacecraft orbital insertion. The locations of the booms and sensors are shown in figure 14-1. The sensor locations and boom lengths used are selected to minimize vehicle shadowing and space charge effects.

To illustrate the principle of operation of the sensor systems, the measurement of pitch is analyzed. Except for the alinement change, the analysis of the yaw measurement is identical. By alining two sensors along the pitch axis as shown in figure 14-2, the current to the collector of each sensor is given by

$$i_1 = N e v a A \cos (45 - \theta) \quad (1)$$

where i_1 is the current to sensor 1, and by

$$i_2 = N e v a A \cos (45 + \theta) \quad (2)$$

where i_2 is the current to sensor 2, and when

N = ambient positive ion density

e = electron charge

v = spacecraft velocity

a = experimentally determined grid transmission factor

A = aperture area of sensors 1 and 2 (identical)

θ = pitch-angle deviation from 0 degrees

Solving equations 1 and 2 for θ ,

$$\tan \theta = \frac{i_1 - i_2}{i_1 + i_2}$$

For θ less than or equal to 20 degrees, $\tan \theta$ is approximately equal to θ , in radians. The output of the sensors may, therefore, be displayed on a meter calibrated in degrees.

A block diagram for the pitch or yaw system is shown in figure 14-3. The output of each sensor is amplified by two electrometer amplifiers. To obtain desired accuracy over the current range of 10^{-6} to 10^{-10} amps, linear amplifiers with range switching are employed. The outputs of the electrometers, designated V_1 and V_2 , are then electronically added, subtracted, integrated, and compared. The final output, $\tan \theta$, referred to as the compared output, is indicated on a meter in the crew station and transmitted by telemetry to the ground stations. To fully evaluate the experiment, the direct outputs of the electrometers, the range analog indication, and the calibrate monitor signal are also transmitted by the spacecraft telemetry. These outputs would not be required in an operational attitude control system. The experiment was designed for precise pitch and yaw angular measurements over the range of ± 20 degrees; however, there is no basic limitation to the magnitude of the angle which can be measured.

Sensor system characteristics are as follows for each of the two systems:

Weight (including electronics and sensors), lb	7
Power (at 28 V), watts	3.5
Electronics response time, milliseconds	<1
Dimensions, in.	11 by 6.5 by 6
Angular measurement range, deg	±20

PROCEDURES

Seven principal modes of operation were requested for the Gemini X mission and four were accomplished. These were as follows:

- (a) Mode-C, Roll Attitude Study: This procedure consisted of rolling the spacecraft through 720 degrees at a rate of approximately 3 deg/sec while holding the spacecraft pitch and yaw constant at zero.
- (b) Mode-D, Pitch Attitude Study: This procedure consisted of maintaining a fixed yaw and roll attitude, then varying the pitch angle through a specified angular range at a rate of approximately 0.1 deg/sec. This rate was specified to insure good comparison of the experiment results with the Inertial Guidance System. The rate of 0.1 deg/sec was determined by the telemetry bandwidth available for the experiment.
- (c) Mode-E, Yaw Attitude Study: This procedure consisted of maintaining a fixed pitch and roll position, then varying the yaw angle through a specified angular range at the rate of approximately 0.1 deg/sec.
- (d) Mode-G, Random Data Accumulation: The ion-sensor switch was left on in this mode while the spacecraft was in drifting flight.

The other three modes of operation consisted of mode-B, ambient ion accumulation under controlled spacecraft conditions, mode-F, the study of photo-emission effects on the sensor, and mode-H, the study of translation-thruster effects. These were not accomplished because of the real-time constraint placed on use of spacecraft propellants.

RESULTS AND CONCLUSIONS

Discussions with the flight crew at the experiment debriefing provided information on the flight operation of the experiment. These discussions resulted in the following conclusions:

(a) In both mode-D and mode-E, the crew were able to compare the two flight-direction meters. One meter showed the output of the Inertial Guidance System and one showed the experiment sensor output of pitch plus yaw. The results showed that the experiment sensors agreed very well with the spacecraft Flight Director Indicator.

(b) The response of the experiment sensors to variations in pitch and yaw was extremely rapid.

(c) When the spacecraft thrusters were firing, the experiment sensor indications went off-scale due to the varying charge on the vehicle and/or the contamination in the immediate vicinity of the spacecraft. Readings returned to normal rapidly after the thrusters ceased firing.

(d) The experiment operated for approximately 12 hours: 2 hours 15 minutes in mode-A, 8 hours in mode-G, approximately 1 hour in mode-E, 35 minutes in mode-D, and 15 minutes in mode-C.

Both the postflight analysis of the transmitted data and the astronauts' inflight comparison of the ion-sensing system with the inertial guidance system showed that the two systems agreed in absolute magnitude very well in the measurement of both pitch and yaw angles. The response of the experiment to variations in angular position was extremely rapid, of the order of milliseconds.

An example of the simultaneous measurement of the ion yaw sensor output and the inertial yaw data during a controlled maneuver is shown in figure 14-4. The magnitudes of the angles at a given time agree within the experimental error of the systems. The inertial yaw measurement accuracy is of the order of 2° . The ion yaw accuracy for the Gemini spacecraft is $\pm 0.25^\circ$. The inertial data given in figure 14-4 illustrate certain characteristics which introduce difficulties in the manual control of the spacecraft. That is, when the yaw angle is varied, a lag in the response time of the order of 8 seconds occurs. The step-like variations in yaw angle, giving jumps of the order of $1-1/2^\circ$ in the inertial measurement, are partly due to the synchronous detectors used in the inertial guidance system, but also partly due to the manner in which the data are digitized through the telemetry system. The addition of an ion yaw sensor alone would therefore be a significant improvement in existing attitude systems.

The existing inertial system requires about 40 minutes to stabilize and warm up after power turnon. This is partly due to the electronic circuits used and the adjustment of the gyroscopes on the unit; however, the astronauts have found that the use of the ion yaw angular measurements significantly decreases the time for platform alinement.

An example of the simultaneous measurement of pitch angles with the ion sensor and inertial systems is given in figure 14-5. It is seen that the absolute values of the angles agree within a fraction of a degree over the angular range of $\pm 20^\circ$. A good illustration of the response time of the two systems is seen in figure 14-5 between 66 hours, 0 minutes and 66 hours, 5 minutes. While individual maxima and minima in pitch agree very well, the faster response of the ion sensor makes it easier to detect angular changes. Operationally, this should be of particular importance in conserving thruster fuel and under conditions where very precise angular positioning is desired.

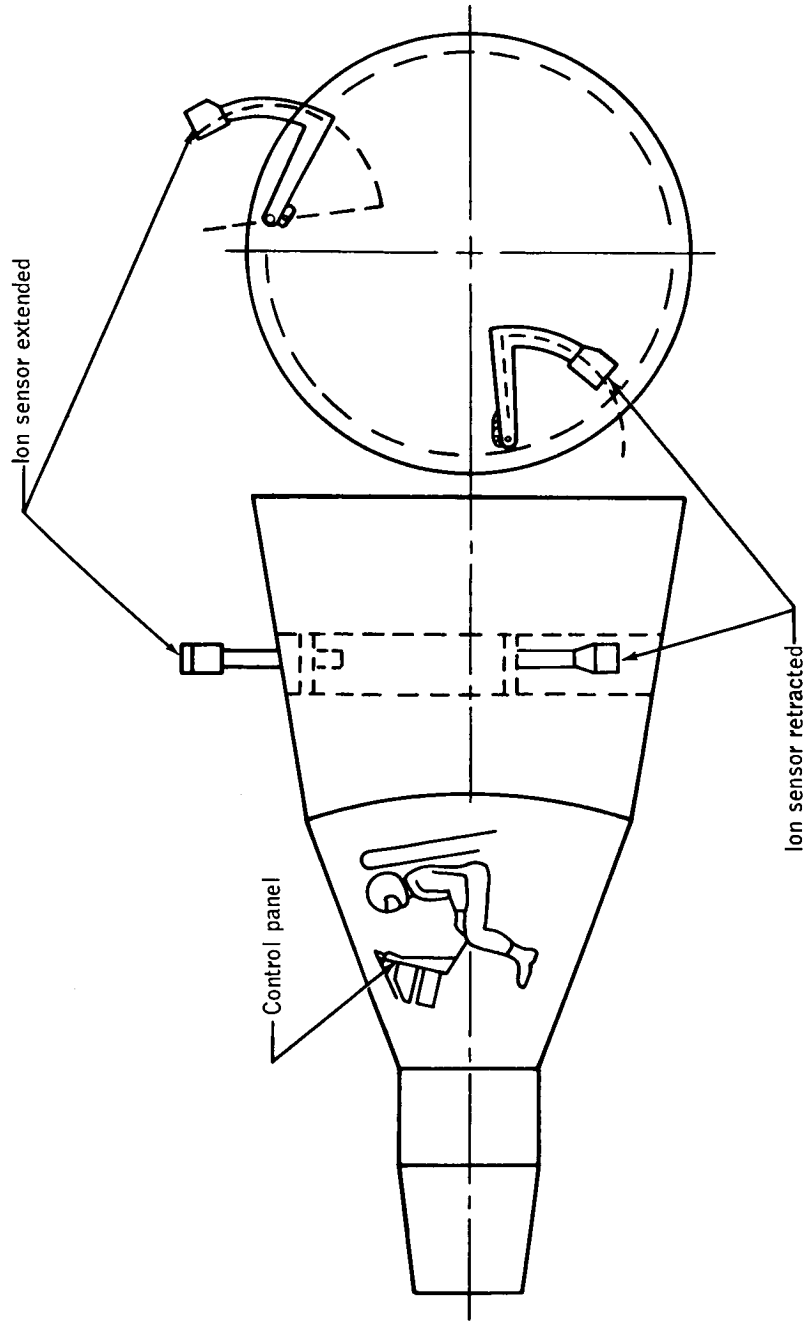


Figure 14-1. - Location of ion-sensing attitude control equipment.

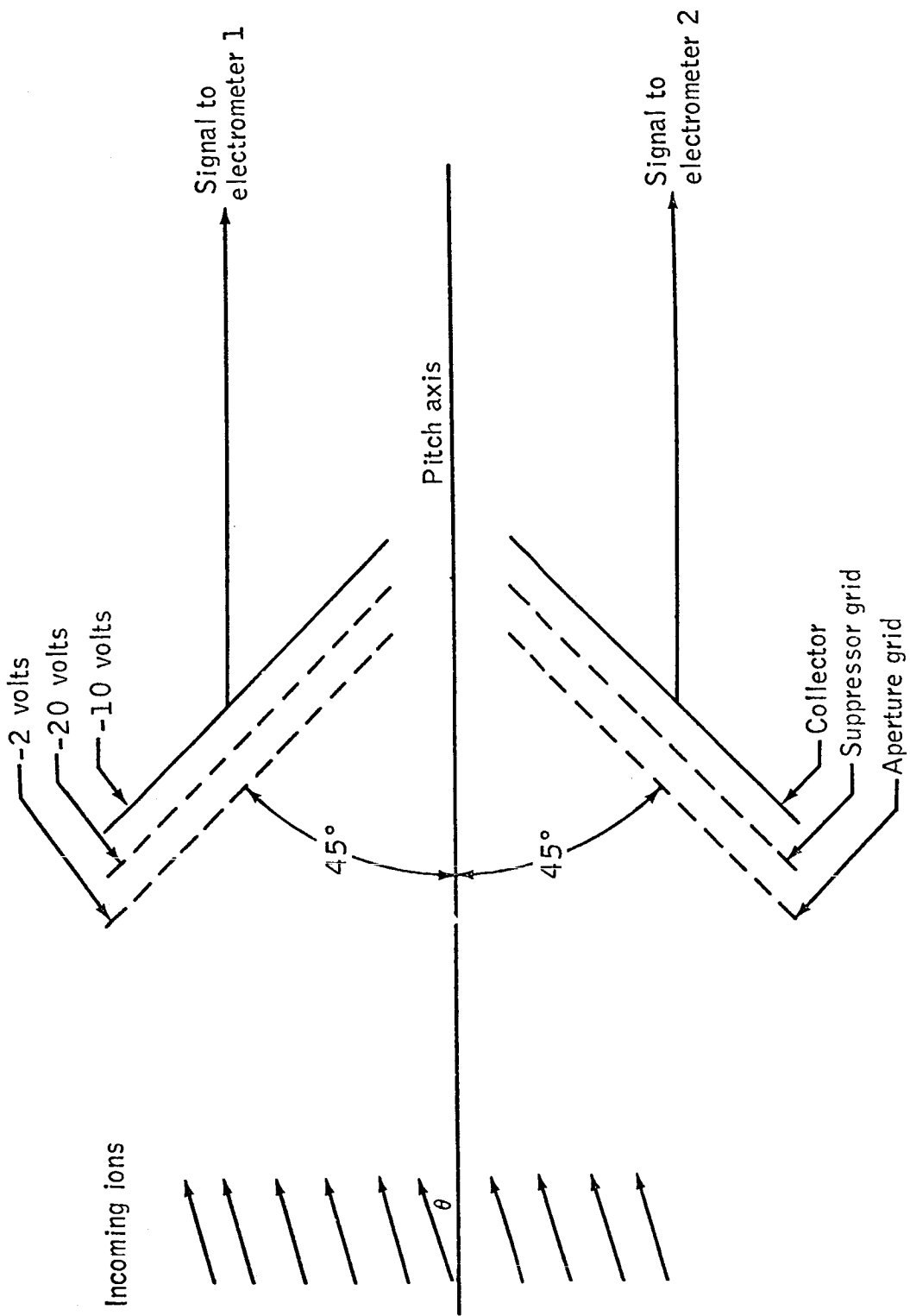
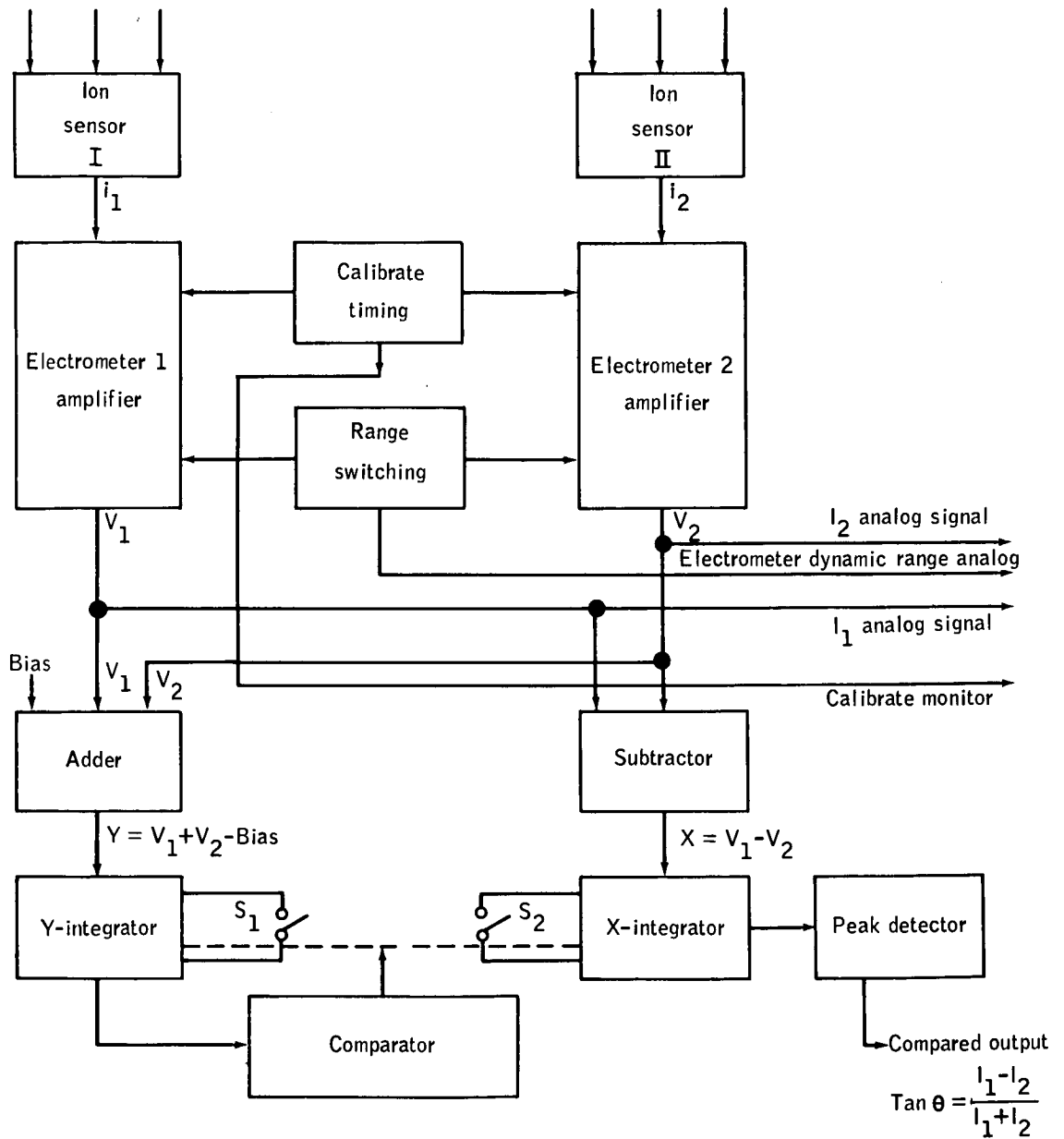
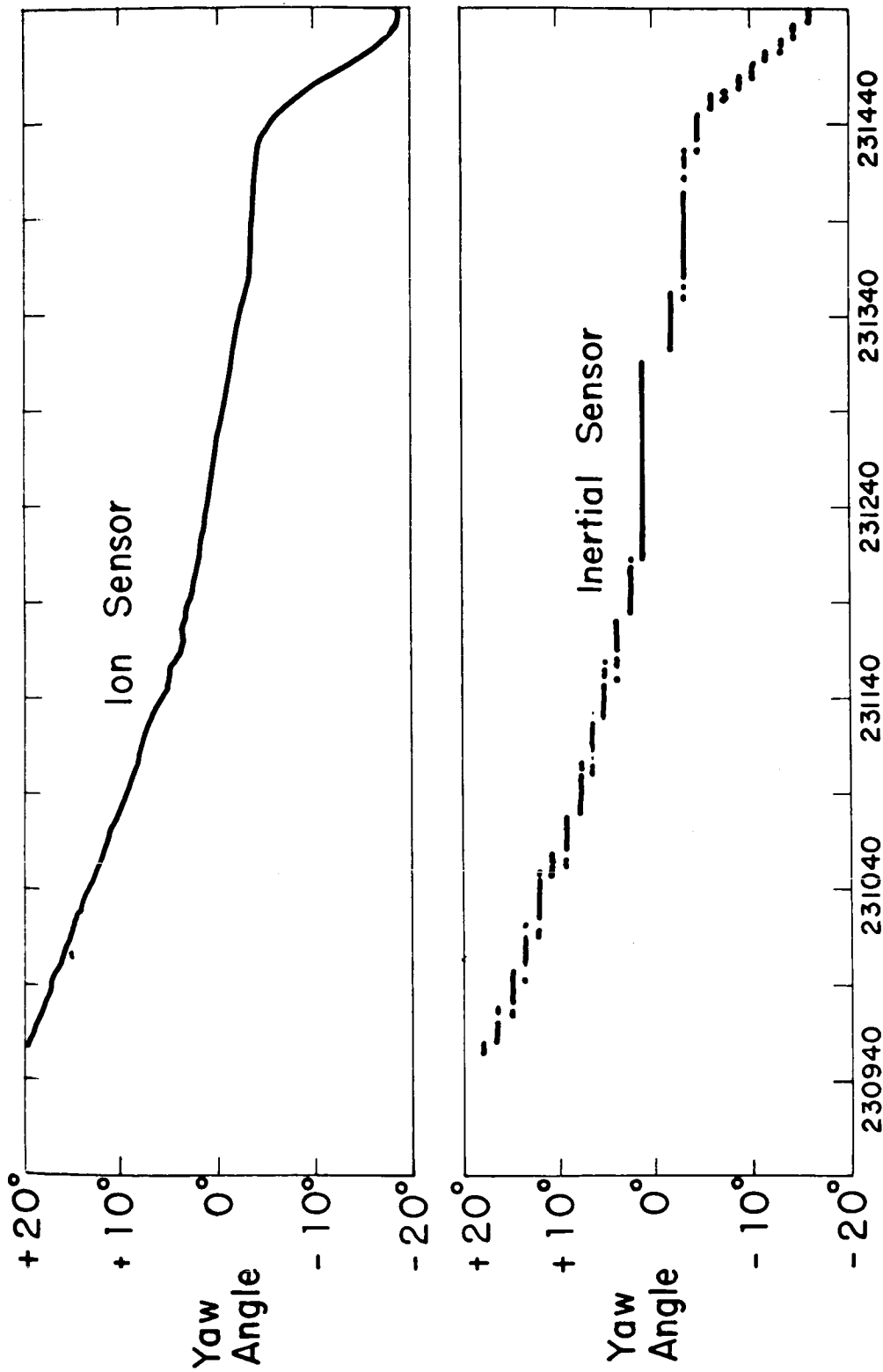


Figure 14-2.- Ion-sensing configuration.



Note: $i_{1,2}$ = Ion sensor current signals
 $V_{1,2}$ = Ion sensor voltage signals

Figure 14-3. - Ion-sensing attitude control electronics system.



Time from Launch (seconds)

Figure 14-4. - Comparison of ion attitude yaw angle measurements with inertial system.

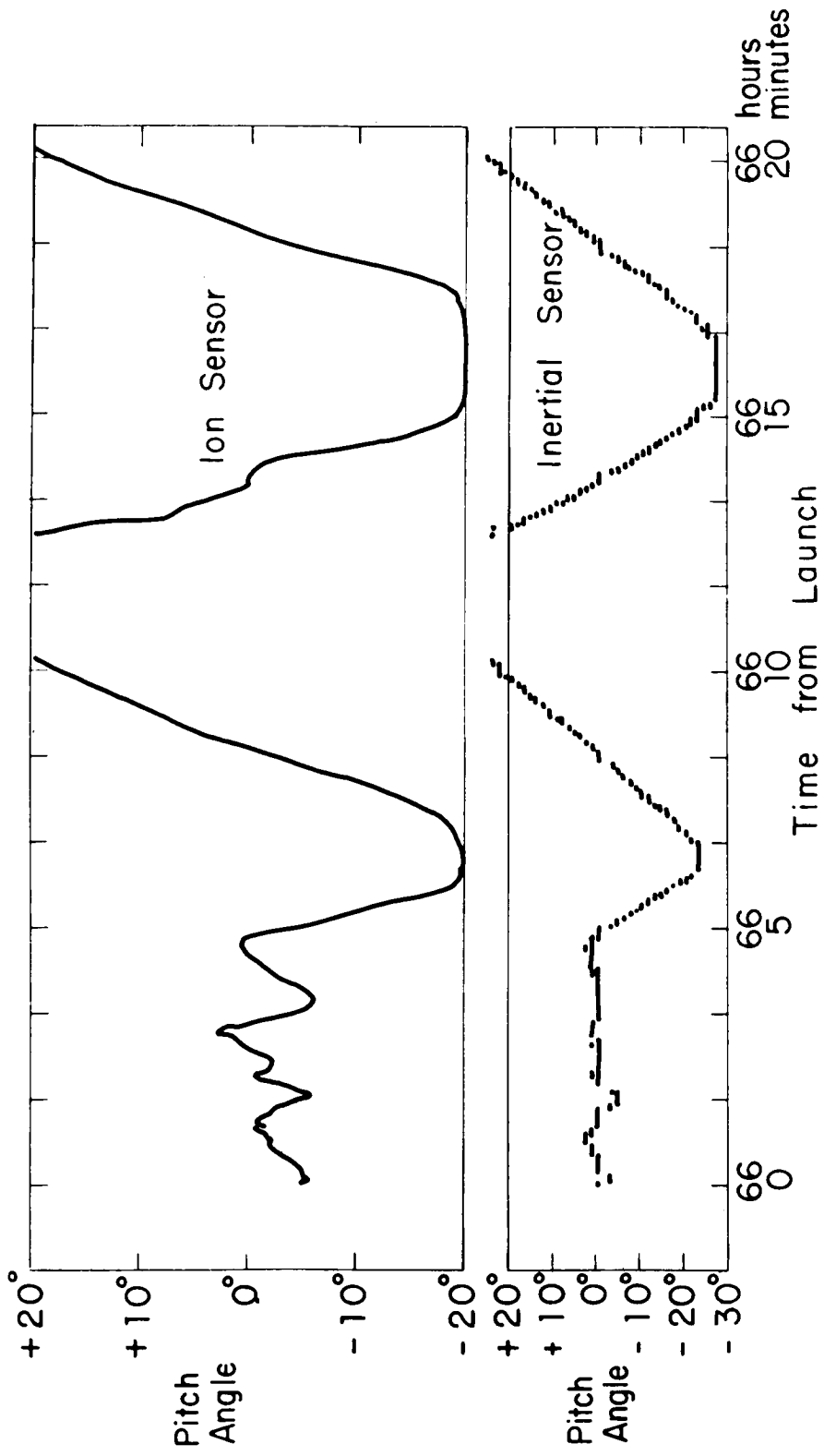


Figure 14-5. - Comparison of ion attitude pitch angle measurements with inertial system.

DISTRIBUTION LIST

Number of copies	Addressees
2	Dr. Mac C. Adams, R Associate Administrator for Advanced Research and Technology National Aeronautics and Space Administration Washington, D.C. 20546
2	Dr. Luis W. Alvarez Lawrence Radiation Laboratory University of California Berkeley, California 94720
1	Dr. H. Anderson Rice University Houston, Texas 77001
30	William O. Armstrong, MB National Aeronautics and Space Administration Washington, D.C. 20546
2	Dr. Stanley Bennett Dean, Medical School University of Chicago Chicago, Illinois 60637
2	Dr. Lloyd Berkner President Graduate Research Center of the Southwest P. O. Box 30365 Dallas, Texas 75230
2	Brigadier General Jack Bollerud, MM Acting Director of Space Medicine Office of Manned Space Flight National Aeronautics and Space Administration Washington, D.C. 20546
2	Dr. Allan H. Brown Department of Biology University of Pennsylvania Philadelphia, Pennsylvania 19104

DISTRIBUTION LIST - Continued

Number of copies	Addressees
2	Dr. Loren D. Carlson Chairman, Department of Physiology and Biophysics University of Kentucky Medical Center Lexington, Kentucky 40506
2	Dr. Francis Clauser University of California Santa Cruz, California 95060
2	Mr. G. A. Derbyshire National Academy of Sciences 2101 Constitution Avenue Washington, D.C. 20418
2	Dr. Lee A. DuBridge President California Institute of Technology Pasadena, California 91109
2	Mr. Lawrence Dunkelman Goddard Space Flight Center National Aeronautics and Space Administration Greenbelt, Maryland 20771
2	Dr. Alfred J. Eggers, R Deputy Associate Administrator Office of Advanced Research and Technology National Aeronautics and Space Administration Washington, D.C. 20546
2	Major General Harry L. Evans USAF SAF-SL MOL Program Office The Pentagon, Room 5D227 Washington, D.C. 20330

DISTRIBUTION LIST - Continued

Number of copies	Addressees
2	General James Ferguson SCG, Hq AFSC Andrews Air Force Base, Maryland 20331
2	Dr. John W. Findlay Deputy Director National Radio Astronomy Observatory P. O. Box 2 Green Bank, West Virginia 24944
2	Mr. Daniel J. Fink OSD DDR&E The Pentagon Washington, D.C. 20301
10	Mr. Willis B. Foster, SM Director of Manned Flight Experiments Office of Space Science and Applications National Aeronautics and Space Administration Washington, D.C. 20546
2	Dr. John French Brain Research Institute University of California Medical School Los Angeles, California 90024
2	Dr. Herbert Friedman Superintendent, Atmosphere and Astrophysics Division Code 7100 U.S. Naval Research Laboratory Washington, D.C. 20390
10	Dr. Jocelyn R. Gill, SM National Aeronautics and Space Administration Washington, D.C. 20546

DISTRIBUTION LIST - Continued

Number of copies	Addressees
1	Dr. T. Gualtierotti Ames Research Center National Aeronautics and Space Administration Moffett Field, California 94035
2	Dr. Leo Goldberg Harvard College Observatory Department of Astronomy Cambridge, Massachusetts 02138
2	Mr. George Trimble, MT Advanced Manned Missions Program Office of Manned Space Flight National Aeronautics and Space Administration Washington, D.C. 20546
10	Dr. Curtis L. Hemenway Dudley Observatory 140 South Lake Avenue Albany, New York 12200
2	Dr. Karl G. Henize Dearborn Observatory Northwestern University Evanston, Illinois 60201
1	Mr. Robert G. Hertz Dept. 650 Building 523 Lockheed Missiles and Space Company P. O. Box 504 Sunnyvale, California 94088
2	Dr. Harry H. Hess Department of Geology Princeton University Princeton, New Jersey 08540

DISTRIBUTION LIST - Continued

Number of copies	Addressees
1	Dr. Francis Johnson Graduate Research Center of the Southwest P. O. Box 30365 Dallas, Texas 75221
2	Dr. William W. Kellogg Associate Director National Center for Atmospheric Research Boulder, Colorado 80301
2	Mr. John E. Kirk OSD DDR&E Room 3E153, The Pentagon Washington, D.C. 20301
10	Mr. Martin J. Koomen U.S. Naval Research Laboratory Code 7141-K Washington, D.C. 20390
2	Dr. T. William Lambe Massachusetts Institute of Technology Cambridge, Massachusetts 02139
2	Dr. John H. Lawrence Donner Laboratory University of California Berkeley, California 94720
10	Mr. Douglas R. Lord, MTS National Aeronautics and Space Administration Washington, D.C. 20546
2	Dr. Paul Lowman Theoretical Division, Code MSSD Goddard Space Flight Center National Aeronautics and Space Administration Greenbelt, Maryland 20771

DISTRIBUTION LIST - Continued

Number of copies	Addressees
2	Dr. Gordon J. F. MacDonald University of California Los Angeles, California 90024
2	Dr. Nicholas U. Mayall Director, Kitt Peak National Observatory 950 North Cherry Avenue Tucson, Arizona 85717
2	Dr. David Medved Electro-Optical Systems, Inc. 300 North Halstead Pasadena, California 91107
2	Dr. George E. Mueller, M Associate Administrator for Manned Space Flight National Aeronautics and Space Administration Washington, D.C. 20546
2	Mr. Kenneth M. Nagler Chief, Space Operations Support Division U.S. Weather Bureau Gramax Building, Room 1415 Washington, D.C. 20689
2	Dr. John E. Naugle, SS Deputy Associate Administrator (Sciences) Office of Space Science and Applications National Aeronautics and Space Administration Washington, D.C. 20546
2	Dr. William Neuman University of Rochester Rochester, New York 14627
2	Dr. Homer E. Newell, S Associate Administrator for Space Science and Applications National Aeronautics and Space Administration Washington, D.C. 20546

DISTRIBUTION LIST - Continued

Number of copies	Addressees
2	Dr. Edward P. Ney School of Physics and Astronomy Institute of Minnesota Minneapolis, Minnesota 55455
10	Mr. David Novick, RNV National Aeronautics and Space Administration Washington, D.C. 20546
2	Dr. Hugh Odishaw National Academy of Sciences 2101 Constitution Avenue Washington, D.C. 20418
2	Mr. J. P. T. Pearman National Academy of Sciences 2101 Constitution Avenue Washington, D.C. 20418
2	Dr. Max Peterson Department of Aeronautics and Astronautics Instrumentation Laboratory 68 Albany Street Cambridge, Massachusetts 02139
2	Professor Courtland D. Perkins Chairman, Department of Aerospace and Mechanical Sciences Princeton University Princeton, New Jersey 08540
2	Dr. Martin A. Pomerantz Director, Bartol Research Foundation Swarthmore, Pennsylvania 19081
2	Dr. Richard W. Porter Engineering Services General Electric Company 570 Lexington Avenue New York, New York 10022

DISTRIBUTION LIST - Continued

Number of copies	Addressees
10	Dr. Leonard Reiffel, MA-6 National Aeronautics and Space Administration Washington, D.C. 20546
2	Dr. Bruno B. Rossi Laboratory for Nuclear Science Massachusetts Institute of Technology Cambridge, Massachusetts 02139
2	Miss Rita C. Sagalyn Hqs Air Force Cambridge Research Laboratories Laurence G. Hanscom Field Bedford, Massachusetts 07130
2	Dr. F. Saiedy Meteorological Office Damascus, Syria
2	Professor Leonard I. Schiff Executive Head, Department of Physics Stanford University Stanford, California 94305
2	Mr. Lyle C. Schroeder Instrument Research Division Langley Research Center National Aeronautics and Space Administration Hampton, Virginia 23365
2	Dr. William G. Shepherd Vice President, Academic Department 200 Morrill Hall University of Minnesota Minneapolis, Minnesota 55455
2	Dr. H. G. Shepler National Academy of Sciences 2101 Constitution Avenue Washington, D.C. 20418

DISTRIBUTION LIST - Continued

Number of copies	Addressees
2	Dr. William Shockley Stanford University Palo Alto, California 94305
2	Dr. John A. Simpson Laboratory of Astrophysics and Space Research Enrico Fermi Institute for Nuclear Studies The University of Chicago Chicago, Illinois 60637
1	Mr. Stanley Soules Environmental Science Services Administration National Environmental Satellite Center Washington, D.C. 20689
2	Dr. William H. Sweet Massachusetts General Hospital Boston, Massachusetts 02114
2	Dr. Charles H. Townes Provost, Massachusetts Institute of Technology Cambridge, Massachusetts 02139
2	Dr. James A. Van Allen Head, Department of Physics and Astronomy University of Iowa Iowa City, Iowa 52440
10	Dr. Sherman P. Vinograd, MM National Aeronautics and Space Administration Washington, D.C. 20546
2	Dr. John R. Winnery Department of Electrical Engineering Cory Hall University of California Berkley, California 94720

DISTRIBUTION LIST - Continued

Number of copies	Addressees
2	Dr. George P. Woolard Director, Hawaii Institute of Geophysics University of Hawaii Honolulu, Hawaii 96822
<u>MANNED SPACECRAFT CENTER:</u>	
2	AA/Dr. Robert R. Gilruth
1	BL/Mr. J. R. Brinkmann
1	BL/Mr. Richard Underwood
5	BM5/Mr. E. F. Meade
10	BM6/MSC Library
1	CA/Mr. Donald K. Slayton
10	CB2/Mr. John Peterson
2	CF/Mr. Helmut Kuehnel
2	EA/Mr. Warren Gillespie
1	EC7/Mr. W. J. Young
1	EC/Mr. R. S. Johnston
1	EG26/Mr. C. Manry
2	FA3/Mr. R. G Rose
1	FC/Mr. Christopher Kraft
1	FC/John D. Hodge
2	GM/Mr. W. Nesbitt
2	KA/Mr. R. F. Thompson

DISTRIBUTION LIST - Concluded

Number of copies	Addressees
1	PA/Mr. George M. Low
1	PC/Mr. R. Cox
5	PK/Mr. Victor Neshyba
10	RL/Mr. W. E. Davidson
1	TA/Wilmot N. Hess
1	TA/Robert O. Piland
1	TA/Paul R. Penrod
1	TG53/Mr. J. Marback
1	TG53/Mr. R. Lindsey
1	TG/Mr. J. Modisette
1	TH4/R. L. Jones
1	TG5/Mr. D. Womack
1	TG/Mr. P. B. Burbank
1	TG/Mr. J. Lintott
1	TG4/Mr. J. Shafer
1	TG4/Mr. R. Stokes
3	TE/Mr. Bruce Jackson
5	TF/Mr. N. G. Foster
82	TF2/James W. Campbell
10	ZR1/AFSC Field Office